

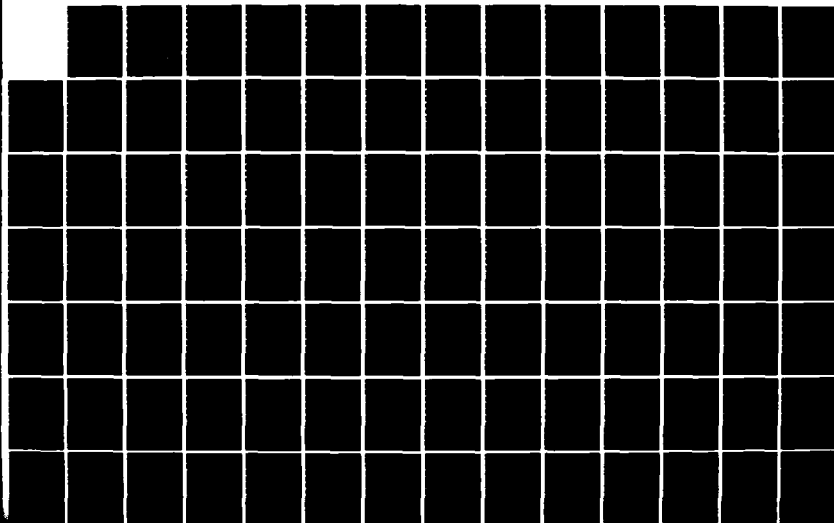
AD-A141 157

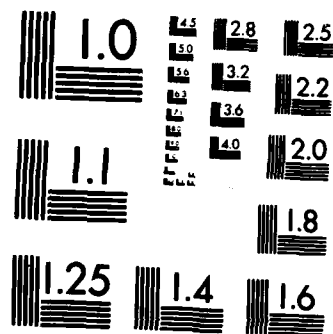
WAVELENGTH SELECTION FOR A GROUND BASED FREE ELECTRON  
LASER WEAPON SYSTEM(U) AIR FORCE INST OF TECH  
WRIGHT-PATTERSON AFB OH SCHOOL OF ENGI... D E KOHLHEPP  
DEC 83 AFIT/GSO/ENP/83D-2 F/G 15/3

1/2

UNCLASSIFIED

NL





MICROCOPY RESOLUTION TEST CHART  
NATIONAL BUREAU OF STANDARDS-1963-A

AFIT/GSO/ENP/83D- 2

AD-A141 157

DTIC FILE COPY

WAVELENGTH SELECTION FOR A GROUND BASED  
FREE ELECTRON LASER WEAPON SYSTEM  
THESIS

Douglas E. Kohlhepp  
Captain, USAF

AFIT/GSO/ENP/83D- 2

DTIC  
ELECTRONIC  
S MAY 16 1984  
A

Approved for public release; distributed unlimited

84 05 15 039

WAVELENGTH SELECTION FOR A GROUND BASED  
FREE ELECTRON LASER WEAPON SYSTEM

THESIS

Presented to the Faculty of the School of Engineering  
of the Air Force Institute of Technology  
Air University

In Partial Fulfillment of the  
Requirements for the Degree of  
Master of Science in Space Operations



Douglas E. Kohlhepp, B.S., M.S.S.M.  
Captain, USAF

December 1983

AI

Approved for public release; distribution unlimited

## Preface

The purpose of this study was to examine the various wavelength dependent issues which would impact the selection of an operating wavelength for a ground based free electron laser weapon system. As a non-specialist in the laser field, my approach to this problem was to develop rather simple scaling relationships and combine them in a straightforward manner. In fact, time itself precluded a more thorough treatment. The results of the study do not present a single optimum wavelength but show, to an approximate degree, how the selection is sensitive to various parameters.

No analysis is a solo effort, and this study was no exception. My thesis advisor, Lt Col John Erkkila, showed tremendous patience and understanding throughout this project and deserves my highest praise. I would also like to thank Dr. Charles Brau, director of the FEL Project Office at Los Alamos, who sponsored this research and provided invaluable information and assistance. Also, much thanks is due Mr. Frank Jinks of the Wright Aeronautical Lab who helped me enormously in getting the programs FASCODE and LOWTRAN up and running. Finally, a special thank you goes to my dearest friend, India Radford. Her love, constant support and encouragement have truly made the entire effort possible.

Douglas E. Kohlhepp

## Table of Contents

	Page
Preface . . . . .	ii
List of Figures . . . . .	v
List of Tables. . . . .	viii
Abstract. . . . .	ix
I. Introduction . . . . .	1
Background. . . . .	1
Research Objectives . . . . .	3
Basic Assumptions . . . . .	4
Basic Methodology . . . . .	5
Organization of the Report. . . . .	7
II. Free Electron Laser Efficiency Model . . . . .	8
Basic Concepts. . . . .	10
Energy Exchange in the Wiggler. . . . .	14
Efficiency Enhancements . . . . .	18
Cavity Restrictions . . . . .	20
Diffraction Spreading . . . . .	20
Mirror Damage . . . . .	22
Cavity Alignment. . . . .	23
Energy Recovery . . . . .	27
Efficiency Scaling. . . . .	28
III. Development of the Propagation Model . . . . .	38
Overview. . . . .	39
Laser Beam Propagation in a Vacuum. . . . .	41
Laser Beam Attenuation. . . . .	44
Molecular Absorption. . . . .	45
Aerosols. . . . .	47
Rayleigh Scattering . . . . .	48
Atmospheric Transmission Codes. . . . .	50
LOWTRAN . . . . .	51
FASCODE . . . . .	57
Atmospheric Turbulence. . . . .	58
Refractive Index Structure Parameter. . . . .	60
Turbulence Induced Beam Radius. . . . .	66

Effects of Jitter . . . . .	68
Thermal Blooming. . . . .	69
Model Resolution. . . . .	84
IV. Target Interactions. . . . .	88
Basic Theory. . . . .	88
Discussion of the Approach. . . . .	94
V. The Program. . . . .	98
Program Limitations . . . . .	108
VI. Analysis Results . . . . .	110
Selection of Parameters for the Base-	
line Case. . . . .	110
Baseline Results. . . . .	113
Thermal Blooming . . . . .	126
Atmospheric Transmission . . . . .	127
Beam Radius. . . . .	131
Extensions to the Base Case . . . . .	138
Effects of Turbulence Compensa-	
tion (1). . . . .	139
Effects of Altitude and Aerosols . . . . .	141
Effects of Turbulence Compens-	
tion (2). . . . .	145
Effects of Aperture Size . . . . .	145
VII. Conclusions and Recommendations. . . . .	149
Conclusions . . . . .	149
Recommendations . . . . .	151
Appendix A: Modifications to the Program - LOWTRAN . . .	153
Appendix B: Modifications to the Program - FASCODE . . .	156
Appendix C: Program Listing - SORT . . . . .	158
Appendix D: Program Listing - WAVLEN . . . . .	161
Bibliography. . . . .	173
Vita. . . . .	177

## List of Figures

Figure	Page
1. Free Electron Laser Components . . . . .	9
2. Electron / Wiggler Field Interactions. . . . .	13
3. FEL Power and Gain Versus Electron Energy. . . . .	16
4. FEL Energy / Phase Relationship. . . . .	17
5. Misalignments in the Optical Cavity. . . . .	25
6. Maximization of $F_K$ Over Variable $x$ and $g$ . . . . .	30
7. Optimum Values of $x$ and $g$ . . . . .	31
8. Optimum Values of $F_K$ . . . . .	32
9. Optimum Values of Resonant Phase . . . . .	33
10. Optimum Values of Scaled FEL Efficiency. . . . .	34
11. FEL Efficiency Versus Wavenumber With Energy Recovery. . . . .	37
12. Atmospheric Transmission (0.5 to 1.7 micro- meters). . . . .	46
13. Attenuation Coefficients for Atmospheric Aerosols and Rayleigh Scattering . . . . .	49
14. Aerosol Concentrations Versus Altitude in LOWTRAN. . . . .	54
15. Attenuation Coefficients for Rural Aerosol Model in LOWTRAN . . . . .	54
16. Ozone Attenuation in the Atmosphere (Visible and Ultraviolet Regions). . . . .	56
17. Hufnagel's Model of the Structure Parameter vs. Altitude . . . . .	65
18. Thermal Blooming Effects on Refractive Index . . . . .	71

19.	Beam Reduction Factor, Irel, vs. Distortion Parameter . . . . .	80
20.	Mean Horizontal Wind vs. Altitude . . . . .	82
21.	Specific Heat Atmosphere vs. Altitude . . . . .	83
22.	Absorptivity of Common Aerospace Materials vs. Wavenumber. . . . .	92
23.	Regression Curve of Experimental Absorp- tivity Data of Al-2024 and Al-7075. . . . .	96
24.	Program Flow for the Analysis . . . . .	99
25.	Flow Chart of Program WAVLEN. . . . .	103
26.	Overall System Efficiency (8750-9500 $\text{cm}^{-1}$ ). . . . .	114
27.	Overall System Efficiency (9500-10500 $\text{cm}^{-1}$ ) . . . . .	115
28.	Overall System Efficiency (10500-11500 $\text{cm}^{-1}$ ). . . . .	116
29.	Overall System Efficiency (11500-12450 $\text{cm}^{-1}$ ). . . . .	117
30.	Overall System Efficiency (12450-13500 $\text{cm}^{-1}$ ). . . . .	118
31.	Overall System Efficiency (13500-14500 $\text{cm}^{-1}$ ). . . . .	119
32.	Overall System Efficiency (14500-15500 $\text{cm}^{-1}$ ). . . . .	120
33.	Overall System Efficiency (15500-16500 $\text{cm}^{-1}$ ). . . . .	121
34.	Overall System Efficiency (16500-17500 $\text{cm}^{-1}$ ). . . . .	122
35.	Overall System Efficiency (17500-20200 $\text{cm}^{-1}$ ). . . . .	123
36.	Overall System Efficiency (20200-24600 $\text{cm}^{-1}$ ). . . . .	124
37.	Overall System Efficiency (24600-29000 $\text{cm}^{-1}$ ). . . . .	125
38.	Aerosol Transmission. . . . .	128
39.	Ozone Transmission. . . . .	129
40.	Rayleigh Scattering Transmission. . . . .	130
41.	Beam Radius Due to Diffraction. . . . .	133

42.	Beam Radius Due to Turbulence . . . . .	134
43.	Total Beam Radius . . . . .	135
44.	Top Line Structure of Baseline Case . . . . .	137
45.	Efficiency Curve With 100% Turbulence Correction. . . . .	142
46.	Efficiency Curve With Laser at 3.0 km Altitude. . . . .	146

## List of Tables

Table	Page
I. Variation of Turbulence Compensation Parameter . . . . .	140
II. Variation of Turbulence Compensation Parameter (No Ozone Absorption) . . . . .	140
III. Variation of Altitude and Sea Level Visibility. . . . .	144
IV. Variation of Turbulence Compensation Parameter (Laser Altitude of 3000 meters) . . . . .	144
V. Variation of Aperture Size. . . . .	147

Abstract

↓  
A computer model was developed to examine the wavelength dependent relationships which would impact in a selection of the operating wavelength for a ground based free electron laser weapon system employed in a strategic role. The program considers the device efficiency of the free electron laser, the propagation of laser radiation in the atmosphere, and the coupling of laser energy into the target material. The program employs modified versions of the atmospheric transmission codes LOWTRAN and FASCODE.

⑦ The optimum laser wavelength for a specific selection of laser parameters is determined. However, equally acceptable wavelengths could be found with a .2 micrometer region surrounding this optimum value. In addition, the wavelength selection process is very sensitive to the mean sea level altitude of the laser device and the degree to which atmospheric turbulence induced beam spread can be compensated for by adaptive optics. ↗

# WAVELENGTH SELECTION FOR A GROUND BASED FREE ELECTRON LASER WEAPON SYSTEM

## I. Introduction

### Background

Over the past decade, enthusiasm over the military uses of directed energy weapons has increased dramatically. Specifically, considerable interest has been placed on the development of ground based laser weapon systems. Such a system could be employed as an anti-satellite weapon, or as some have proposed, in a strategic defense role (1:17). In this latter mission, the ground based laser would work in concert with high quality relay mirrors in space to intercept ICBM's, and possibly, high altitude bomber aircraft.

Basing such a laser weapon on the ground rather than in space offers many advantages. Generally, size and weight are not the critical considerations on the ground as they would be in space. Ground basing allows ease of servicing and repair. Perhaps the most important advantage, however, is the high survivability that basing within national boundaries offers over space basing.

Yet, the ground basing of a laser weapon poses a very severe disadvantage as well. Such a weapon system would be required to propagate a laser beam through the intervening

atmosphere. Atmospheric attenuation, turbulence, and self-induced thermal blooming all contribute to reduce the laser energy that reaches the target. These effects are very much dependent on the wavelength of the laser radiation; slight changes in wavelength can drastically alter the beam's ability to propagate through the atmosphere. In addition, the degree to which a laser's energy is absorbed by a target also determines the overall effectiveness of a laser weapon system. This phenomenon is dependent on the laser wavelength as well. Finally, there may be efficiencies within the laser itself which are functions of wavelength.

Previously, designers of laser systems for defense applications were restricted to only the specific, discrete wavelengths produced by conventional lasers. With the advent of the free electron laser (FEL), however, a designer would now have the ability to select the wavelength which would maximize the effectiveness of the weapon system.

The free electron laser produces coherent electromagnetic radiation through interactions between a relativistic electron beam, a spatially periodic magnetic field, and an optical radiation field propagating in the same direction as the electron beam. It is unusual in that, unlike a conventional laser, it does not rely on energy transitions between atomic or molecular energy levels. Because of this fact, the operating wavelength of the free electron laser is continuously selectable. In theory, any wavelength from the microwave

region to the x-ray portion of the spectrum is possible (2). The free electron laser is still very much in the experimental stage of development, but the eventual scaling to the high power levels required of a laser weapon appears promising (3:60).

Review of the current literature and discussions with the Free Electron Laser Project Office at the Los Alamos National Laboratory indicate that, previously, no one has studied atmospheric propagation, target absorption, and FEL device efficiency issues in an overall system analysis with an eye towards selecting the wavelength which best accomplishes a specific mission. This analysis is necessary if one is ever to take advantage of this unique tunability feature of the FEL.

#### Research Objectives

The objective of this study is to examine the many wavelength dependent relationships which affect the overall effectiveness of a ground based free electron laser weapon system and to select that wavelength which provides the maximum effectiveness for the system. Specifically, this objective will include the following subtasks.

- A. To determine the significant wavelength dependent issues which affect weapon system efficiency.
- B. To develop a parametric computer model which evaluates the overall effectiveness of a ground based FEL at a given wavelength.

- C. To validate the model, test model assumptions and identify inaccuracies in the model
- D. To analyze a range of wavelengths in hopes of finding a single wavelength or a small range of wavelengths which maximizes the system of effectiveness for the input parameters chosen.
- E. To identify the key issues which affect the wavelength selection process.

#### Basic Assumptions

The following basic assumptions will be made in the analysis:

- A. The free electron laser weapon system is ground based in a mid-latitude region of the United States and in a relatively pollutant free, low humidity environment.
- B. The FEL weapon system is being employed in a strategic mission, i.e. anti-satellite, ballistic missile defense, anti-aircraft.
- C. The laser can be used in a direct attack mode for a target in space, or in concert with a 100% reflecting spaced based relay mirror. It is assumed that the optimum wavelength would be nearly the same in either case.
- D. The free electron laser produces an output with a long pulse length which can be assumed to be continuous wave. Hence, the device peak power is es-

entially equal to the average power (2).

- E. The target is composed of common aerospace materials such as aluminum alloys.
- F. The kill mechanism of the weapon system is a thermal burnthrough of the target's outer skin.
- G. The wavelength dependence in the reflectances of optical mirrors will not be considered.
- H. Efficiencies associated with power and cooling requirements will not be considered. It is assumed these are insignificant for a ground based system.
- I. Pointing and tracking capabilities will not be addressed.
- J. Further assumptions concerning specific areas will be discussed during the chapters pertaining to model development.

### Basic Methodology

The brunt of the analysis effort will be in the development of the computer model. The model will emphasize a system wide approach to the problem and will cover the following three main areas of an interest in a ground based free electron laser weapon system: FEL device efficiency, atmospheric propagation and target interactions.

The wavelength dependence in the device efficiency arises from the laser's ability to trap and extract energy from the relativistic electron beam and from certain restrictions with-

in the laser cavity (2). Current engineering measures which are used to enhance the overall FEL device efficiency need to be considered as well.

A simplified propagation sub-model will be developed to address the propagation issues. It will consider atmospheric absorption and scattering from both molecular and aerosol constituents in the atmosphere. In addition, the spreading of the laser beam due to diffraction, jitter, and atmospheric turbulence will be included. Finally, the model will address the reduction of the laser beam irradiance from self-induced thermal blooming.

Generally, shorter wavelengths are absorbed by metallic targets more efficiently than longer wavelengths. The basic theory behind such an assumption is the Drude free electron model, and thus, will form the foundation for this portion of the analysis.

Each of the three areas just discussed can be described through a relationship between laser wavelength and a dimensionless value of efficiency between zero and one. The proposed computer model will multiply these three values together to form an overall system efficiency as described below.

$$\eta_{\text{system}} = \eta_{\text{FEL}} \times \eta_{\text{propagation}} \times \eta_{\text{target}} \quad (1)$$

This overall efficiency is the system measure of effectiveness we wish to maximize with respect to laser wavelength. Wavelength selection will be simply based on the maximum

value of overall system efficiency.

At certain times in the analysis process, it is more useful to employ the term wavenumber rather than wavelength. Both are spectral representations of electromagnetic radiation. This report will use the terms wavelength and wavenumber almost interchangeably, the conversion between the two being governed by the following equation.

$$\text{WAVENUMBER (cm}^{-1}\text{)} = \frac{1.0 \times 10^4}{\text{WAVELENGTH (micrometers)}} \quad (2)$$

#### Organization of the Report

In the following three chapters, the theory supporting the modeling of FEL device, propagation, and target coupling efficiencies is presented and pertinent wavelength dependent relationships are developed. Chapter V presents the program which will be used in the analysis. The actual results of the analysis will be presented in Chapter VI. Finally, Chapter VII summarizes with the conclusions and recommendations from the study.

## II. Free Electron Laser Efficiency Model

The free electron laser is unique among laser devices in that it does not rely on the transitions between discrete energy levels of atoms or molecules to generate stimulated emission. Instead, coherent electromagnetic radiation is produced through the interactions of a relativistic electron beam, a spatially periodic magnetic field or 'wiggler', and an optical radiation field propagating in the direction of the electron beam. These major components of a free electron laser can be seen in a cut-a-way view of the device in Figure 1.

Free electron lasers have only been in existence for the past seven years. Madey and others at Stanford University first demonstrated amplification from such a device in 1976 (4:717). A year later, the same group demonstrated laser power from a cavity resonator operating at 3.4 micrometers (5:892). Since those early breakthroughs, much has been published in an effort to advance the theory. One of the earlier works of interest was that of Colson (6) who described free electron laser operation totally in terms of classical physics. Also of note were the theoretical proposals to enhance the efficiency of the device through novel wiggler designs (7) and the efforts to optimize certain design parameters of the system (8).

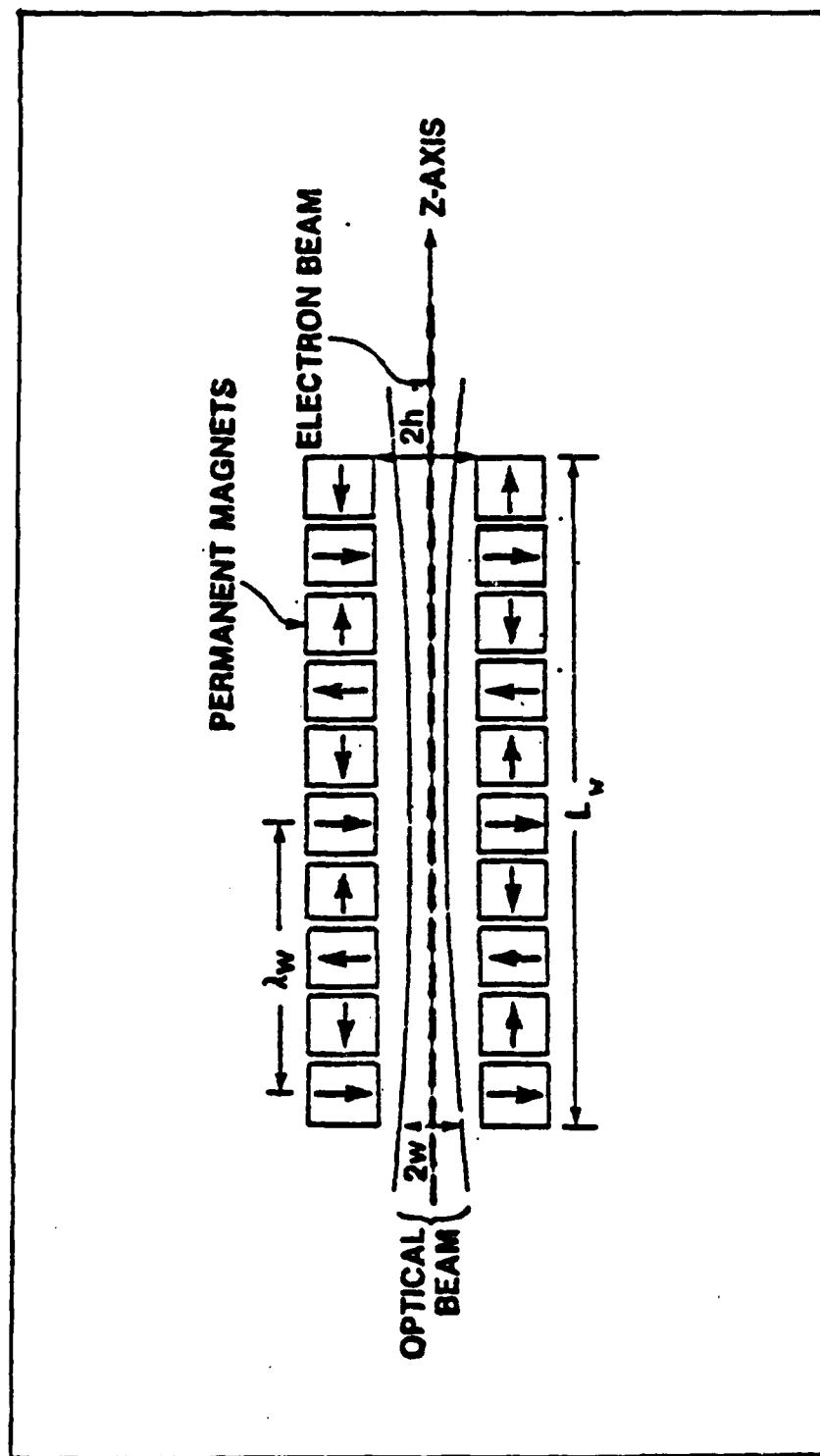


Figure 1. Free Electron Laser Components (11:56)

## Basic Concepts

The largely qualitative discussion of the free electron laser which follows is intended to provide those unfamiliar with the basic concepts of the device an understanding of the efficiency relationships. A full theoretical treatment is beyond the scope of this study and the interested reader is referred to the many excellent references on the subject.

The electron beam and propagating optical beam travel through the interior of the wiggler device. The wiggler is characterized by a magnetic field which is constant in magnitude, but alternating in direction down the length of the wiggler with some spatial period,  $\lambda_w$ . The magnetic field vector,  $\vec{B}$ , is kept perpendicular to the path of the electron beam throughout. This is generally accomplished through a series of permanent magnets as depicted in the figure.

As the electron beam travels down the interior of the wiggler and encounters the magnetic field perpendicular to its path, the electrons will undergo a transverse acceleration described by the following equation.

$$\frac{d}{dt} (\gamma m \vec{v}) = e (\vec{v} \times \vec{B}) \quad (3)$$

where  $m$  = electron rest mass, Kg  
 $e$  = electron charge, coulombs  
 $\vec{v}$  = electron velocity, m/sec  
 $\vec{B}$  = the magnetic field vector, Tesla  
and  $\gamma$  = the relativistic factor,

$$\left[ 1 - \left( \frac{v}{c} \right)^2 \right]^{-\frac{1}{2}}$$

Of course, the direction of acceleration due to the magnetic force is normal to both the electrons' path and the magnetic field because of the cross product terms in the equation. As the electrons undergo this acceleration, they emit energy in the form of electromagnetic radiation. The resulting radiation pattern is symmetric about some mean propagation vector which is normal to the direction of acceleration. In this case, the radiation will peak in the direction of the electrons' path. Due to the relativistic nature of the electron beam, this radiation pattern will be extremely narrow.

If the magnetic field alternates periodically in direction, the electrons will be caused to accelerate first in one direction, then another. Therefore, the electrons will follow an undulating path with a period equal to the spatial period of the magnetic field (hence, the derivation of the term, wiggler).

Consider the radiation produced by the electrons at two points along their path as depicted in Figure 2. The undulating motion of the electrons is exaggerated for clarity. Actually, the electrons deviate very little from their original path. The radiation produced at Point A could be made to combine constructively with the radiation produced at Point B with some judicious selections of parameters. The time necessary for a photon of radiation to travel the distance from A to B is simply

$$\tau_p = \lambda_w / c \quad (4)$$

where  $c$  is the speed of light. An electron, traveling close to but less than the speed of light, will lag behind the photon. Suppose the electrons lag a distance equal to exactly one wavelength of the propagating radiation. In this case, the radiation they produce at point B will be in phase with the radiation produced at point A. The electrons' time to travel from A to B is

$$\tau_e = \lambda_w / v \quad (5)$$

If the difference between the two times corresponds to one wavelength of light,  $\lambda_L$ , we have

$$\left( \frac{\lambda_w}{v} - \frac{\lambda_w}{c} \right) = \frac{\lambda_L}{c} \quad (6)$$

or

$$\frac{v}{c} = \frac{\lambda_w}{\lambda_w + \lambda_L} \quad (7)$$

using the following relativistic relationship and its Taylor series expansion

$$\frac{v}{c} = \left( 1 - \frac{1}{\gamma^2} \right) \approx 1 - \frac{1}{2\gamma^2} - \frac{1}{8\gamma^4} \dots \quad (8)$$

and ignoring the insignificant terms

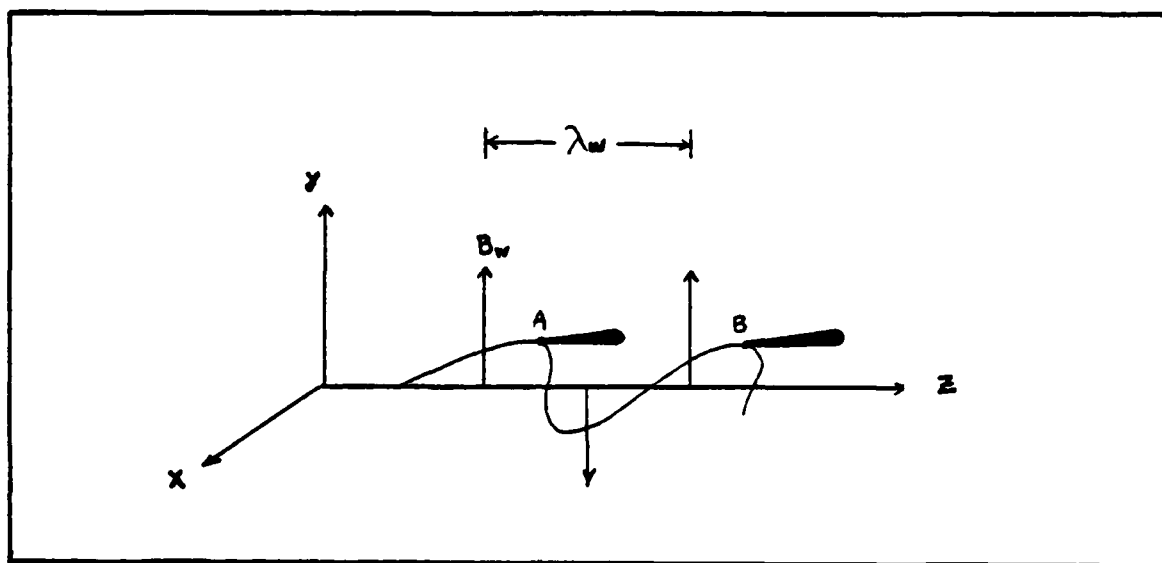


Figure 2. Electron/Wiggler Field Interactions

$$1 - \frac{1}{2\gamma^2} \approx \frac{\lambda_w}{\lambda_w + \lambda_L} \quad (9)$$

we arrive through simple algebraic operations with the expression

$$\lambda_L \approx \frac{\lambda_w}{2\gamma^2} \quad (10)$$

Equation (10) defines the "resonance" condition for a free electron laser and is one of the most important equations in the theory. It points up perhaps the most remarkable characteristic of the free electron laser: tunability. By changing either the wiggler period,  $\lambda_w$ , or the electron kinetic energy,  $\gamma$ , one can specify the wavelength of the

laser radiation. For example, a 100 MEV electron beam equates to a  $\gamma$  of about 196. For a nominal wiggler period of 5 cm, a laser output in the visible region with a wavelength of .65 micrometers could be produced.

This simplistic overview is intended only to illustrate the basic operation of the free electron laser. In reality, equation (10) is applicable only for weak magnetic fields where one can assume the electron velocity is not perturbed appreciably by the wiggler. For stronger fields, this does not hold, and the resonance condition is governed by the following equation (9:245).

$$\lambda_L = \frac{\lambda_w}{2\gamma^2} \left( 1 + A_w^2 \right) \quad (11)$$

where  $A_w$  is the dimensionless wiggler vector potential given by

$$A_w = \frac{e|\vec{B}|\lambda_w}{2mc} \quad (12)$$

Brau (10:16) employs an equivalent expression for the wiggler vector potential based on a characteristic length,  $\lambda_p$ , which depends on the permanent magnet material and wiggler construction, and the separation between the magnet arrays,  $2h$ , as depicted in Figure 1.

$$A_w = \frac{\lambda_w}{\lambda_p} \exp \left( -\frac{2\pi h}{\lambda_w} \right) \quad (13)$$

Energy Exchange in the Wiggler. Let us now consider the

interaction between the electrons and the co-propagating electromagnetic field of the laser beam. This interaction will be determined by the Lorentz force equation.

$$\frac{d}{dt} (\gamma m \bar{v}) = e (\bar{E}_r + \bar{v} \times \bar{B}_r) \quad (14)$$

Here,  $\bar{E}_r$  and  $\bar{B}_r$  refer to the electric and magnetic fields of the laser radiation. The magnetic field accomplishes no work on the electron; therefore, the rate of change of the kinetic energy of the electron can be described by the following expression (11:9).

$$\frac{d}{dt} (\gamma) = \frac{e}{mc^2} (\bar{v} \cdot \bar{E}_r) \quad (15)$$

Equation (15) also gives rise to the inter-related concept of phase between an electron and the laser field. The sign of the change in electron energy depends on the dot product of the electron velocity and the electric field of the laser beam, and, therefore, on the spatial position of the electron with respect to the light wave. Thus, a resonant phase, in this simple example equal to zero, can be defined (11:10).

In a continuous electron beam or electron bunch of large spatial extent compared to the wavelength of the light, the phase of the interaction is completely random. If all of the electrons are at the resonance energy, approximately half will

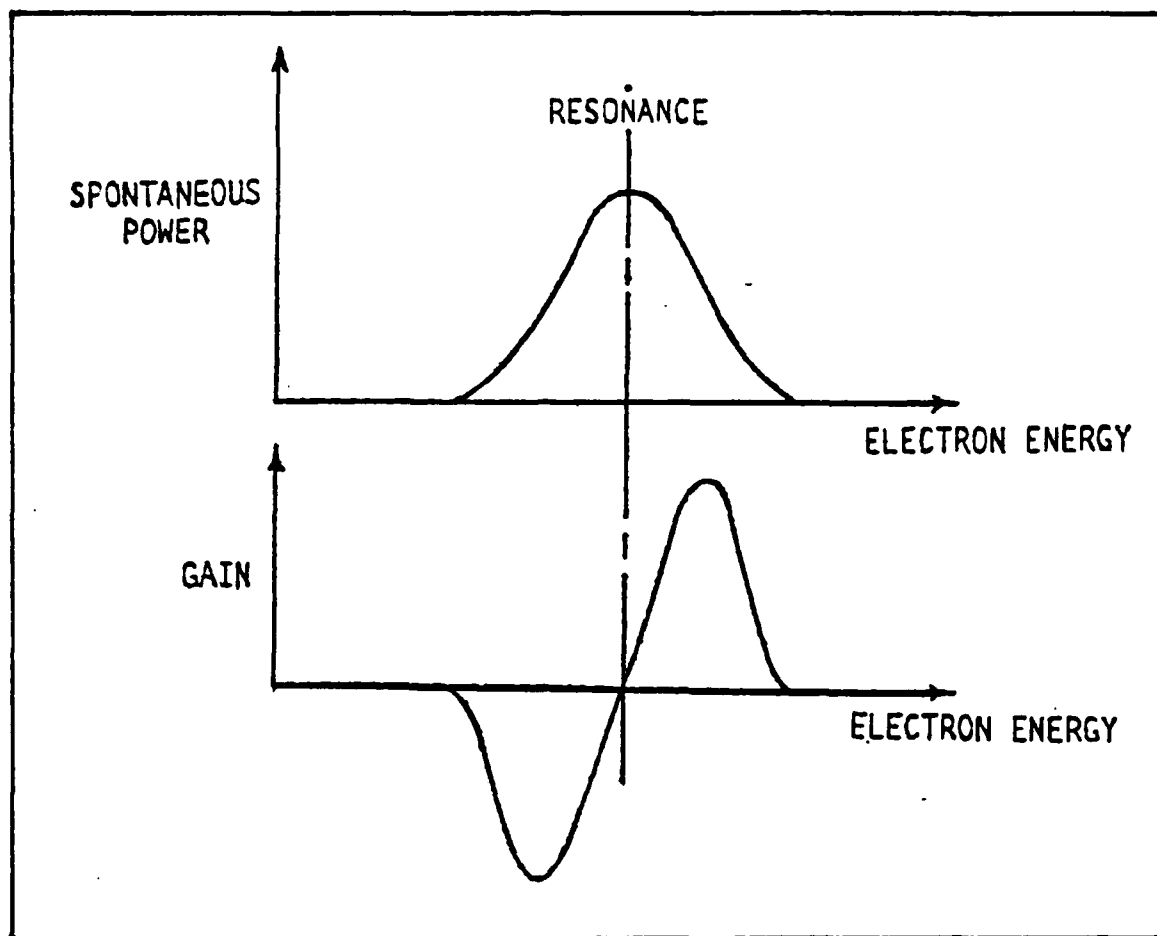


Figure 3. FEL Power and Gain vs. Electron Energy (11:10)

lose energy to the light wave and half will gain energy from the light wave. Hence, at resonance, no net transfer of energy takes place. However, if the electrons are injected into the wiggler at an energy slightly higher than the resonance energy for a given wavelength, then those electrons that absorb energy from the light wave are pushed to higher energies, farther from the resonance condition and proper phase with the light wave. Those electrons that lose energy to the wave are pulled closer to resonance and remain in phase for a longer period of time. Thus, there is a net positive energy exchange from the electron beam to the laser field.

Figure 3 depicts both the stimulated emission curve and

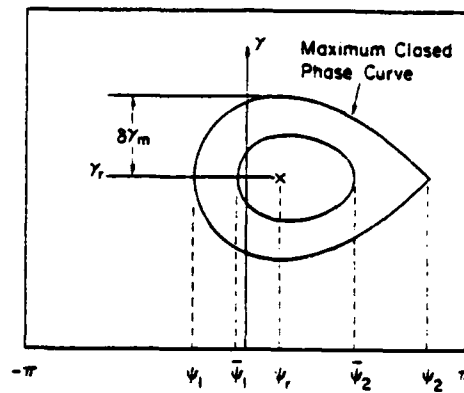


Figure 4. FEL Energy/Phase Relationship (7:99)

the small signal gain curve for a free electron laser. As stated above, for electron beams at the resonant energy, the laser gain is zero. For higher energies, the laser gain is positive representing transfer of energy from the electron beam to the laser field.

Those electrons that are decelerated towards the resonant energy are eventually captured or trapped by the laser field and will oscillate about the resonant values of energy and phase. Simply, if an electron is decelerated below the resonant energy and phase, it will now begin to absorb energy from the laser field as described by equation (15), and thus, will be accelerated back to the resonant energy. Therefore, 'buckets' of electrons, trapped by the laser beam, are formed with the finite dimensions of height and width. Figure 4 depicts the energy/phase diagram of this interaction. The area within the closed curves represents those values of electron energy and phase that result in electrons being captured. These closed curves effectively define the height and width of the

electron buckets as well.

### Efficiency enhancements

Some of the earliest experiments on the free electron laser succeeded in extracting less than .2% of the electrons' energy (4:720). Since those times, many schemes have been proposed to enhance the efficiency of the free electron laser. Perhaps the most effective has been the development of the variable parameter wiggler.

In the discussion which preceded, it was assumed the spatial period and the strength of the magnetic field in the wiggler remained constant. Such an assumption drastically limits the amount of energy that can be extracted from the electron beam. After the electrons decelerate in the wiggler and become trapped, no net energy transfer between the electrons and laser field takes place. However, if the value of the resonant energy is slowly (and adiabatically) decreased along the length of the wiggler, greater amounts of energy can be extracted from the beam (7:108). From the resonance condition defined by equation (11), it can be seen that, holding the laser wavelength constant, the resonant energy can be reduced by decreasing the wiggler period and/or decreasing the wiggler magnetic field potential.

For an adiabatic deceleration of the electrons, the bucket size and shape must vary slowly along the length of the wiggler. This can be assured if the resonant phase is held

constant. Kroll has shown that this resonant phase,  $\psi_r$ , can be found from the following expression (12:116).

$$\frac{d\gamma}{dz} = \frac{-2A_s A_w}{\gamma} \sin \psi_r \quad (16)$$

where  $z$  is the position along the wiggler and  $A_s$  is the dimensionless laser field equal to

$$A_s = \frac{e}{mc^2} (Z_0 I_L)^{\frac{1}{2}} \quad (17)$$

Here,  $Z_0$  is the impedance of free space  $= (\mu_0/\epsilon_0)^{\frac{1}{2}} = 377 \Omega$ , and  $I_L$  is the laser intensity in Watts/m<sup>2</sup>. Note that the resonant phase reduces to a value of zero when the resonant energy is constant as in the case of a constant parameter wiggler.

In the case of variable parameter wigglers, it is useful to think of electrons being captured in buckets and then the buckets being decelerated to extract energy. No longer is it necessary to inject the electrons at an energy above the resonant energy. Instead, the electrons are injected at the resonant energy and are immediately captured. These buckets of captured electrons are then slowly decelerated by decreasing the resonant energy of the wiggler. With such a model, one can define a capture efficiency,  $\eta_C$ , and a deceleration efficiency,  $\eta_D$ , of the free electron laser device. Then the total extraction efficiency,  $\eta_X$ , which measures the device's ability to transfer the kinetic energy of the electrons to the radiation field of the laser, is simply the following

$$\eta_X \approx \frac{A_w A_s L_w}{\gamma^2 r_1} \eta_C \sin \psi_r \quad (22)$$

Note that the extraction efficiency scales inversely with the square of the electron energy, indicating the greater difficulties in decelerating higher energy beams. Since, the square of the resonant energy is likewise inversely proportional to the laser wavelength, equation (22) shows that higher device efficiencies result for longer wavelengths as well.

#### Cavity Restrictions

Of course, the above equation represents an ideal case where there exist no other restrictions to the design of the free electron laser cavity. Brau and others at the FEL Project office at the Los Alamos National Laboratory have extensively studied the efficiency of the free electron laser device when cavity restrictions such as diffraction spreading of the laser beam, mirror damage and mirror alignment are considered (10:4-22). The rest of this section is based on their work.

Diffraction Spreading. The maximum length of the wiggler magnet and thus the extraction efficiency, will be limited by the diffraction spreading of the laser beam. At the entrance and exit to the wiggler, the laser field must not impinge on the surfaces of the permanent magnets. Brau defines the fol-

lowing quantities (10:5).

$$g = \frac{r}{r_L} \quad (23)$$

Here,  $r$  is the  $1/e$  radius of the beam at the entrance (or exit) of the wiggler and  $r_L$  is the radius at the beam waist. It is assumed the beam waist falls at the midpoint of the wiggler. The diffraction spreading is governed by the following equation

$$r^2 = r_L^2 \left( 1 + \frac{z^2}{Z_L^2} \right) \quad (24)$$

where  $z$  is the distance from the beam waist, and  $Z_L$  is the Rayleigh range,

$$Z_L = \frac{\pi r_L^2}{\lambda_L} \quad (25)$$

Brau (10:6) defines the ratio of the wiggler aperture radius,  $h$ , and the beam radius at the entrance to the wiggler,  $r$ , as simply

$$n = \frac{h}{r} \quad (26)$$

Finally, the electric field, equation (17), is defined in terms of the laser power,  $P_L$ , and a characteristic power,  $P_0$  (10:5).

$$A_s = \left( \frac{4P_L}{r^2 P_0} \right)^{\frac{1}{2}} \quad (27)$$

Here,  $P_0$  equals the following.

$$P_0 = \left( \frac{mc^2}{e} \right) \frac{2\pi}{Z_0} = 4.36 \text{ GW} \quad (28)$$

Using these quantities, Brau determines the maximum extraction efficiency,  $\eta_x$ , based on a maximum wiggler length (10:6).

$$\eta_x = \left( \frac{P_L}{P_0} \right)^{\frac{1}{2}} \left( \frac{g^2 - 1}{ng^2} \right)^{\frac{1}{2}} \frac{4A_w}{1 + A_w^2} \ln \left[ \frac{2\gamma_{r1}^2 \lambda_L}{\lambda_p A_w (1 + A_w^2)} \right] \eta_c \sin \psi_r \quad (29)$$

Mirror Damage. For any high power laser device, the maximum power that can be generated is often limited by the thermal distortion of the laser cavity mirrors. This is also the case for the free electron laser. For an assumed Gaussian beam, the peak laser irradiance at the mirror surfaces is given by

$$I_m = \frac{2P_L}{\pi r_m^2} \quad (30)$$

where  $r_m$  is the laser beam radius at the mirrors. For a continuous wave laser such as the free electron laser, mirror damage will most likely limit the time averaged irradiance at the mirror surfaces rather than the peak irradiance. Since the time averaged laser power,  $\bar{P}_L$ , is related to the average electron beam current,  $\bar{I}_B$ , by (10:10)

$$\bar{P}_L = \frac{mc^2}{e} \gamma_{r1} \bar{I}_B \eta_x \quad (31)$$

Brau shows that the extraction efficiency of the device is

further restricted by mirror damage and must satisfy the following (10:11).

$$\eta_x = \frac{\bar{I}_m L_m^2}{P_L} \frac{I_B}{I_0} \frac{g^2 - 1}{g^2} \frac{A_w^2}{\gamma_{r1}^3} \eta_c^2 \sin^2 \psi_r \quad (32)$$

Here,  $\bar{I}_m$ , is the limiting average laser irradiance on the mirror surfaces,  $I_B$ , is the peak electron beam current,  $L_m$  is the distance separating the two cavity mirrors, and  $I_0$  is a characteristic electron beam current given by

$$I_0 = \frac{mc^2}{eZ_0} = 1356 \text{ Amp} \quad (33)$$

Cavity Alignment. It can be seen in equation (32), that maximizing the extraction efficiency requires  $g \gg 1$ . or the radius of the laser beam at the wiggler entrance to be much greater than at the beam waist. This requirement necessitates cavity mirrors with short focal lengths, thus imposing more severe cavity alignment difficulties (10:11).

Figure 5 depicts a nearly concentric stable laser cavity with mirror radii of  $R_m$ . A small angular displacement,  $\theta_m$ , in mirror alignment results in the center of curvature of that mirror being displaced by an amount  $\delta_m$ . We must require that the tilt of the laser beam axis be small compared with the diffraction angle of the beam. Making the approximation  $R_m = L_m/2$ , the fractional displacement of the laser spot on

(10:2).

$$\eta_X = \eta_C \eta_D \quad (18)$$

The capture efficiency of the wiggler is determined by those values of phase at which electrons are captured. Recalling Figure 4, those phase values will fall within the two extremes that define the bucket width,  $\psi_1$  and  $\psi_2$ . Therefore, assuming every phase value between zero and  $2\pi$  is equally likely, the capture efficiency is given by the following expression (10:1)

$$\eta_C = \frac{\psi_2 - \psi_1}{2\pi} \quad (19)$$

The formula for the deceleration efficiency is equally simple (10:2).

$$\eta_D = \frac{\gamma_{r1} - \gamma_{r2}}{\gamma_{r1}} \quad (20)$$

Here,  $\gamma_{r1}$  and  $\gamma_{r2}$  are the resonant energies at the entrance and exit of the wiggler. Integrating equation (16) with respect to  $z$ , the distance along the wiggler, yields

$$\gamma_{r1}^2 - \gamma_{r2}^2 = 2 A_w A_s L_w \sin \psi_r \quad (21)$$

where  $L_w$  is the length of the wiggler. Therefore, for small amounts of deceleration, the extraction efficiency is approximated by the following (10:4).

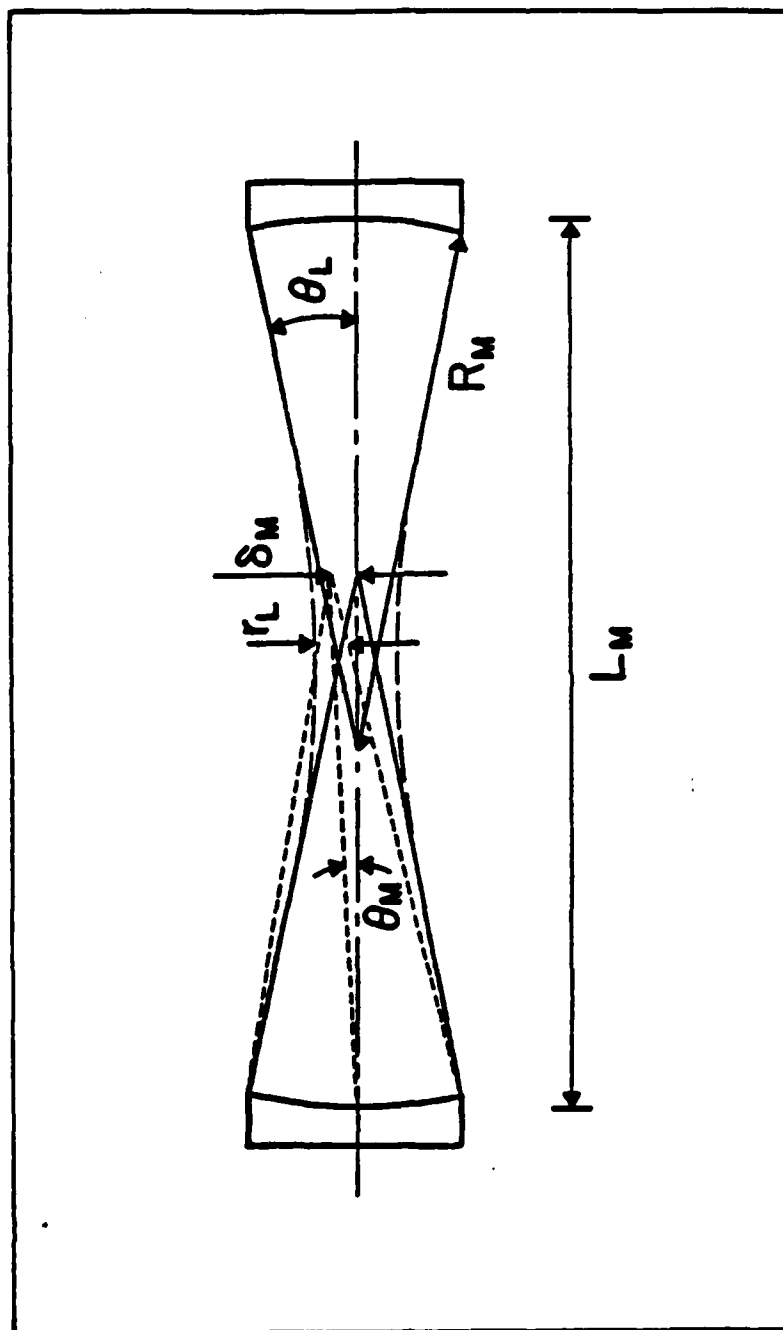


Figure 5. Misalignments in the Optical Cavity (10:20)

the mirrors caused by mirror misalignment is found to be

$$\epsilon_m = \frac{L_m^2 \lambda_L}{4\pi r_L^3} \theta_m \quad (34)$$

which must also be much less than one (10:11). Imposing this final cavity restriction on the extraction efficiency of the device, leads to the following (10:11)

$$\eta_x = \frac{I_m L_m^2}{P_L} \frac{I_B}{I_0} \left( \frac{\lambda_L}{\lambda_P} \right)^{3/2} F_\kappa(g, x) \eta_c^2 \sin^2 \psi_r \quad (35)$$

where the function  $F_\kappa$  is defined by the expression

$$F_\kappa(g, x) = \kappa^{5/4} \left( \frac{2}{x} \right)^{3/2} \frac{g^2 - 1}{g^2} \frac{x^2 \exp(-g/x)}{[\kappa + x^2 \exp(-g/x)]^{3/2}} \quad (36)$$

and where

$$\kappa = \left( \frac{\lambda_P}{4\pi n} \right)^2 \left( \frac{4\pi \epsilon_m}{L_m^2 \lambda_L \epsilon_m} \right)^{2/3} \quad (37)$$

and

$$= \kappa^{1/2} \left( \frac{\lambda_w}{\lambda_P} \right) \quad (38)$$

In terms of the variables just defined, the dimensionless wiggler vector potential is given by the formula

$$A_w = \kappa^{-1/2} x \exp(-g/2x) \quad (39)$$

and the resonant electron energy at the entrance of the wiggler by the expression

$$\gamma_{r1} = \left( \frac{x}{\kappa^{\frac{1}{2}}} \frac{1 + A_w^2}{2} \frac{\lambda_p}{\lambda_L} \right)^{\frac{1}{2}} \quad (40)$$

### Energy Recovery

Another method to enhance the overall efficiency of the free electron laser is to recover the energy of the electrons once they have exited the wiggler. This energy can be converted to radio frequency (rf) power which, in turn, can be used to accelerate the electrons in the beam prior to their entry into the wiggler (13:1). In general, maximizing the extraction efficiency of the wiggler does not maximize the overall efficiency of the system when energy recovery techniques are used (13:1). Therefore, we will consider this last feature of the device in order to develop a wavelength dependent relationship for the overall system efficiency.

When energy recovery is used, the total power required by the electron beam accelerator to sustain operation of the device is given by

$$\bar{P}_R = \bar{P}_A + \bar{P}_I + \bar{P}_M + \eta_D \bar{P}_B \quad (41)$$

where  $\bar{P}_A$  is the power lost in the accelerator device,  $\bar{P}_I$  represents the power lost in the injector,  $\eta_D \bar{P}_B$  is the power lost in the wiggler to the laser field, and  $\bar{P}_M$  is the power lost during energy recovery (13:1). This last quantity rep-

resents the fact that electrons can not be decelerated below some minimum energy,  $\gamma_B$ , before control of the beam is lost to self-repulsive effects. Brau's formulation (13:2) assumes the power lost in the injector is proportional to the power of the beam in the wiggler; therefore, the following simplification is used.

$$\bar{P}_M + \bar{P}_I = \frac{\gamma_B}{\gamma_{r1}} \bar{P}_B \quad (42)$$

Thus, the efficiency,  $\eta_r$ , for converting rf power to laser power is given by the following formula (13:3).

$$\frac{1}{\eta_r} = \frac{\bar{P}_R}{\bar{P}_L} = \frac{\bar{P}_A}{\bar{P}_L} + \left( \frac{\gamma_B^{-1}}{\gamma_{r1}^{-1} - 1} \right) \frac{1}{\eta_x} + \frac{1}{\eta_c} \quad (43)$$

From the earlier expression for the extraction efficiency, equation (35), the overall system efficiency becomes (13:3)

$$\frac{1}{\eta_r} = \frac{\bar{P}_A}{\bar{P}_L} + \frac{\delta}{\eta_c^2 \sin^2 \psi_r} + \frac{1}{\eta_c} \quad (44)$$

where the variable  $\delta$  equals

$$\delta = \left( \frac{\gamma_B^{-1}}{\gamma_{r1}^{-1} - 1} \right) \frac{\bar{P}_L I_0}{I_m L_m^2 I_B} \left( \frac{\lambda_P}{\lambda_L} \right)^{3/2} \frac{1}{F_K(g, x)} \quad (45)$$

### Efficiency Scaling

In the design of a free electron laser, equation (44) would presumably be optimized over all variables subject to the laser power,  $\bar{P}_L$ , being fixed. The only way to approach

such a complex optimization problem is through an iterative procedure on a computer. Fortunately for this study, this procedure has already been accomplished.

Brau has assumed that all parameters except the resonant phase,  $\psi_r$ , can be satisfactorily optimized by first maximizing the extraction efficiency of the device (13:5). Having done this, equation (44) can then be optimized as a function of the resonant phase,  $\psi_r$ . The process proceeds as follows. The parameter  $\kappa$ , described by equation (37), is used as input to the first optimization, from which, the maximum value of  $F_\kappa$  is determined over the variables  $g$  and  $x$ . Figure 6 illustrates this procedure, where for a fixed  $\kappa$ , different values of  $g$  and  $x$  are iteratively combined to find the maximum value of  $F_\kappa$ . Once accomplished, the optimum value of  $F_\kappa$  is used to compute  $\delta$ . With  $\delta$  so fixed, the maximum value of system efficiency,  $\eta_r$ , is found through numerical iteration of  $\psi_r$ .

The results of Brau's optimizations are depicted in the next four figures. The optimum values of  $g$  and  $x$  are found in Figure 7 for values of  $\kappa$  and the corresponding maximum values for the function  $F_\kappa$  are depicted in Figure 8. Figures 9 and 10, respectively, show the optimum value for the resonant phase,  $\psi_r$ , and a scaled value of optimum system efficiency for the fixed parameter  $\delta$ . Of interest, the dashed lines in these last two figures represent the optimum values had just the extraction efficiency of the device been maximized.

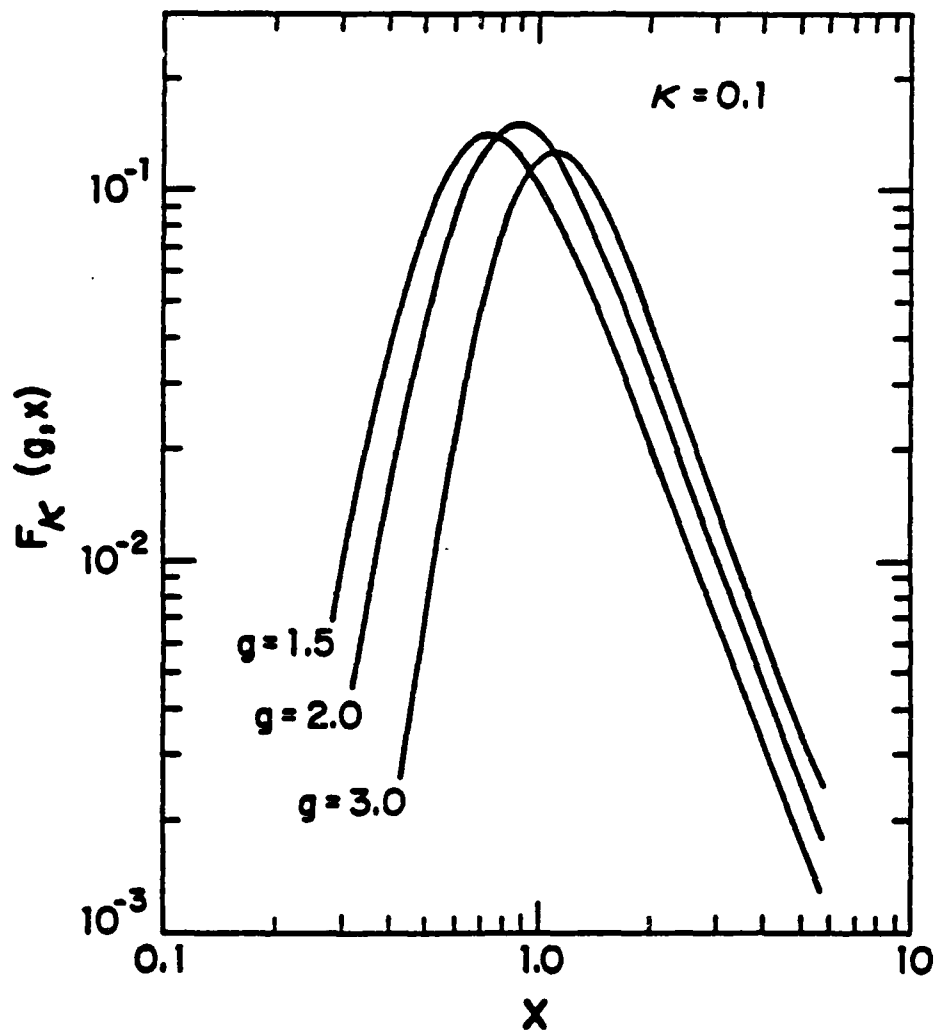


Figure 6. Maximization of  $F_K$  over  
Variables  $g$  and  $x$  (10:13)

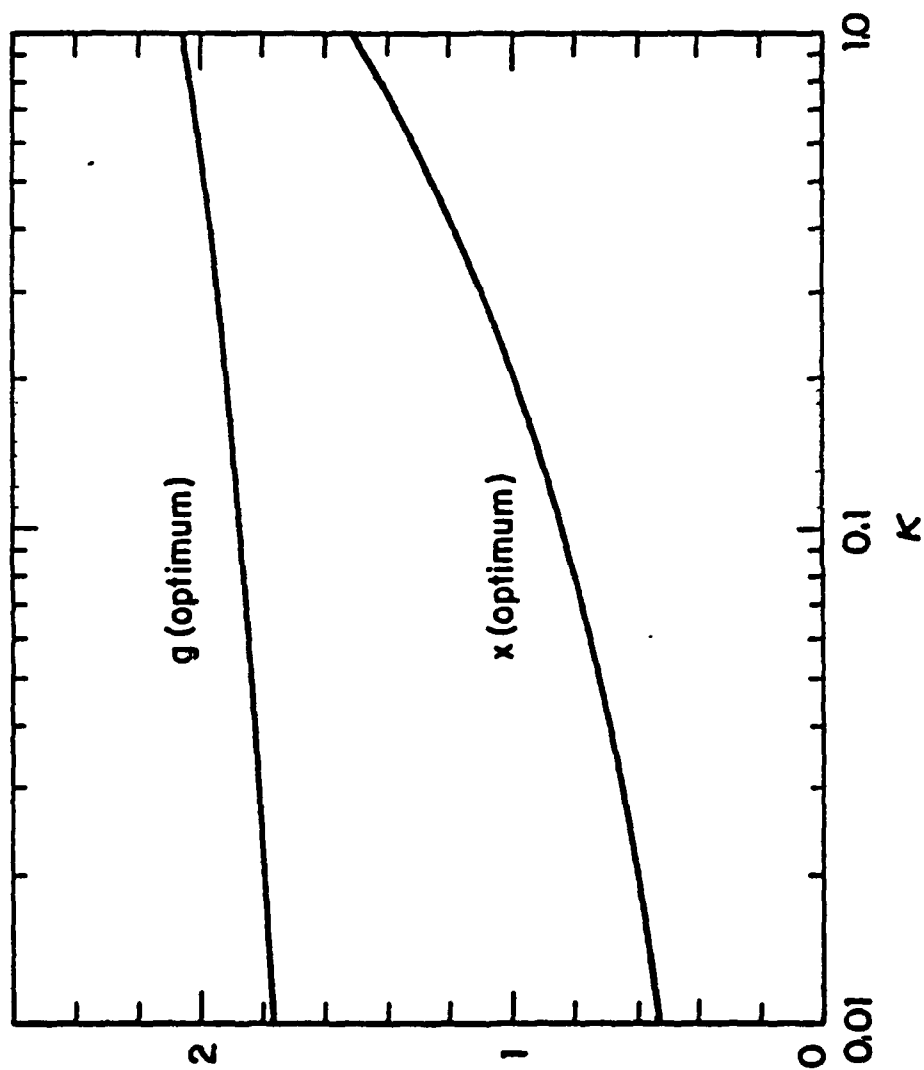


Figure 7. Optimum Values of  $g$  and  $x$  (10:15)

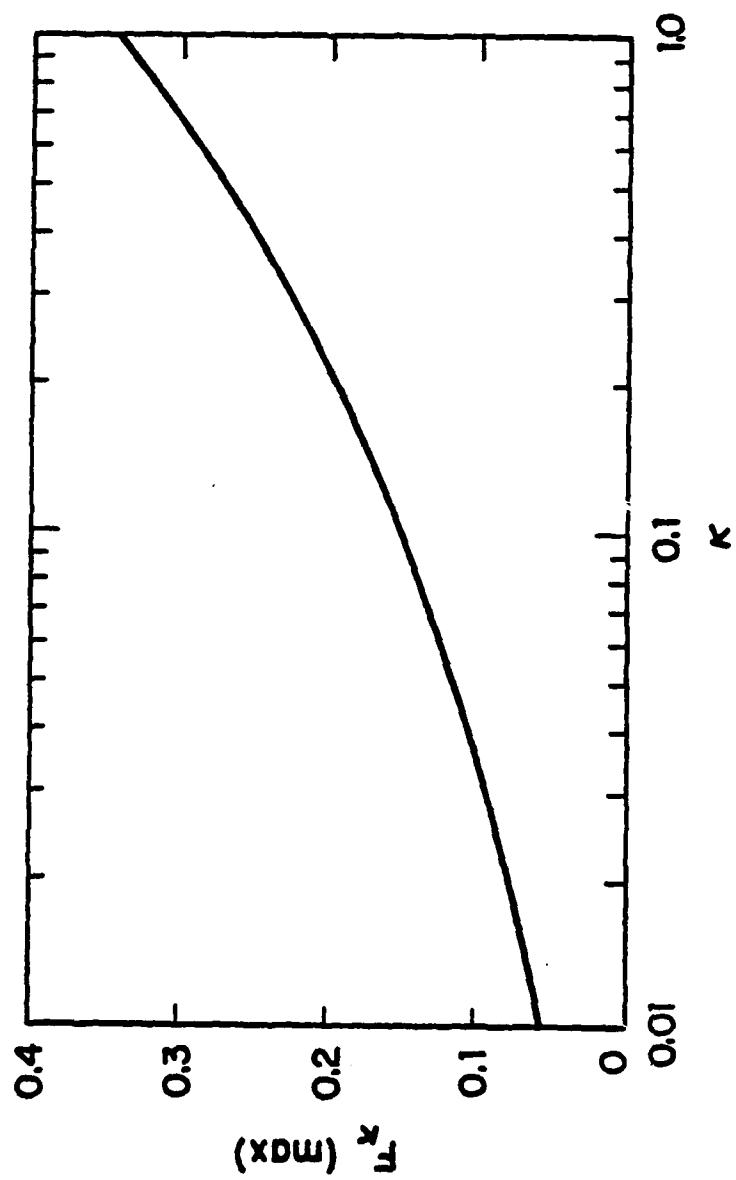


Figure 8. Optimum Values of  $F_{\kappa}$  (10:14)

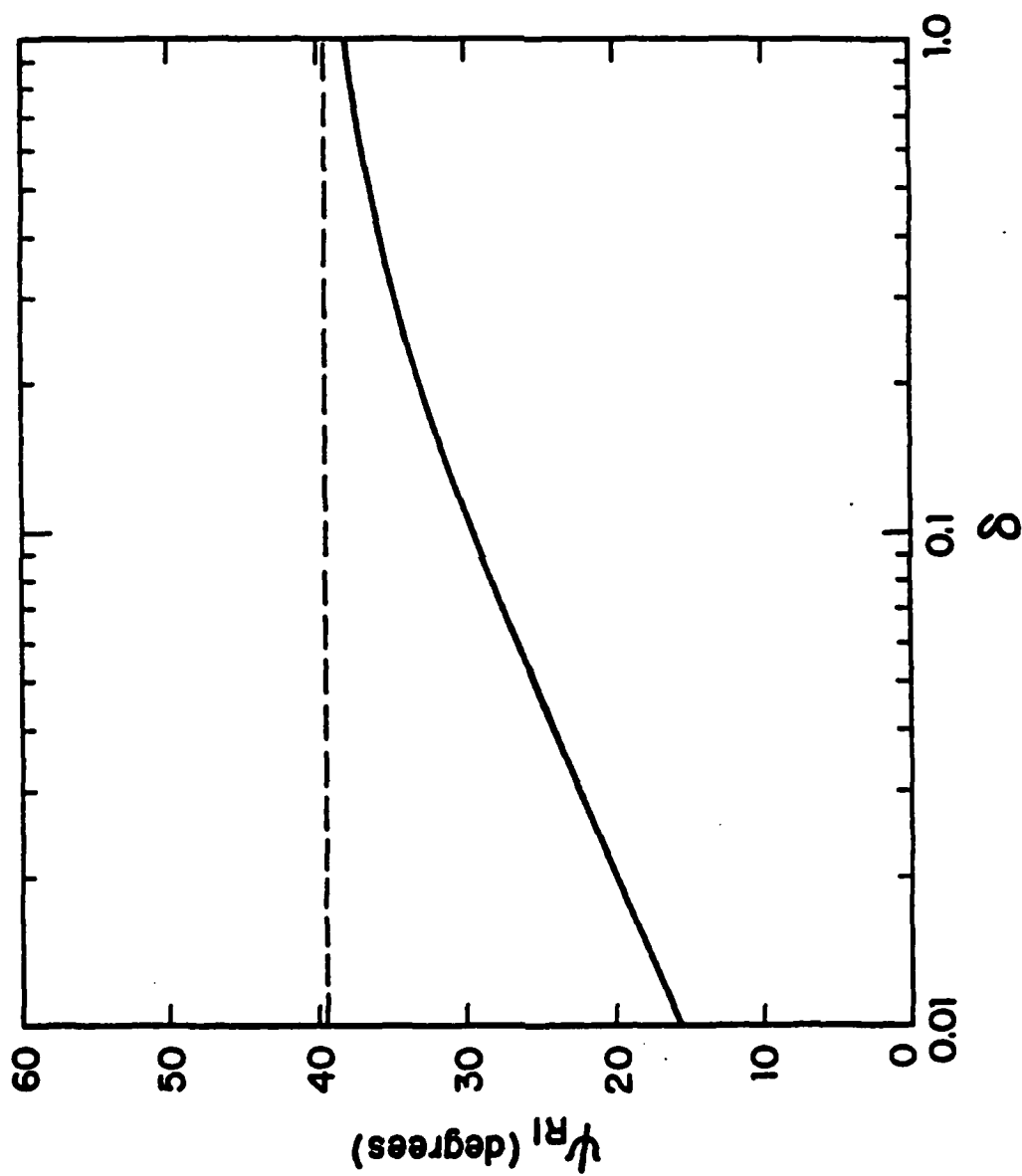


Figure 9. Optimum Values of Resonant Phase (13:8)

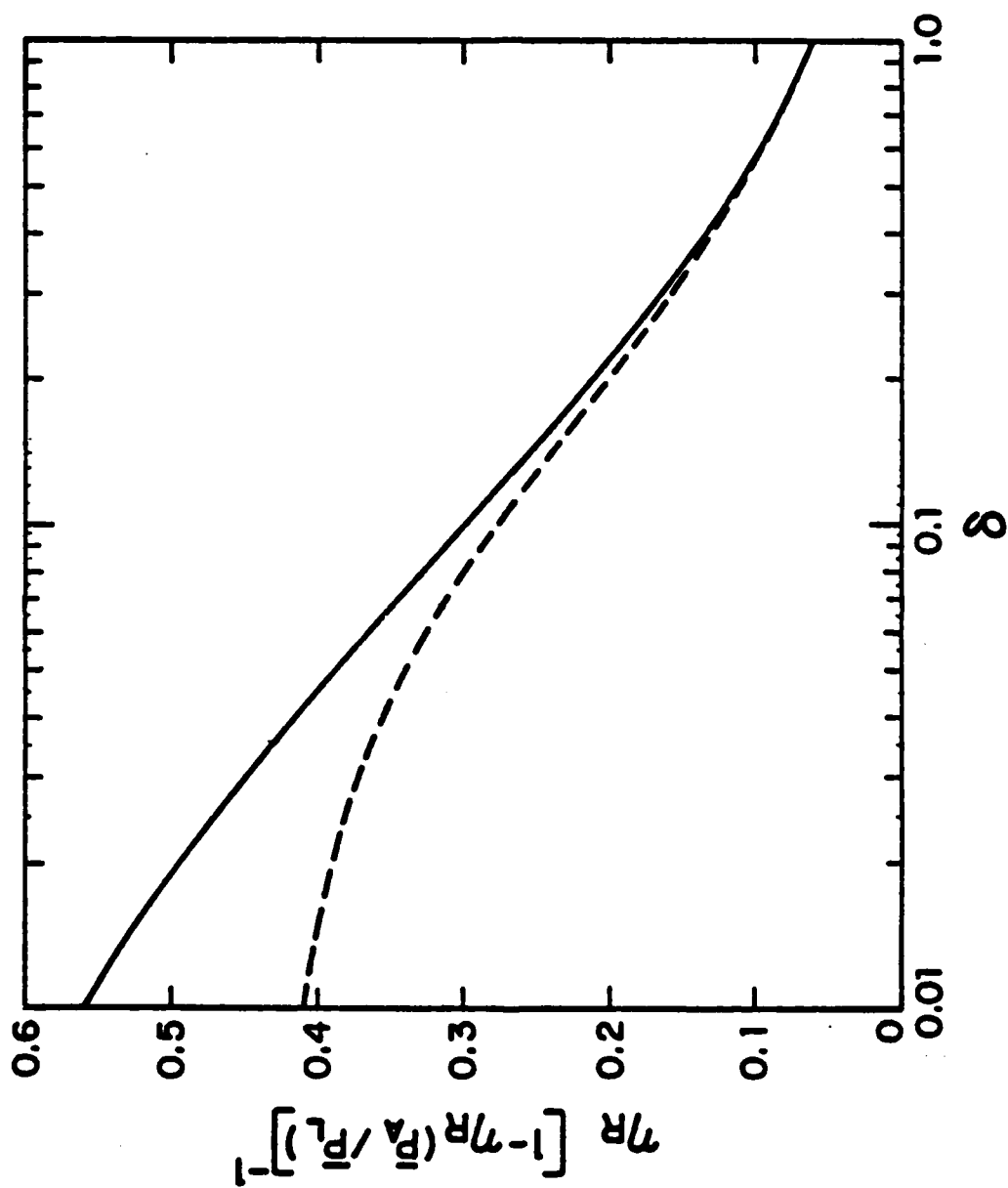


Figure 10. Optimum Values of Scaled FEL Efficiency (13:7)

There exists no optimum wavelength in the free electron laser; however, the choice of laser wavelength will indeed affect the optimum value of system efficiency. Figure 11 depicts this relationship between wavenumber and the optimum system efficiency. The approach taken in this study will begin by assuming that, given a desired wavelength for the free electron laser output, all other parameters will be chosen to maximize the system efficiency with energy recovery,  $\eta_r$ . Nominal values for certain engineering parameters for a high power free electron laser device (i.e. permanent magnet sizes, distance between cavity mirrors, cavity alignment tolerances, etc.) were provided by the FEL project office at Los Alamos (14:1-17). With these nominal values, an optimum system efficiency is determined for a given wavelength. We are assuming these nominal values would not change significantly over the range of wavelengths under study.

Instead of accomplishing a full optimization of the system efficiency on the computer for each wavelength, optimum values will be determined through the curves found in Figures 7 thru 10. The data from these curves were extracted and inserted into a least-squares polynomial curve fit routine to determine the relationship between variables. The optimum values of  $g$  and  $x$  can thus be found for a given  $\kappa$  by the following expressions.

$$g = (-3.6495 \kappa^2) + (1.4410 \kappa) + 1.76241 \quad (46)$$

$$x = (-8.8528 \kappa^2) + (4.0284 \kappa) + .52725 \quad (47)$$

from which the optimum values for  $F_{\kappa}$ ,  $A_w$ ,  $\gamma_{r1}$ , and thus,  $\delta$ , are determined. Then the value of  $\delta$  is used to find the scaled system efficiency by

$$\text{Scaled Efficiency} = (11.9642 \delta^2) + (-3.7919\delta) + .55284 \quad (48)$$

The scaled efficiency is then converted to an actual efficiency by the relationship

$$\eta_r = \left( \frac{1}{\text{Scaled Efficiency}} + \frac{\bar{P}_A}{\bar{P}_L} \right)^{-1} \quad (49)$$

This curve fit approach was validated against typical efficiency results provided by the FEL Project Office which were obtained by the full computer optimization (14:9). It was found that, near the center of the curve in Figure 11, the results from the two approaches agreed within 2%. At either end of the curve, however, the differences grew to approximately 4%. It is felt that this error is quite acceptable and well within the assumed errors within the rest of the model.

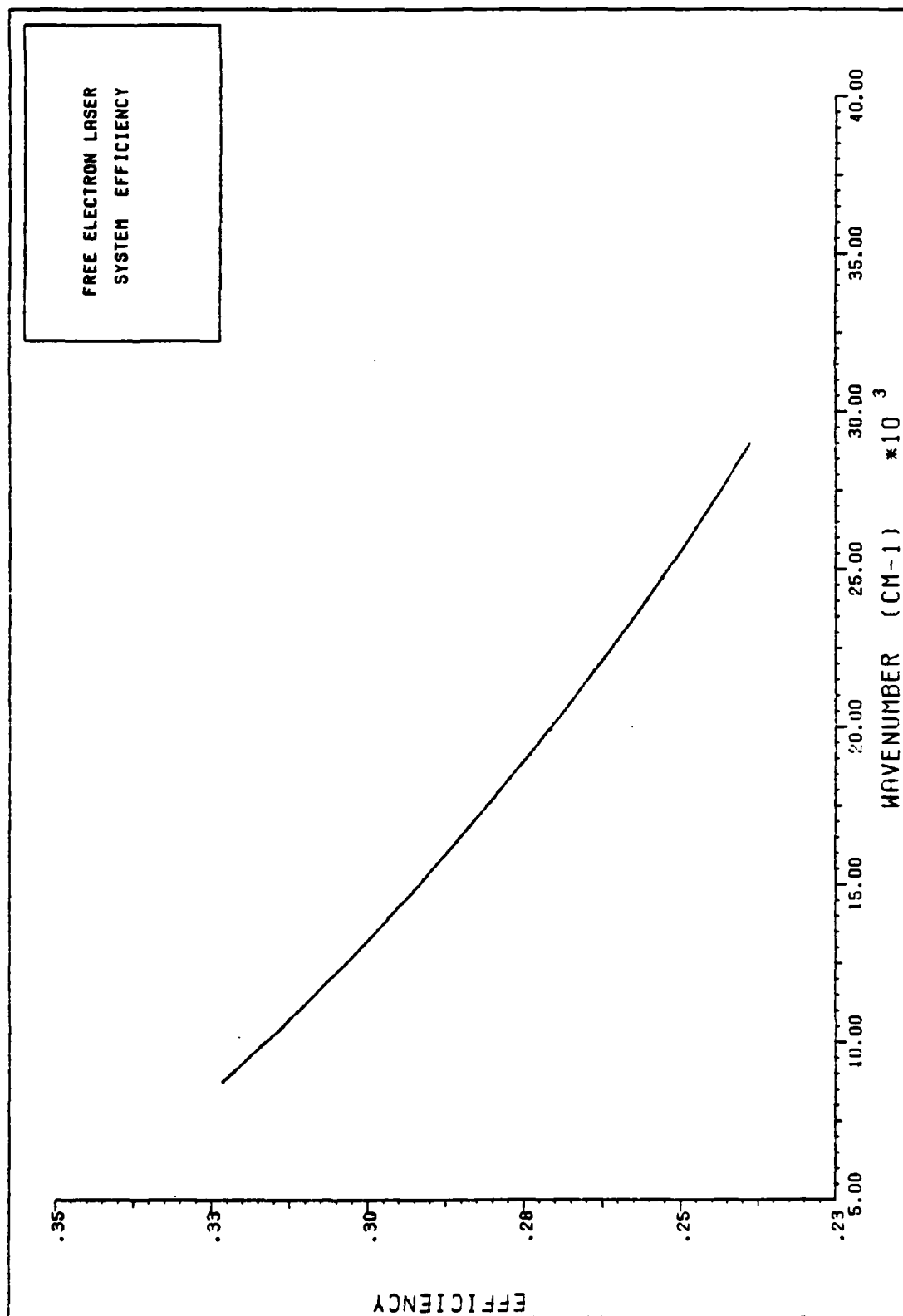


Figure 11. FEL Efficiency vs Wavenumber with Energy Recovery

### III. Development of the Propagation Model

The vast majority of the overall system efficiency in a ground based laser weapon lies in the ability to propagate the laser energy through the atmosphere to the target. Further, most of the important effects are strongly wavelength dependent. One must consider linear effects such as the absorption and scattering due to the molecular and aerosol constituents in the atmosphere, and the spreading of the beam due to atmospheric turbulence, diffraction, and platform jitter. For most power levels of interest, the nonlinear thermal blooming effects caused by the self-induced heating of the atmosphere along the path of the laser beam must also be considered.

Many computer codes have been developed to model these propagation effects with widely varying degrees of complexity. Camphausen developed a simplified high energy laser propagation code, HELIM, which is suitable for use on a hand held calculator (15). Lilly's propagation code (16) and the program GUTS (Ground Up To Space) used by the Air Force Weapons Laboratory (17) both rely on Fourier optics for their calculations. Lying somewhere between in complexity is the code developed by Peckham and Davis (18). Their code

has the advantage that it employs relatively simple algebraic expressions and is better suited for the system analyst. The propagation model we will develop for this study will be similar in form and sophistication to Peckham and Davis's code.

### Overview

For this study, we will assume a laser beam profile that approximates an infinite Gaussian distribution. This irradiance profile is given by

$$I = I_0 \exp(-2r^2/a_0^2) \quad (50)$$

where  $I_0$  = the peak irradiance at beam center  
 $r$  = the lateral distance from beam center  
 and  $a_0$  = the  $1/e^2$  radius of the beam, within which 86.5% of the beam energy is found

Therefore, at the exit aperture of the laser, the average irradiance across the beam equals

$$I_{AV} = \frac{\text{Power}}{\text{Area}} = \frac{.865 P_t}{\pi a_0^2} \quad (51)$$

where  $P_t$  is the total average power contained in the beam. After propagating a distance  $z$  from the device, the

average irradiance is given by

$$I_{AV}(z) = \frac{.865 P_t e^{-\alpha z} I_{rel}}{\pi a^2} \quad (52)$$

where  $\alpha$  = the attenuation coefficient of the atmosphere  
 $I_{rel}$  = the power reduction factor due to thermal blooming  
 and  $a$  = the average spot size of the laser beam at a distance  $z$

The average spot size can be approximated by combining in a root-mean-squared technique the calculated spot sizes resulting from the effects of diffraction, turbulence and platform jitter (19:1480).

$$a^2 = a_D^2 + a_t^2 + a_j^2 \quad (53)$$

To define a propagation efficiency for a given wavelength, we will calculate the average irradiance incident on the target and divide by the average irradiance produced at the laser device.

$$\eta_{prop} = \frac{I_{AV}(z)}{I_{AV}(z=0)} \quad (54)$$

The above constitutes an overview of the basic approach we will take in developing the propagation model. Each of the

wavelength dependent factors that affect laser beam propagation will be discussed in greater detail in the following sections.

### Laser Beam Propagation in a Vacuum

Even without the presence of an intervening, attenuating medium, a laser beam will spread simply by diffraction due to the wave nature of light. This effect can be reduced, with restrictions, through optical focusing of the output laser beam. For an assumed infinite Gaussian beam profile, the spot size of the beam at a distance  $z$  from the laser can be found through wave diffraction theory. Yariv gives the following results for such a calculation (20:33).

$$a_D^2(z) = a_0^2 \left[ 1 + \left( \frac{\lambda z}{\pi a_0^2} \right)^2 \right] \quad (55)$$

where  $a_0$  equals the radius of the output optics of the laser device and  $\lambda$  is the propagating wavelength. For an unfocused beam, the minimum beam radius or beam waist is found at the output optics. For a focused beam, however, the beam waist occurs at a point between the laser and the focal length of the output optics. The spot size at the waist for a focused

beam is also given by Yariv as

$$a_w = a_o \frac{(f \lambda / \pi a_o^2)}{\left[1 + (f \lambda / \pi a_o^2)\right]^{1/2}} \quad (56)$$

where  $f$  equals the focal length of the output optics (20:38). Also, the focal range,  $z_w$ , the distance from the laser to the beam waist, is related to the focal length by the following expression (20:38).

$$z_w = f \left[ 1 - \frac{1}{1 + (\pi a_o^2 / f \lambda)^2} \right] \quad (57)$$

A curious result of the above equations should be noted. If the focal length is equal to the Rayleigh range,  $z_L$ , defined as

$$z_L = \frac{\pi a_o^2}{\lambda} \quad (58)$$

the spot size at the beam waist is minimized and would be equal to

$$a_w = \frac{a_o}{\sqrt{2}} \quad (59)$$

In addition, the focal range is maximized. In this case, the beam waist is located exactly halfway between the laser and the focal length. If one attempts to focus at a range beyond the Rayleigh range, the spot size at the beam waist increases and the location of the beam waist draws nearer the source. In this case, the spot size at the target is greater than if no focusing were employed.

The effects of focusing and diffraction beam spread have been combined into one equation by Gebhardt (19:1480), Camp-hausen (15:13) and others. The  $1/e^2$  radius of a Gaussian laser beam at a distance  $z$  from the source is given by

$$a_D^2(z) = a_0^2 \left[ \left( 1 - \frac{z}{z_w} \right)^2 + \left( \frac{\beta \lambda z}{\pi a_0^2} \right)^2 \right] \quad (60)$$

The term,  $\beta$ , in equation (60) is known as the beam quality factor. Beam quality is used to incorporate imperfections in the phase uniformity of the beam at the exit of the laser device. The term is usually defined as 'times diffraction limited' at some empirically derived quantity greater than one.

## Laser Beam Attenuation

Transmission of a light source through an attenuating medium is defined by Beer's Law (21:19). From the reference point of  $z=0$  to a point  $z$  along the propagation path, the fraction of power remaining in the beam is given by

$$\frac{I(z)}{I(z=0)} = \exp(-\alpha z) \quad (61)$$

The attenuation term,  $\alpha$ , represents a combination of many different loss processes. Included in this term are the absorption and the scattering losses from both molecular and aerosol constituents in the atmosphere. Each loss mechanism can be represented by its own attenuation coefficient. Addition of each term yields the total attenuation coefficient for the atmosphere.

$$\alpha_{\text{Total}} = \alpha_{\text{molecular absorption}} + \alpha_{\text{aerosol absorption}} + \alpha_{\text{aerosol scattering}} + \alpha_{\text{molecular scattering}} \quad (62)$$

where for each individual process

$$\alpha(\lambda, z) = n(z) \sigma(\lambda) \quad (63)$$

Each  $\alpha$  is dependent upon,  $n$ , the number density of

absorbers or scatterers the beam encounters along the propagation path which, of course, is a function of altitude in the atmosphere (21:41). The wavelength dependence of each process is contained in the  $\sigma$  term which measures the cross-sectional probability of an interaction occurring (21:41). Each of the major attenuation processes represented in equation (62) will be briefly discussed.

Molecular absorption. Molecular absorption is the direct result of the discrete quantum energy states of the molecules in the atmosphere. When a photon 'collides' with an air molecule, and the energy of the photon equals the energy necessary to excite the molecule from a lower energy state to a higher energy state, the photon will be absorbed by the molecule. Naturally, since radiative energy is a function of photon wavelength ( $E=h\lambda/c$ ), the spectral absorption curve is also a function of wavelength. In addition, each discrete absorption wavelength or 'line' is widened by collisional and Doppler broadening processes (21:43).

At wavelengths longer than .75 micrometers, atmospheric attenuation is most strongly influenced by the contribution of molecular absorption. The structure of the spectral transmission curve in this region exhibits enormous complexity and irregularity, reflecting the discrete energy levels of the molecular absorbers. Figure 12 is a low resolution plot of

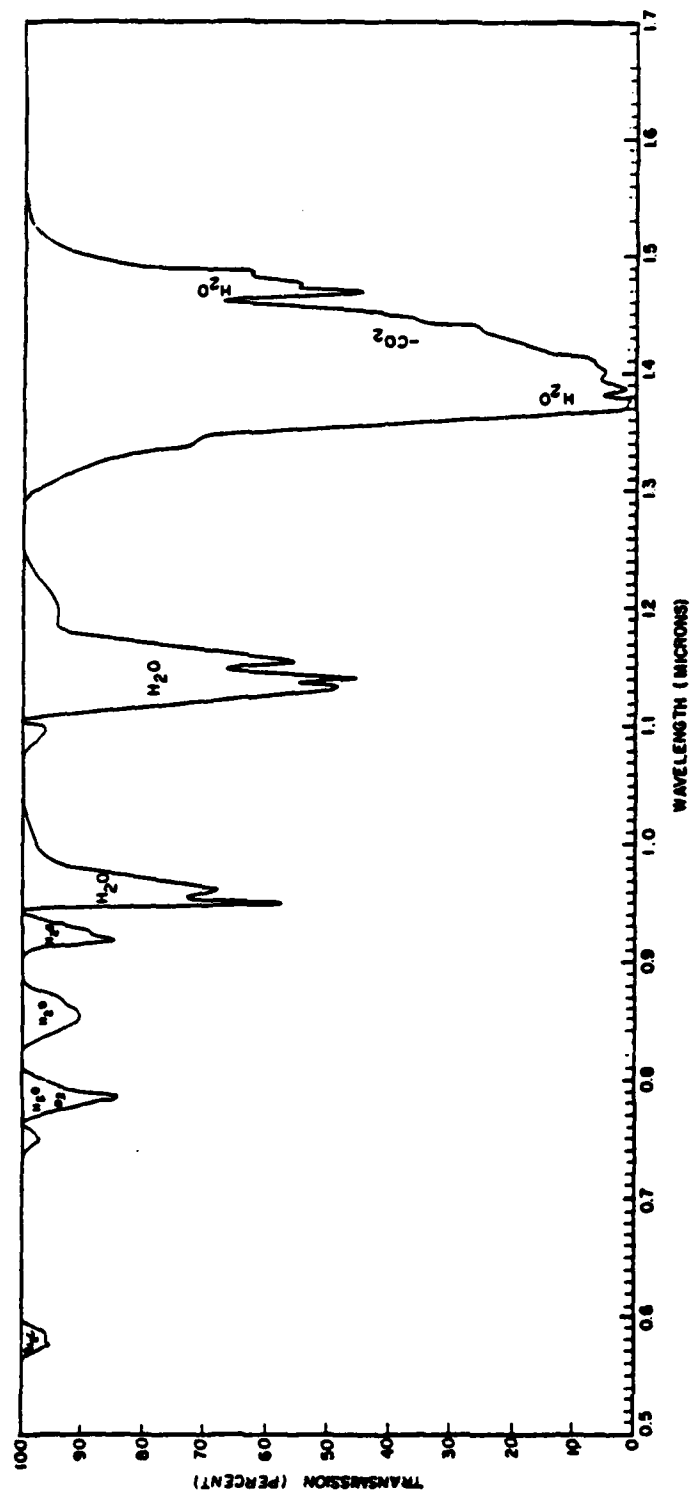


Figure 12. Atmospheric Transmission ( 0.5 to 1.7 microns) (22:53)

atmospheric transmission for the short wavelength infra-red and visible regions of the spectrum and illustrates this complexity. For the region of interest in this study, the major atmospheric absorbers are water, carbon dioxide, oxygen, and ozone (22:146).

Aerosols. As shorter wavelengths are approached in the visible spectrum, the contribution of aerosol attenuation begins to dominate the spectral transmission curve (21:56). This is in spite of the fact that aerosol number densities are generally many orders of magnitude less than atmospheric molecules. The theory of aerosol absorption and scattering, based on the work of Gustav Mie, treats atmospheric aerosols as small dielectric spheres (21:57). The interaction of a light ray with an aerosol can cause the light ray to be reflected or refracted out of the propagation path or to be internally reflected and absorbed by the aerosol. The absorbing and scattering properties of aerosol particles is, therefore, a function of the particle radius, the wavelength of the propagation radiation, and the difference in the refractive indices of the aerosol and the surrounding air. Although, Mie theory is well understood, major difficulties arise in application due to the extreme altitude and geographical variations in the sizes, shapes, and dielectric constants of the atmospheric aerosols. Generally, however, aerosol attenuation

is a slowly varying function of wavelength. As Figure 13 illustrates, shorter wavelengths are somewhat more strongly attenuated than longer wavelengths. Mie theory is applicable when the size of the aerosol is comparable to the wavelength of the propagating radiation. When the radius of the aerosol becomes much larger than the laser wavelength (as in heavy clouds, fog, and rain) attenuation increases dramatically and becomes wavelength independent (21:63). Therefore, this type of propagation effect will not be considered in this study. Conversely, when the laser wavelength is much larger than the scattering particle (such as individual molecules), attenuation becomes a strong function of wavelength (21:64). This process is called molecular or Rayleigh scattering.

Rayleigh Scattering. Rayleigh scattering results from the interaction of the oscillating electromagnetic field of the laser beam and the individual electrons of an atmospheric molecule. By assuming the laser wavelength is much greater than the physical dimensions of the molecule, spatial variations of the electromagnetic field over the molecule can be ignored. The propagating laser field induces oscillations in the bound molecular electrons which, in turn, radiate energy at the same laser frequency. However, not all of this energy is radiated in the direction of propagation, and thus, power is lost from the laser beam. Using this approach results in

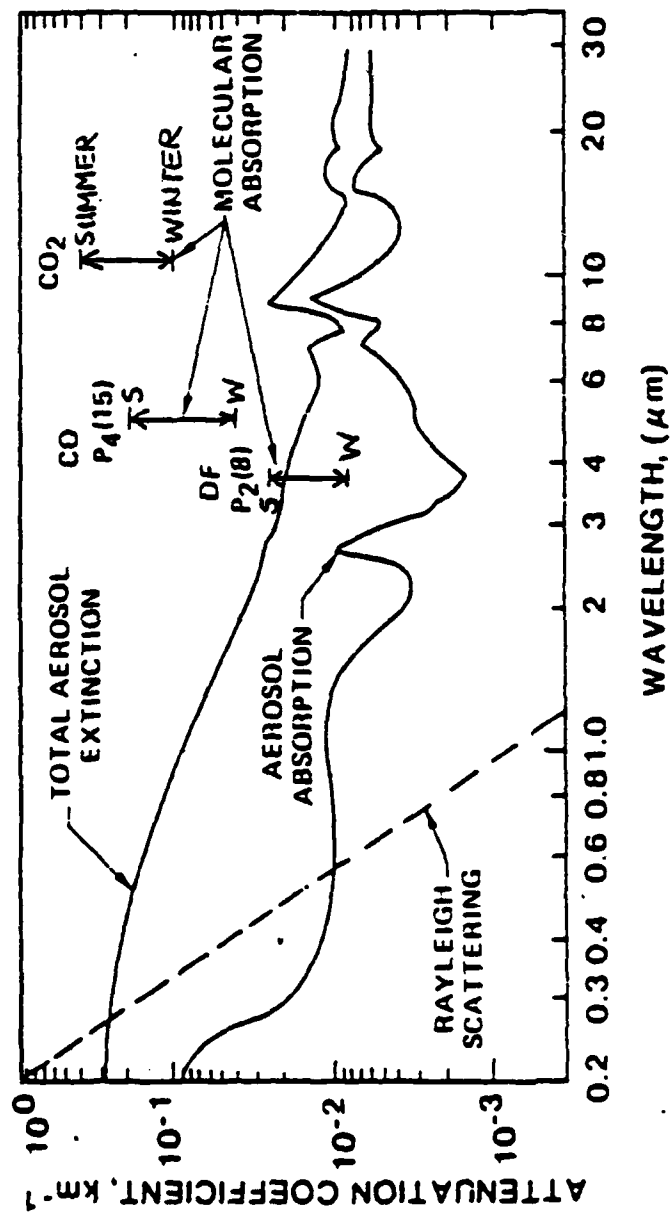


Figure 13. Attenuation Coefficients for Atmospheric Aerosols and Rayleigh Scattering (23:146)

a cross-sectional probability for Rayleigh scattering which is proportional to  $\lambda^{-4}$  (21:67). This strong wavelength dependence can be seen in Figure 13. At wavelengths above 1.0 microns, Rayleigh scattering is only a minor contributor to laser beam attenuation; however, in the short wavelength portion of the visible spectrum, it can be seen that Rayleigh scattering is comparable in magnitude to total aerosol attenuation.

Atmospheric Transmission Codes. To tackle the complexity of atmospheric attenuation, several computer codes have been developed. Two such codes, developed by the Air Force Geophysics Laboratory, which were available for this research were the Fast Atmospheric Signature Code (FASCODE) (24) and the Low Resolution Atmospheric Transmission Code (LOWTRAN) (25).

Both codes employ the concept of a 'layered' atmosphere such that within a given layer, atmospheric properties are assumed constant. The altitude, pressure, temperature, water vapor density, and ozone density for the 1962 U.S. Standard atmosphere and five seasonal model atmospheres are provided as basic input data to both LOWTRAN and FASCODE. The five supplemental models offer the user a selection of varying atmospheric conditions. They include models which represent: 1) Tropical (15 N Latitude), 2) Midlatitude Summer (45 N, July), 3) Midlatitude Winter (45 N, January), 4) Subartic

Summer (60 N, July), and 5) Subarctic Winter (60 N, January). There are, however, major differences between these two codes.

LOWTRAN is designed to provide low to moderate spectral resolution results to the user. It computes atmospheric transmission in increments of five wavenumbers and the data for each wavenumber has been averaged over twenty wavenumbers (25:3). It does consider in its calculations all loss mechanisms which comprise the attenuation coefficient of equation (62). FASCODE, on the other hand, offers the highest possible resolution by adding the contributions from individual molecular absorption lines to compute transmission at a given wavenumber; however, for the region of interest in this study, it does not include aerosol loss mechanisms, ozone absorption, or Rayleigh scattering (24:14). Therefore, neither code provides the moderate to high resolution data and includes every attenuation process which is needed for this analysis. In order to achieve these study objectives, it will be necessary to use both codes: FASCODE for the complex molecular absorption determination and LOWTRAN for the more slowly varying functions of aerosol absorption and scattering, and Rayleigh scattering. The data generated by each code will then be used in the model developed for this study. Each code will now be discussed in greater detail.

LOWTRAN. In the visible region of the spectrum, aerosol absorption and scattering become very important contributors

to the overall attenuation of the laser beam. LOWTRAN employs an aerosol model which is divided into four regions, each containing a different type and distribution of aerosols (25:21). In the boundary layer region from sea level to 2 km, the size and composition of the aerosols are assumed to be invariant with altitude, changing only as a function of relative humidity and the user selected environmental conditions (25:21). In LOWTRAN, the user may chose from Rural, Urban, and Maritime boundary layer aerosol models, and further specify in kilometers the meteorological range or visibility at the surface. The number density of aerosols in this lowest region is assumed to vary exponentially with altitude but only under high visibility conditions. Under low visibilities, aerosol concentrations become independent of altitude up until the altitude of the first temperature inversion (approximately 1 km) and decrease dramatically above. Above this boundary layer in the upper tropospheric region (2 to 10 km), the size and distribution of aerosols become less sensitive to surface conditions and seasonal influences dominate (25:22). In summer months, tropospheric aerosol concentrations are somewhat higher. In LOWTRAN's third aerosol region, the lower stratospheric (10 to 30 km), particle size and distribution is determined by the degree of recent volcanic activity, which at times, can increase aerosol concentrations by a factor of 100 over the normal background (25:34). This region is also

scaled by LOWTRAN to compensate for seasonal variations. Finally, at altitudes above 30 km, aerosols composed of meteoric and cometary dust form the major component of the normal upper stratospheric aerosol model in LOWTRAN (25:36). Figure 14 shows the vertical profiles of the aerosol constituents used in LOWTRAN.

The cross-sectional probabilities for aerosol absorption and scattering are computed in LOWTRAN based on two size distributions of aerosols, the so-called accumulation (small) and coarse (large) particles (25:25), the result being that the absorption and scattering (also referred to as extinction) coefficients are not smooth functions. This fact can be seen in Figure 15 which depicts the coefficients for the Rural aerosol model, normalized to 1.0 at .55 micrometers. These coefficients are also scaled in LOWTRAN to the local relative humidity. As the relative humidity increases, water vapor condenses out of the atmosphere onto the existing aerosol particles. This condensed water thus increases both the size and effective refractive index of the aerosol particles (25:26). This can be seen as well in Figure 15.

LOWTRAN's treatment of molecular scattering is fairly straightforward. The number density of scatterers is scaled to the local pressure and temperature of the atmosphere. The cross-sectional probabilities for each wavenumbers were

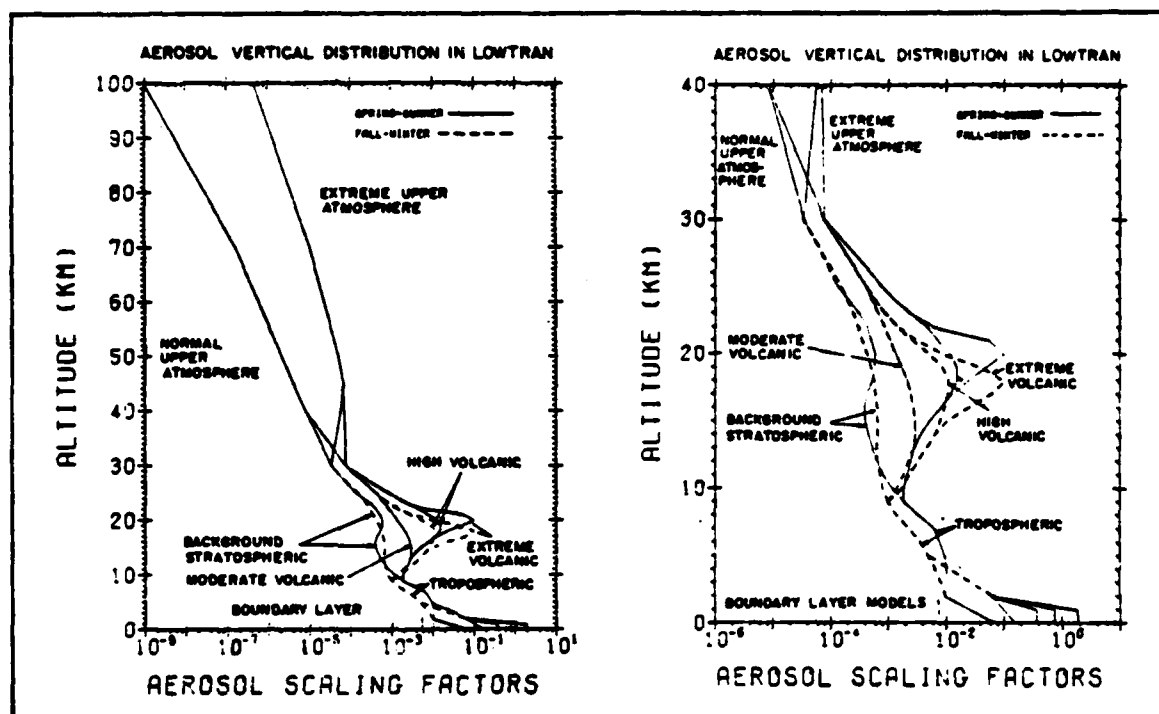


Figure 14. Aerosol Concentrations vs Altitude  
in LOWTRAN (25:24)

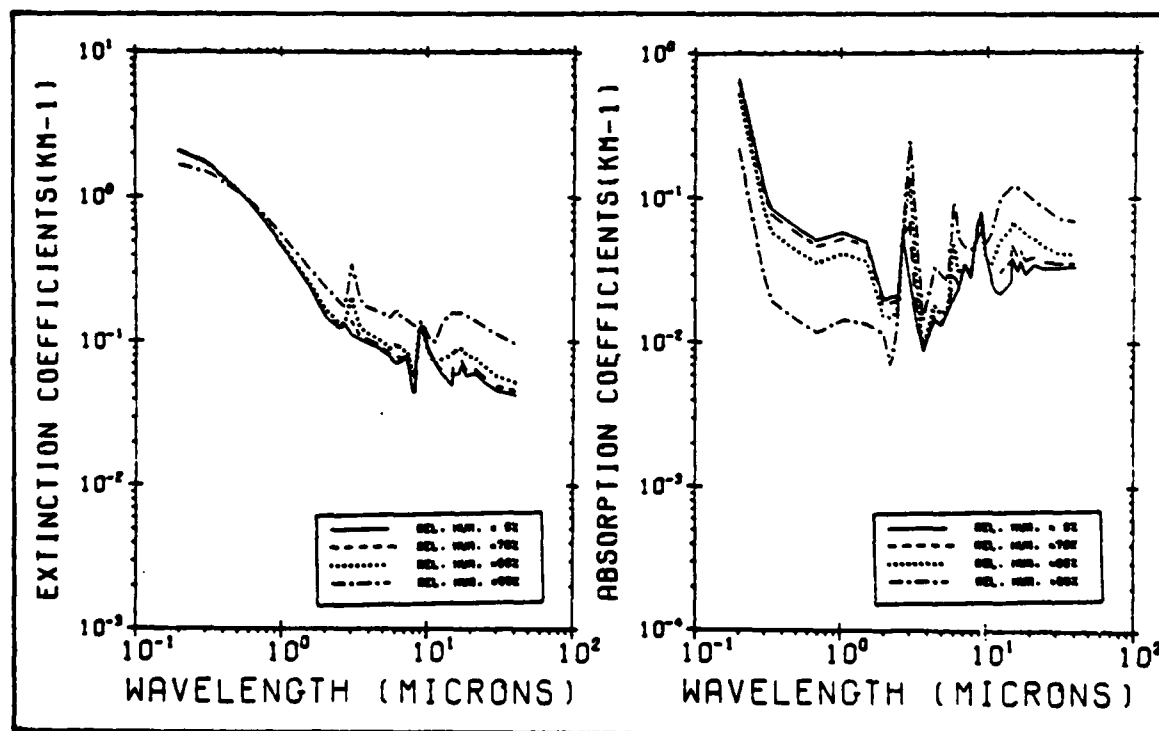


Figure 15. Attenuation Coefficients for Rural  
Aerosol Model in LOWTRAN (25:26)

obtained from least-square curve fits of molecular scattering data and closely follow the theoretical functions. The errors in this curve fit are less than .5% in the region of interest of this study (25:57).

LOWTRAN will also provide molecular absorption data for ozone in the visible and ultraviolet region of the spectrum since FASCODE data does not extend into this region. Figure 16 depicts the two spectral regions where ozone absorption is found. Of note is the fact that the ozone absorption in the ultraviolet region is much stronger than the weak ozone absorption in the mid-visible. Ozone does not vary exponentially with altitude (25:48). Instead, ozone concentrations peak at an altitude of approximately 18 km, the so-called ozone layer. Each of the six atmospheric models in LOWTRAN contains separate ozone profiles. For the ultraviolet and visible ozone molecular absorption lines, the cross-sectional probabilities were digitized from the spectral curves of McClatchey et al, in intervals of 500 wavenumbers and 200 wavenumbers respectively (25:48). Therefore, there is considerable interpolation required in LOWTRAN to achieve the advertised five wavenumber resolution.

Continuum absorption due to collision induced line broadening of water vapor and nitrogen is available in both FASCODE and LOWTRAN; however, the regions where continuum absorption is important are outside the region of interest

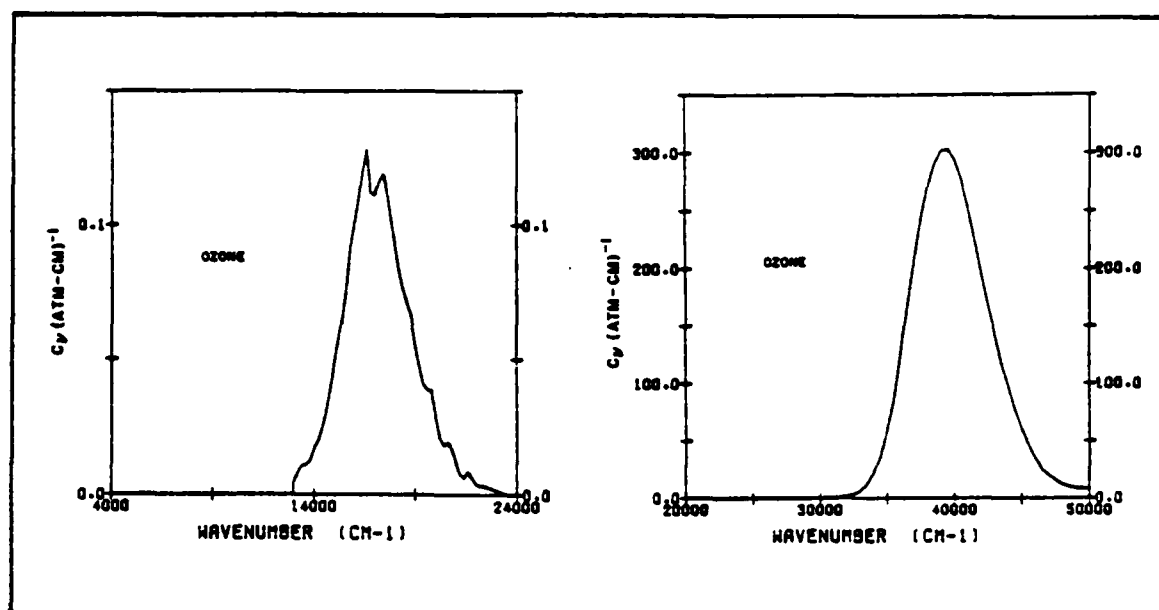


Figure 16. Ozone Attenuation in LOWTRAN (25:53)

in this analysis (25:61)

For LOWTRAN, each of the six atmospheric models is divided into 32 layers: in 1 km layers from sea level to 25 km, in 5 km layers from 25 km to 50 km with the final two layer boundary at 70 km and 100.

LOWTRAN provides only a value for total transmission along a selected path in the program output. In order to model non-linear effects in this study, it was necessary to have absorption and scattering information for points along the beam's path. Therefore, LOWTRAN was modified to extract this data at each of the 32 altitude layers and write the results to a data file for use later. The specifics of this program modification are included in Appendix A to this report.

FASCODE. As mentioned earlier, FASCODE computes molecular absorption by adding contributions from individual absorption lines. At lower altitudes, collision broadening mechanisms dominate the overall width of the molecular absorption lineshape. In the lower atmospheric pressures of higher altitudes, the weaker Doppler broadening mechanisms will begin to dominate. FASCODE convolves the collision broadened lineshape, approximated by a Lorentz function, with the Doppler broadened lineshape, approximated by a Gaussian function, into a Voigt lineshape (24:10). This convolution gives an effective description of the overall molecular absorption lineshape at any altitude. The accuracy of this approximation is nominally 0.5% with a maximum error of 3.0% occurring in the wings of the Voigt line profile (24:15). This maximum error is still generally less than the errors associated with the knowledge of both the lineshape and the broadening mechanism.

For program efficiency, FASCODE samples across a 'panel' or block of wavenumbers of interest in order to calculate atmospheric transmission. The sampling interval is determined by the average width of the molecular absorption lines within the block of wavenumbers (24:11). Since the average linewidth changes with altitude, the sampling interval is also a function of altitude. As the results of each altitude layer are merged with preceding layers, FASCODE employs a four-point Lagrangian interpolation to match the different sampling

intervals (24:12)

FASCODE allows the user to either specify layer boundaries or employs an auto-layering subroutine. Of course, for this study, boundary layers were chosen to coincide with the preset layer boundaries in LOWTRAN.

Like LOWTRAN, FASCODE had to be modified to extract absorption information for each of the 32 altitude layers. These modifications are described in Appendix B. In one respect, this was a simpler process since FASCODE computes absorption data one layer at a time. However, the fact that FASCODE's sampling interval varied for each layer required modifications to the basic program. It was necessary to fix the sampling interval for each layer to coincide with the desired resolution of the overall analysis. As in LOWTRAN, absorption data was written to a data file. In addition, the FASCODE data was reconfigured to be compatible with the data format of LOWTRAN and the main program used in this study. Since this proved to be a non-trivial matter, this additional program is presented in Appendix C.

#### Atmospheric Turbulence

Reduction of the average irradiance on the target will occur due to turbulence within the propagating medium. As a laser beam propagates through the atmosphere, it encounters numerous cells or eddies of air where the index of refraction

is slightly different from that of the neighboring cells. These small changes in the refractive index are primarily due to the small variations (.1 to 1.0 degrees Kelvin) in the temperature of these eddies of air (21:70). Irregular solar heating of the Earth's surface produces these temperature variations in the atmosphere. Naturally, when a laser beam encounters a cell with a non-uniform refractive index, its direction and phase are perturbed by a small amount. This process is entirely random, but by dealing with statistically averaged quantities, one can successfully approximate the effects of turbulence. While the refractive index variations are quite small, long propagation distances can produce cumulative effects which are very significant (21:70). A small angular deflection near the laser source can translate to miss distances of hundreds of meters for targets in geosynchronous orbits.

Atmospheric turbulence effects can be separated into two components: instantaneous small scale beam spread and beam wander (21:71). When the lateral diameter of the refractive index cells are small compared to the local diameter of the beam, turbulence causes small scale distortions in the size and shape of the laser beam spotsize. This short term beam spread component, therefore, describes the beam spotsize at any instant of time. Similarly, when the size of the turbulent cell is large compared to the beam diameter, the entire

beam follows a refracted path. This component of turbulence thus causes the beam centroid to wander about some central point in the target plane. Each component is typically represented by a statistically derived characteristic beam radius. A total beam radius for both turbulence effects is then found by a root-sum-squaring of the two radii (21:72).

Refractive Index Structure Parameter. The single most important factor in describing turbulence effects in the atmosphere is the refractive index structure parameter,  $C_n^2$  (26:20). It can be considered a measure of the strength of the refractive index fluctuations within the atmosphere. The derivation of this parameter is based on the work of Kolmogorov and Tatarskii (26:20) and is assumed valid over a range of eddy sizes--the so-called inertial subrange  $r$  where:

$$l_0 \ll r \ll L_0 \quad (64)$$

Here  $l_0$  and  $L_0$  are the inner and outer scales of turbulence (note: also referred to as the microscale and macroscale of turbulence in the literature). The turbulent eddies introduced into the atmosphere by the irregular convective currents from the Earth's surface and wind shear, are of a large scale. Gradually, the turbulent motion of these cells causes their breakup and the formation of smaller and smaller cells. The value  $l_0$  corresponds to the eddy size below which

dissipation of energy in the eddy through viscous effects becomes important, while  $L_0$  is the largest scale size for which the eddies may still be considered isotropic. Near ground level,  $l_0$  may be on the order of millimeters and  $L_0$  on the order of several meters (26:20).

As one might expect, the value of  $C_n^2$  decreases with increasing altitude as the effects of surface thermal convection and frictional wind shear become less noticeable. The surface of the Earth can have such a strong effect that the value of the structure parameter near the surface can easily change two orders of magnitude depending on the solar elevation angle, local wind conditions and cloud cover (26:21). Therefore, predictive models of the behavior of the structure parameter with altitude at best represent nominal values. In addition, models which are useful near the surface are of little applicability in the so-called free atmosphere.

Near the surface, the structure parameter decreases proportionally with altitude to the  $-2/3$  power during quiet periods in the atmosphere, i.e. dawn and dusk. However, with the unstable conditions of a sunny summer day at noon-time, a more appropriate scaling would be with altitude to the  $-4/3$  power (26:22-25). Wyngaard et al have developed such a model for the latter case (27:1646-1650). The

model is valid from the surface to the first temperature inversion in the atmosphere, which on a warm summer day may be over 1000 meters high.

$$C_n^2(h) = \frac{(dn/dT)^2 (2 \times 10^{-3}) Q^{4/3} h^{-4/3}}{\left[ 1 + \frac{14000 U_*^3}{hQ} \right]^{2/3}} \quad (65)$$

where  $h$  = height in meters above the ground  
 $dn/dT$  = the change in refractive index, per unit change in temperature,  $K^{-1}$ , per  
 $Q$  = the upward convective heat flux,  $W/m^2$   
 and  $U_*$  = a characteristic frictional velocity with the surface,  $m/sec$

Typically,  $U_*$  is an order of magnitude smaller than the local wind speed and may be approximated by

$$U_* = 0.35 \left[ h (dU/dh) \right] \quad (66)$$

where  $dU/dh$  equals the vertical gradient of the mean horizontal wind (28:6.11). For many conditions, the term  $\left[ h (dU/dh) \right]$  becomes independent of altitude. A nominal value for this factor from Wyngaard's experimental data over the plains of Kansas would be  $1.0 m/sec$  (27:1648). The value of  $Q$  depends on the amount of sunlight falling on the ground and the properties of the ground itself. As an estimate of  $Q$ , one may take

$$Q = Q_0 \sin \xi \quad -50 \quad (67)$$

where  $\xi$  is the solar elevation angle and  $Q_0$  is a constant containing the effects of cloud cover and surface composition (28:6.11). For a clear sky and dry fields,  $Q_0$  has a value of  $400 \text{ w/m}^2$  (28:6.12).

An approximate formula for the refractive index of dry air at optical frequencies was obtained from Clifford (26:10).

$$n = 1 + \frac{(7.76 \times 10^{-5})P}{T} + \frac{(5.84 \times 10^{-19})P}{T \lambda^2} \quad (68)$$

where  $P$  is atmospheric pressure in millibars,  $T$  is temperature in degrees Kelvin and  $\lambda$  is the wavelength of the propagating light in meters. Differentiating equation (68) with respect to temperature yields an appropriate expression for the change in refractive index for a unit change in temperature.

$$\frac{dn}{dT} = - \frac{(7.76 \times 10^{-5})P}{T^2} - \frac{(5.84 \times 10^{-19})P}{T^2 \lambda^2} \quad (69)$$

At altitudes near the first temperature inversion, there is typically a local peak in the structure parameter curve (28:6.12). However, even at much higher altitudes in the free atmosphere, the behavior of the structure

parameter is characterized by sharp peaks of possibly two orders of magnitude (28:6.18). A particularly significant peak occurs in the 9-15 kilometer region near the tropopause. Yet, beyond the tropopause, the structure parameter quickly approaches zero (28:6.19).

Hufnagel (26:24) has incorporated this highly active tropopause region in the derivation of his latest model of the behavior of the structure parameter in the free atmosphere. The model is valid for altitudes above the first temperature inversion to 25 km. The mean values of  $C_n^2$  as a function of altitude,  $h$ , is given by

$$C_n^2(h) = 2.7 \left\{ (2.2 \times 10^{-53} h^{10}) \exp(-h/1000) + 10^{-16} \exp(-h/1500) \right\} \quad (70)$$

A plot of Hufnagel's model is shown in Figure 17.

As stated before, the region which most influences turbulence effects in the far field is near the surface where the laser source is located. Therefore, this study will use the two models just described to determine the behavior of the structure parameter with altitude. Wyngaard's model will be used from the surface to 1000 meters, an appropriate value for the first temperature inversion for sunny daytime conditions, above which, Hufnagel's model is

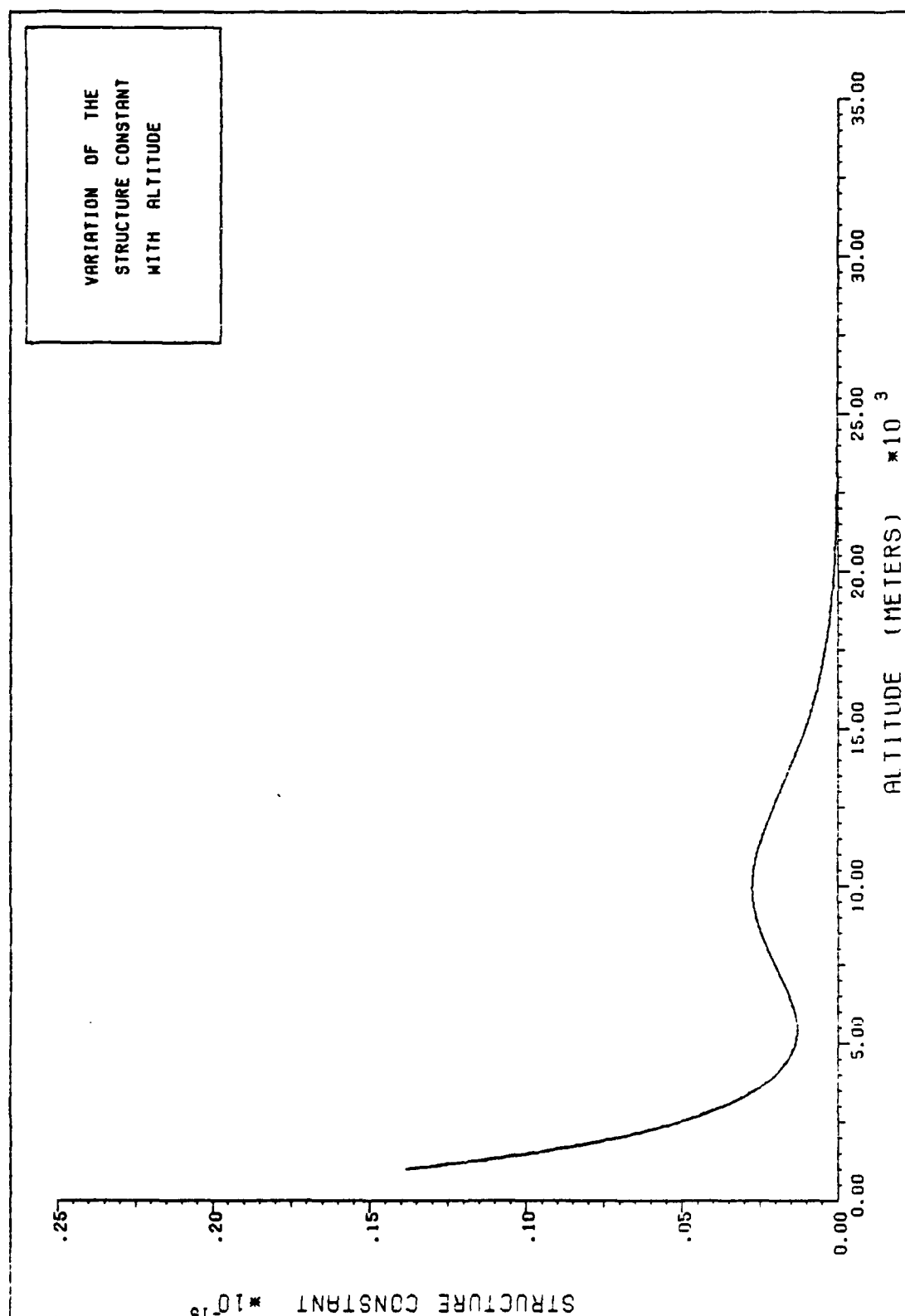


Figure 17. Hufnagel's Model of the Structure Parameter vs Altitude

employed to an altitude of 25 km. Above this altitude, the structure parameter can be assumed to be zero. The two models merge at a value of approximately  $1.5 \times 10^{-16} \text{ m}^{-2/3}$  at an altitude of 1000 meters when a mid-afternoon sun angle of 40 degrees is used.

The use of a structure parameter model near the surface which essentially describes a worse case scenario in terms of turbulence effects is very conservative but justified by the fact that the operational use of a ground based laser weapon system would require an immediate response even under such unstable atmospheric conditions.

Turbulence Induced Beam Radius. The theoretical development of the effects of turbulence on a propagating laser beam follows the work of Yura (29). The key parameter in his formulation is  $\rho_o$ , the lateral coherence length. This quantity can be thought of as the separation between points in a plane perpendicular to the propagation direction where a spherical wavefront remains coherent. Yura presents the following formula for this quantity valid over the propagation range  $Z_1 \ll Z \ll Z_2$  (29:2771).

$$\rho_o = \left[ 1.45 k^2 \sec \phi \int_0^Z Cn^2(z') \left( \frac{z-z'}{z} \right)^{5/3} dz' \right]^{-3/5} \quad (71)$$

where

$$z_1 = (.4 k^2 Cn^2 (L_0/2\pi)^{5/3})^{-1} \quad (72)$$

$$z_2 = (.4 k^2 Cn^2_{\ell_0}{}^{5/3})^{-1} \quad (73)$$

Here,  $k$  is the propagating wavenumber  $= 2\pi/\lambda$ ,  $\phi$  is the zenith angle, and  $Cn^2$  is the refractive index structure parameter in units of  $\text{meters}^{-2/3}$ . Note that the integration of the structure parameter is weighted more heavily toward values located near the source of the laser. Consider visible frequencies and a constant ground level value for the structure parameter of  $2.0 \times 10^{-16}$ . The propagation ranges of validity according to equations (72) and (73) lie between .5 and 400,000 meters. Propagating vertically through the atmosphere would mean average values of  $Cn^2$  several orders of magnitude below a ground level value. Therefore, it can be seen that Yura's theory is valid over the ranges of interest in this study, and in fact, over most ranges for any high powered laser system study.

Yura assumes an infinite Gaussian profile for the laser source in his formulation. Through his statistical treatment of turbulence, the beam profile in the far field

also approximates a Gaussian profile. Yura proceeds by approximating a  $1/e$  characteristic total beam radius dependent on the lateral coherence length parameter (29:2771). Converting this formula to a  $1/e^2$  radius yields a total beam spread radius due to turbulence effects which will be used in the model for this study.

$$a_t = \frac{2 \sqrt{2} z}{k \rho_0} = \frac{\sqrt{2} z}{\pi \lambda \rho_0} \quad (74)$$

The effects of turbulence might be compensated for through the use of adaptive optical systems. Without correction, the beam characteristics of a ground based laser device would quickly be dominated by turbulence effects and significantly reduce the weapon's utility. The degree to which this compensation can be accomplished remains an open question and will be treated parametrically in the model developed for this study.

#### Effects of Jitter

Vibrations in or near a high energy laser device can cause small angular deflections in the laser beam at the source. Over long propagation distances, these small deflections can translate to significant errors in the target plane. These vibrations can be the result of

frictional forces within moving parts of mechanical devices or merely the relatively constant seismic activity within the Earth. Most can be isolated; however, even a free electron laser device, with few mechanical parts, will experience a minor amount of jitter.

These jitter effects on the laser beam are normally treated statistically in laser system studies. A mean squared radial displacement of the laser spotsize at a propagation distance  $z$  can be determined by the following formula (19:1480).

$$a_j^2 = 2 \langle \theta_x^2 \rangle z^2 \quad (75)$$

where  $\langle \theta_x^2 \rangle$  is the variance of the single axis jitter angle. This formula assumes an isotropic jitter, i.e.

$\langle \theta_x^2 \rangle = \langle \theta_y^2 \rangle$ . Even though jitter is not a wavelength dependent phenomenon, it will be included in this study in order to evaluate non-linear effects through the atmosphere.

### Thermal Blooming

When a high power laser beam passes through an absorbing medium, the phenomenon of thermal blooming will act to distort the laser beam profile and could significantly

reduce the laser beam power which reaches the target. In fact, this process is often the limiting factor in determining the maximum amount of power which can be transmitted through the atmosphere at a given wavelength.

The essential features of thermal blooming can be explained through relatively simple physical processes. Consider an ideal gas which is initially in thermal equilibrium and with an ambient index of refraction. If the gas absorbs radiation at the wavelength of the laser, this absorbed energy gives rise to local heating of the gas. The increase in temperature produces a small increase in pressure. The medium, expanding at the speed of sound in response to this pressure imbalance, decreases in density, and thus, causes a proportional decrease in the local refractive index.

Consider also a laser beam which initially has a Gaussian intensity profile as in Figure 18a. On the axis of the beam, heating of the medium will be at a maximum; therefore, the local index of refraction will be at a minimum value as shown in Figure 18b. The index of refraction returns to the ambient value near the edges of the laser beam. Thus, light rays near the center of the beam will be refracted radially outward toward the more dense regions of the gas. The laser beam, therefore, diverges or 'blooms' as the heating of the gas continues.

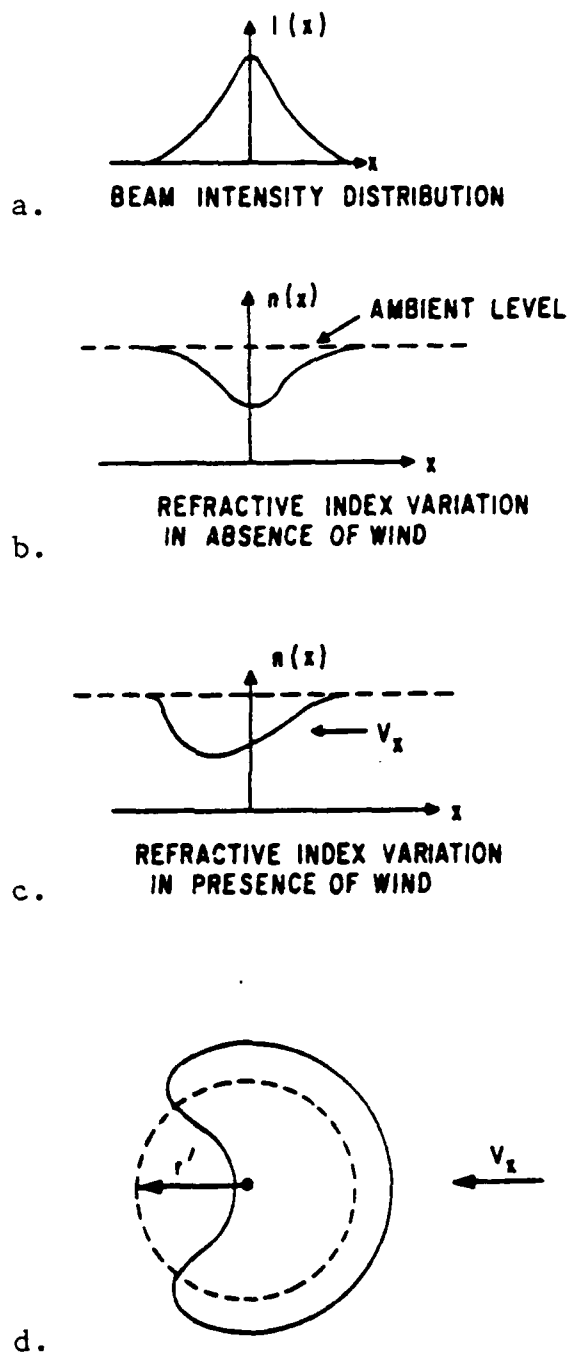


Figure 18. Thermal Blooming Effects on Refractive Index (18:76)

An interesting complication occurs when the absorbing medium is flowing transverse to the direction of propagation by means of either a natural crosswind or a slewing of the laser device. Under these conditions, the refractive index profile will be skewed as in Figure 18c. The transverse motion of the medium continuously replaces that portion of the medium which has been heated by the laser beam with unheated medium. Therefore, the upwind region of the beam is cooler and more dense than the downwind region which has undergone laser heating longer. As before, light rays are refracted toward these cooler regions. In this case, the process produces an asymmetric, crescent shaped beam profile depicted in Figure 18d.

If the laser beam power and absorbtivity of the atmosphere are sufficiently large, the beam will simply be obliterated by thermal blooming effects after propagating only a short distance. Studies have shown that this can occur on time frames of milliseconds (30:222). Yet, for modest power levels and absorbtivity, convective cooling in the beam and the transverse flow of air across the beam can combine to create a steady-state condition for thermal blooming (31:63).

Not only is the beam expanded by the self-induced thermal blooming, but the effective center of the beam is displaced in the direction of the wind (31:64). This

effect could complicate aiming of the beam; however, for laser beams which survive the effects of thermal blooming, thermal 'bending' effects are small and will not be considered in this analysis.

A quantitative description of the thermal blooming process can follow several approaches. The problem can be treated through sophisticated wave optics calculation; however, this methodology has one key disadvantage. Most non-specialists would quickly lose sight of the approach and the basic physical processes involved. An alternate avenue might be the one taken by Gebhardt and Smith (31). They employed relatively simple geometric optics approximations to develop a thermal blooming 'distortion' parameter. This parameter is then used as an argument to enter a series of curves to obtain the amount of irradiance reduction on the target due to thermal blooming. The curves were fit from experimental data and results from detailed wave optics computer codes. The approach to thermal blooming by Gebhardt and Smith is the one which will be developed here and used in the model for this study.

As laser energy is absorbed by the medium, it is transmitted to cooler surroundings through either convection or conduction. The change in temperature across the medium is governed by the following energy balance equation (31:64).

$$\rho C_p V_x \left( \frac{dT}{dx} \right) + K \nabla^2 T = \alpha I \quad (76)$$

where  $\rho$  = atmospheric density in  $\text{kg/m}^3$   
 $C_p$  = specific heat in  $\text{joules/kg-K}$   
 $V_x$  = wind velocity transverse to the  
propagation path in  $\text{m/sec}$   
 $\alpha$  = absorption coefficient of the atmosphere  
 $K$  = the conductivity of the atmosphere  
and  $I$  = the laser irradiance in  $\text{watts/m}^2$

In this theoretical development, convective heat transfer is assumed to dominate over thermal conduction; therefore, the second term in equation (76) is ignored. Furthermore, it is assumed that the time for the conversion of absorbed laser energy to thermal motion is small compared to some characteristic convective heat transfer time equal to  $a/V_x$  where  $a$  is the local radius of the beam. Finally, energy losses due to re-radiation of the absorbed laser energy are neglected.

The refractive index of the medium will vary about some ambient value,  $n_0$ , due to the small spatially varying temperature changes across the beam (31:64). For an arbitrary position vector,  $\vec{r}$ , we have

$$n(\vec{r}) = n_0 + \left( \frac{dn}{dT} \right) \Delta T(\vec{r}) \quad (77)$$

If we assume these variations in the refractive index are small and occur over dimensions large compared to the laser wavelength (easily satisfied at optical frequencies), the following scalar wave equation can be used to describe laser propagation (31:64).

$$(\nabla^2 + k^2 n^2 + ik\alpha) \bar{U}(\bar{r}) = 0 \quad (78)$$

where  $k$  is the vacuum wavenumber and  $\bar{U}(\bar{r})$  is the complex electric field of the laser radiation.

Geometric optics assumes that, for sufficiently short wavelengths, one can describe surfaces of constant phases called phase fronts such that normals to these surfaces represent the direction of local energy flow (32:235). Consider as a trial form of the fixed time complex electric field of the laser,

$$\bar{U}(\bar{r}) = A(\bar{r}) \exp \left[ ikS(\bar{r}) \right] \quad (79)$$

where  $\bar{r}$  is the position vector of a point along a given ray of light and  $S(\bar{r})$ , independent of the magnitude,  $A(\bar{r})$ , is a scalar function of position which locates these surfaces of constant phase (32:235). Substituting equation (79) into Maxwell's equations yields, in the short wavelength limit,

$$\left[ \nabla S(\vec{r}) \right]^2 = n(\vec{r})^2 \quad (80)$$

where  $n(\vec{r})$  becomes the position dependent value of refractive index along the ray. The function  $S(\vec{r})$  is often called the eikonal and equation (80), the eikonal equation. Both  $n(\vec{r})$  and the gradient of  $S(\vec{r})$  are normal to the surface of the phase front. From Born & Wolf (33:121-122), the eikonal equation can be developed into a differential equation for the ray vector.

$$\frac{d}{ds} (\nabla S(\vec{r})) = \nabla n(\vec{r}) \quad (81)$$

Here,  $s$  represents the scalar measure of distance along the propagating ray. Note that a constant refractive index implies an unvarying gradient of  $S(\vec{r})$  and no beam divergence.

By assuming a plane wave form for  $S(\vec{r})$  and the paraxial ray approximation, i.e. the ray vector is nearly parallel to the axis of propagation, Gebhardt and Smith developed an irradiance distribution of the thermally bloomed laser beam (31:65).

$$\begin{aligned}
 I(x, y, z) &= \\
 I_u(x, y, z) e^{-\alpha z} \exp \left\{ - \int_0^z \left( \nabla_t + \frac{\nabla_t I_u}{I_u} \right) \cdot \int_0^{z'} \frac{\nabla_t n}{n_0} dz'' dz' \right\} \\
 &= I_u(x, y, z) e^{-\alpha z} e^{\psi}
 \end{aligned} \tag{82}$$

Where  $I_u$  is the unbloomed irradiance distribution at propagation distance  $z$  and  $\nabla_t$  is the transverse gradient operator  $= d/dx \hat{x} + d/dy \hat{y}$ . The attenuation factor,  $e^{-\alpha z}$ , accounts for absorption in the medium. This expression conveniently describes the effect of refractive index variations across the laser beam in terms of an exponential factor,  $e^{\psi}$ , that modifies the unbloomed irradiance,  $I_u$ . For a Gaussian beam profile given previously by equation (50), the total useable power within the  $1/e^2$  radius of the beam is found through integration.

$$P_t = \int_0^a I_0 \exp(-2r^2/a^2) 2\pi r dr = \frac{.865}{2} I_0 \pi a^2 \tag{83}$$

therefore one can write

(84)

$$I_u(x, y, z) = \frac{2P}{.865 \pi a^2} \exp \left[ -\frac{(2x^2 + 2y^2)}{a^2} \right]$$

The change in temperature across the beam is obtained from equation (76).

(85)

$$\Delta T(x, y, z) = \frac{\alpha}{\rho C_p V_x} \int_{-\infty}^x I_u(x', y, z) dx'$$

Combining equations (77) and (85) yields the following (31:66).

(86)

$$\frac{\nabla_t n}{n_0} = \frac{1}{n} \left( \frac{dn}{dT} \right) \nabla_t T = \epsilon \left( \hat{x} I_u + \hat{y} \int_{-\infty}^x \frac{dI_u}{dy} dx' \right)$$

where

(87)

$$\epsilon = \frac{2 (dn/dT)^2 \alpha}{.865 n_0 \rho C_p V_x} = \epsilon(z)$$

Hence, all the elements in equation (82) have been defined. Through rather straightforward, albeit laborious, mathematics and again invoking the paraxial ray assumption and ignoring the  $z$  dependence on the transverse coordinates,  $x$  and  $y$ , an expression for  $\Psi$  can be determined (18:32).

$$\Psi = NI \left( \text{constants independent of } z \right) \quad (88)$$

Here,  $NI$  is Gebhardt and Smith's thermal blooming distortion parameter defined as

$$NI = \frac{4.89P_t}{\pi} \int_0^z \frac{1}{a(z')} \int_0^{z'} \frac{\left( \frac{dn(z'')}{dT} \right) \alpha(z'') \exp(-\alpha(z'')z'')}{n_o(z'') \rho(z'') c_p(z'') v_x(z'') a^2(z'')} dz'' dz' \quad (89)$$

They argue that the reduction of laser beam irradiance due to thermal blooming effects can be determined solely by this single distortion parameter,  $NI$  and have developed an empirical model based on this parameter. Figure 19 shows the dependence of an irradiance reduction factor,  $I_{rel}$ , on the distortion parameter,  $NI$ . The curve was developed from experimental data points, depicted by open circles in the figure, and through theoretical results of nonlinear wave optics propagation codes, shown as solid circles. The curve fit results predict the following

relationship (19:1484).

$$I_{rel} = \frac{1}{1 + .0625 NI^2}$$

(90)

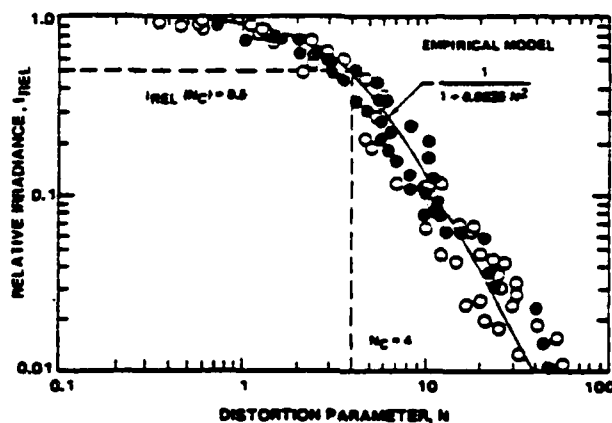


Figure 19. Beam Reduction Factor,  $I_{rel}$ ,  
vs. Distortion Parameter (19:1484)

The elements under the integrands in equation (89) are functions of  $z$ , the coordinate along the propagation path. Therefore, in order to determine a distortion parameter for thermal blooming, the  $z$  dependence for these elements must be stated. Of course, in the case of this study, the  $z$  dependence is primarily an altitude dependence.

The radius of the beam along the path can be determined through equation (53) after considering the effects of diffraction, focusing, jitter, and turbulence. In addition,

the use of LOWTRAN and FASCODE in this study provides values of absorption and scattering coefficients for molecular and scattering processes at various layers of the atmosphere. Thus, total attenuation coefficients and total absorption coefficients can likewise be determined at each layer through addition. For intermediate values, exponential interpolation can be used. Also, LOWTRAN will provide values of pressure, temperature and density for each layer boundary and average values for each layer in the assumed model atmosphere. Again, interpolation is used for intermediate altitudes. Using values for pressure, temperature, and the propagation wavelength, the value of the refractive index,  $n(z)$ , can be computed through equation (68) and the differential of the refractive index with respect to temperature,  $dn/dT$ , can likewise be computed through equation (69). Both equations were discussed previously under turbulence effects.

Expressions for the specific heat at constant pressure,  $C_p$ , and the nominal crosswind,  $V_x$ , were borrowed from Peckham and Davis (18:58). We will assume in this study that a horizontal wind always exists and this wind continuously increases with altitude until the tropopause, at which point, the average wind begins to decrease. Peckham and Davis' curve for nominal wind velocity versus altitude was based on data contained within Reference 34. A plot of this

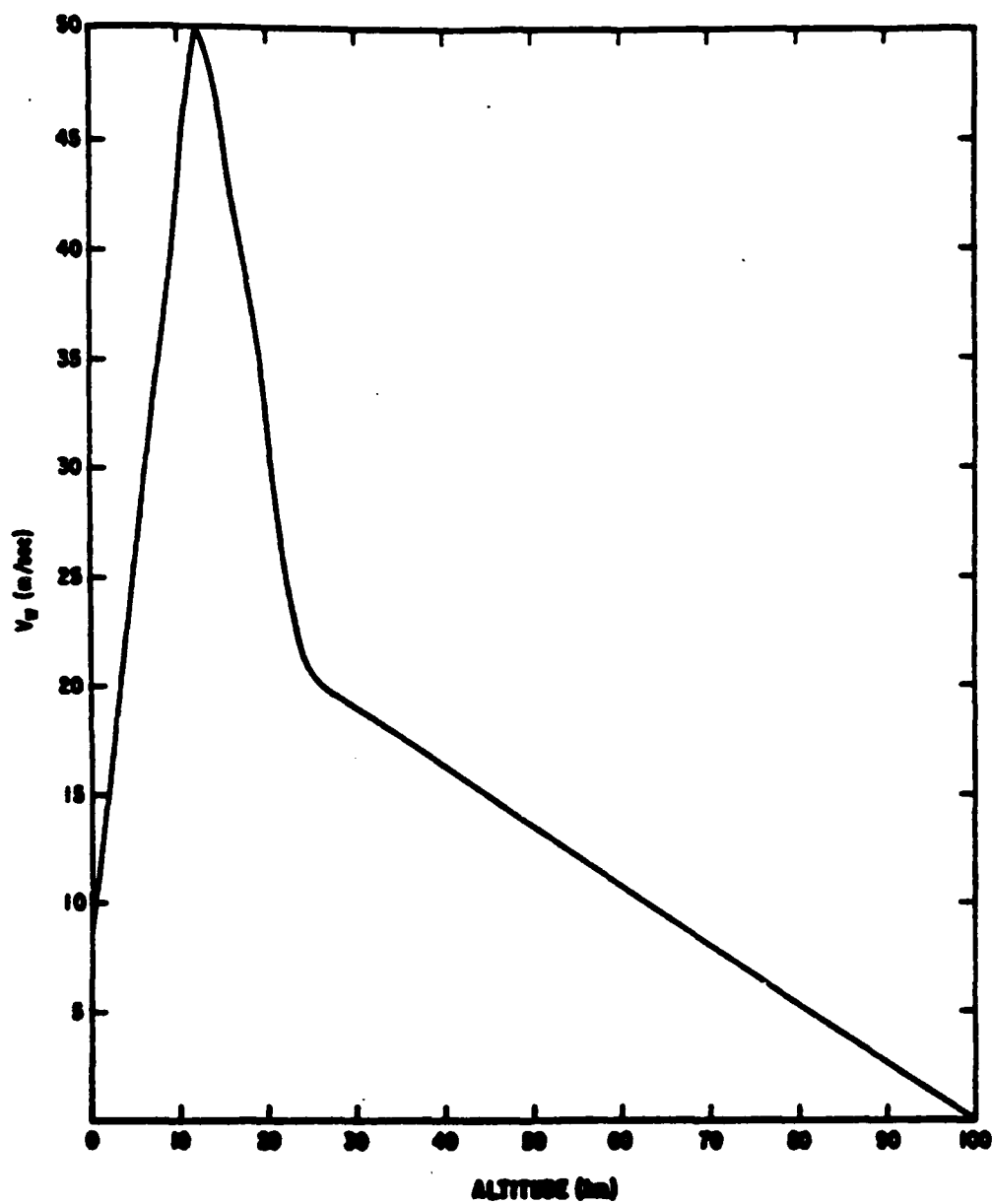


Figure 20. Mean Horizontal Wind vs. Altitude (18:60)

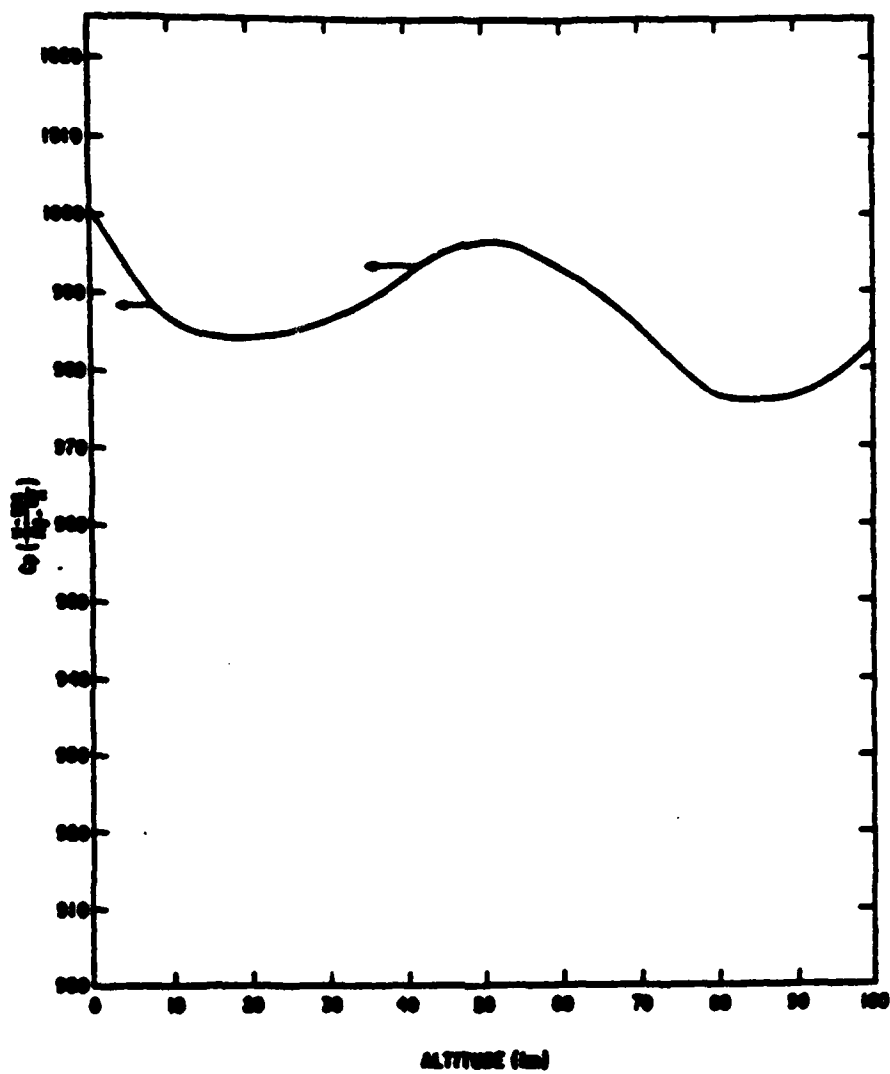


Figure 21. Specific Heat of the Atmosphere  
vs. Altitude (18:61)

curve is found in Figure 20. Their formulation for the specific heat curve was a 2nd degree polynomial curve fit with temperature based on data in Reference 35. A plot of this curve is found in Figure 21.

### Model Resolution

One of the important issues in the development of the model was the choice of resolution, or the separation between successive wavelengths which would be compared. The model itself will pose no restrictions; however, a trade-off between computer time and the discrimination in the output data was necessary. The important factors bearing on this decision will be discussed.

As described earlier, the structure of the molecular absorption curve is very complex in wavelength regions longer than about .55 micrometers. Each absorption line has a finite width. At sea level, collision broadening mechanisms dominate, widening the average absorption line to approximately 0.1 wavenumbers  $\text{cm}^{-1}$  (24:10). At higher altitudes, the linewidth is determined primarily by the weaker Doppler broadening to be approximately  $0.01 \text{ cm}^{-1}$  (24:10). FASCODE samples across a spectrum at a specified interval. Conceivably, if that interval is greater than the average linewidth at a given altitude, the entire line contribution would be missed. In fact, the original FASCODE

program has been structured to sample at intervals equal to one quarter of the average linewidth for this reason (24:14).

Also to be considered are the limitations in the free electron laser device. First, the relationship between the linewidth of the laser and the absorption linewidth must be explored. As with conventional lasers, the free electron laser has a small signal gain curve, broadened about some central value. The width of that curve is based, however, on relativistic dynamics (11:11). The definition of which electrons are or are not in phase can only be determined within the length,  $L_w$ , of the wiggler. Based on the Uncertainty Principle, it can be shown that the fractional linewidth,  $\nabla\nu/\nu$ , is (11:11):

$$\frac{\nabla\nu}{\nu} = \frac{\lambda_w}{2L_w} \quad (91)$$

Typical values of  $L_w=30$  meters and  $\lambda_w=0.02$  meters gives a linewidth of approximately  $6.67 \text{ cm}^{-1}$  for visible frequencies. However, this gain curve can be treated as a homogeneously broadened gain curve of a conventional laser; the laser will saturate on the highest gain cavity mode closest to the center of the gain profile. The emitted linewidth will, therefore, be determined by the

cavity mirror stability and could be on the order of  $10^{-4}$   $\text{cm}^{-1}$ , many orders of magnitude narrower than the average absorption linewidth in the atmosphere (11:12). Thus, the laser linewidth does not restrict the model resolution.

Presumably, with a little judicious cavity adjustments, any wavelength of interest could be selected. However, an open question remains concerning the stability of the laser wavelength based on the stability of the electron beam. No reference could be found in the open literature on this subject. According to the Free Electron Laser Program office at Los Alamos, the energy stability of the electron beam can be controlled by feedback devices to one part in 10,000 or better (36). As a gross estimate of wavelength stability, one may begin with equation (10)

$$\lambda_L \approx \frac{\lambda_w}{2\gamma^2} \quad (10)$$

Differentiating with respect to  $\gamma$ , we get,

$$d\lambda_L = \frac{-\lambda_w}{\gamma^3} d\gamma \quad (92)$$

Assuming  $\lambda_w = 0.02$  meters,  $\lambda_L = .5$  microns, and  $d\gamma = .00005$ , gives a spread in the laser output of approximately  $2.0 \text{ cm}^{-1}$ .

A preliminary test run of the model indicated that approximately 0.3 seconds of central processing time was

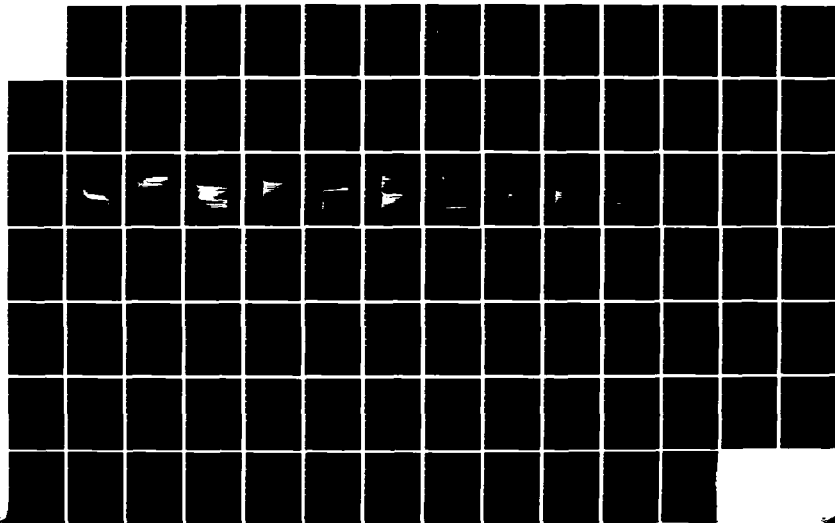
ND-A141 157

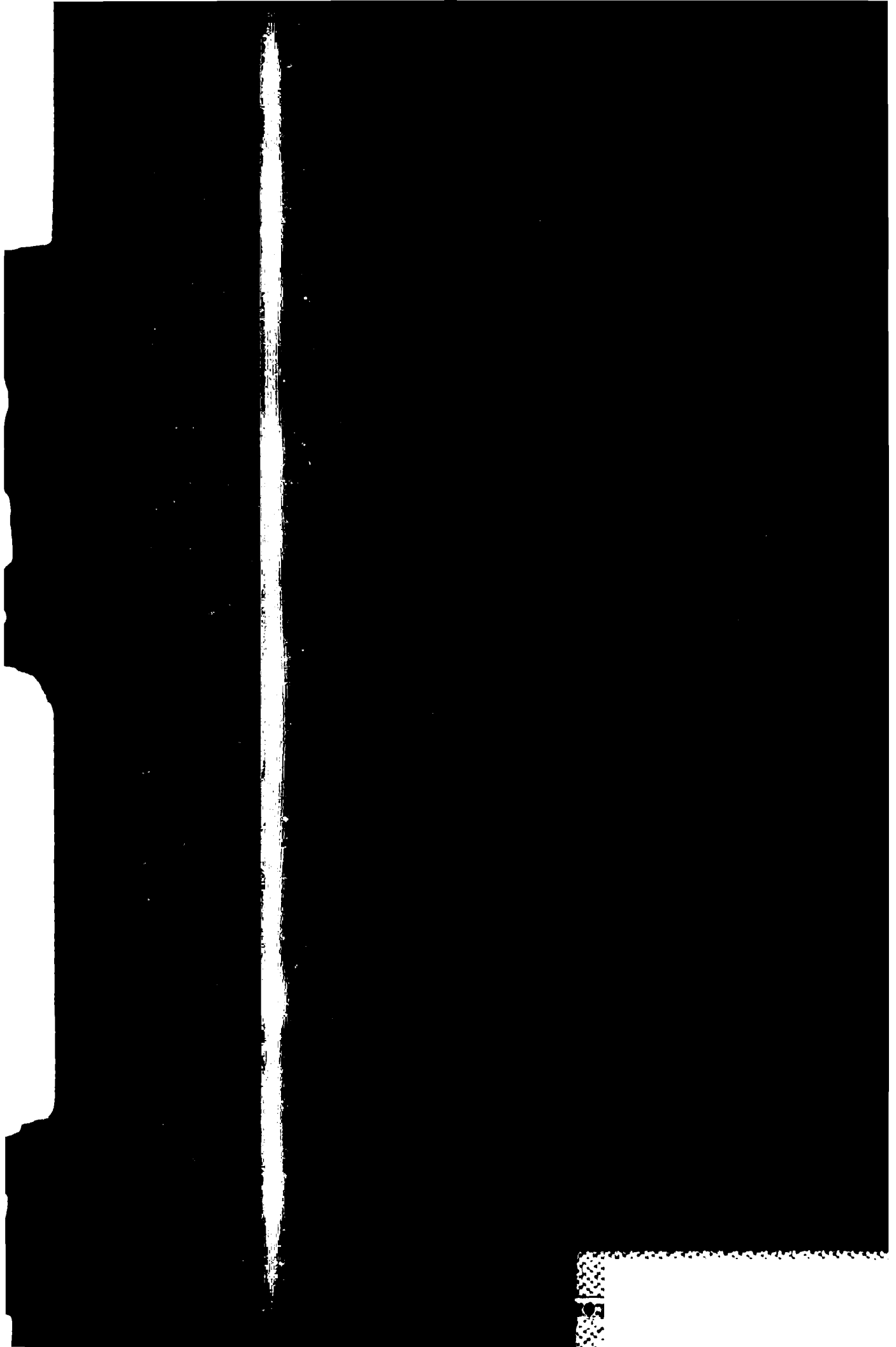
WAVELENGTH SELECTION FOR A GROUND BASED FREE ELECTRON  
LASER WEAPON SYSTEM(U) AIR FORCE INST OF TECH  
WRIGHT-PATTERSON AFB OH SCHOOL OF ENGI... D E KOHLHEPP  
DEC 83 AFIT/G50/ENP/83D-2 F/G 15/3

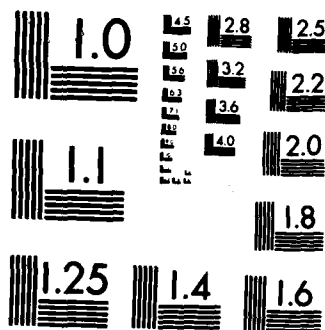
2/2

UNCLASSIFIED

NL







MICROCOPY RESOLUTION TEST CHART  
NATIONAL BUREAU OF STANDARDS-1963-A

required for each wavelength calculation. Therefore, a trade-off between capturing the majority of the structure in the molecular absorption curve and computer time led to a decision to sample in intervals of 0.2 wavenumbers. It was felt that the structure missed by this choice represented secondary consequences. Finally, in the wavelength region shorter than .55 micrometers where molecular absorption is non-existent, the spectrum will be sampled at a conservative 1.0 wavenumbers.

#### IV . Target Interactions

Electromagnetic radiation incident on a metallic target will either be absorbed or reflected. Of course, for laser weapon system effectiveness, one is interested in the degree of absorption of laser energy into the target material.

The free electron laser normally is operated to produce a long pulsed output of high average power (2) . Therefore, the primary kill mechanism is a thermal burn through of the target's outer skin. The laser energy absorbed in the skin is converted to heat, which is gradually transported through the target by simple conduction. Such thermal kill mechanisms can be assumed to be linear processes, and therefore, scale directly with the absorptivity of the target. In certain regions of the spectrum, absorptivity can be a strong function of the incident laser wavelength.

##### Basic Theory

Consider the following simple model. A monochromatic plane wave is incident perpendicular to a smooth conducting plane surface. The electric field in the wave causes oscillating motion in the loosely bound valence electrons of the metal at the same frequency of the incident wave. If totally free to oscillate, the electrons will produce a reflected wave of the same magnitude, exactly 180 degrees out of phase with the incident wave. In this case , no

radiation is absorbed by the target material and accounts for the highly reflective nature of metallic conductors like silver. However, viscous damping forces arising from the collisions between the oscillating electrons and the atomic lattice of the metal will restrict the movement of the electrons, and thus, reduce the conductivity. These collisions dissipate the electrons' energy into thermal motion, and produce heat within the target.

The above discussion constitutes the basic assumptions behind the Drude free electron model (37:434). The theory pre-supposes a complex index of refraction,

$$\tilde{n} = n + ik \quad (93)$$

where  $n$  is the real index of refraction and  $k$  is an extinction coefficient of an incident wave. The extinction component can be more easily seen when the complex index of refraction is used in the formula for the wave's electric field.

$$E(z) = E(z = 0) e^{-\frac{k\omega}{c} z} e^{\frac{in\omega}{c} z} \quad (94)$$

The Fresnel expression for the fraction of reflected radiation from a homogenous surface due to a normally incident wave is given by the following (37:395).

$$R_n = \frac{(n-1)^2 + k^2}{(n+1)^2 + k^2} \quad (95)$$

For optical frequencies metals are opaque; therefore, by Kirchoff's Law and energy conservation (37:395), the fraction of radiation reflected plus the fraction absorbed must equal one. This gives an expression for the absorptance of normally incident waves.

$$A_n = \frac{4n}{(n+1)^2 + k^2} \quad (96)$$

If one assumes the frequency of the radiation is less than the frequency of the induced electron collisions within the target material, then the currents in the metal are in phase with the electric field of the radiation. In this case, the absorption depends on just the incident wavelength,  $\lambda$ , and the conductivity of the material,  $\sigma$ . This expression is widely known as the Hagen-Rubens formula (37:437).

$$A_n = 4 \sqrt{\frac{\epsilon_0 c}{\sigma \lambda}} \quad (97)$$

where  $c$  is the speed of light, and  $\epsilon_0$  is the permittivity of free space.

By this expression, the absorptivity of a metallic target scales as  $\lambda^{-\frac{1}{2}}$  and therefore, tends to favor shorter wavelengths for a laser weapon system analysis. For pure metals at room temperature, equation (97) is usually not

valid in the visible portion of the spectrum. Since visible frequencies are generally greater than the induced electron collision frequencies, this model would tend to over estimate the absorptance of the metal. However, for alloys of common aerospace materials where impurities exist in the atomic lattice, the experimental data suggests that this expression may be quite appropriate.

Figure 22 shows the spectral absorptivities for four common alloys used in satellites, missiles, and aircraft as a function of wavenumber. In the visible region, 10000 to 29000  $\text{cm}^{-1}$ , the absorptivity does seem to indeed scale as equation (97). This assumption will be tested later in this chapter.

However, this simple scaling is far from explaining the coupling of laser radiation to a target. The spectral absorption curve is greatly modified by the existence of resonance wavelengths. This phenomenon is not unlike the natural frequencies of an oscillator system. This behavior can be observed in the Aluminum-2024 curve in figure 22 where an absorption peak occurs in the visible spectrum at approximately 12000  $\text{cm}^{-1}$  (.83 micrometers).

In addition, the surface conditions of metallic targets play a dominant role in their radiative properties. The degree of surface roughness can be severe enough to require a statistical treatment in order to explain the optical behavior of the surface. If the surface irregularities are much smaller than the wavelength of light, diffraction

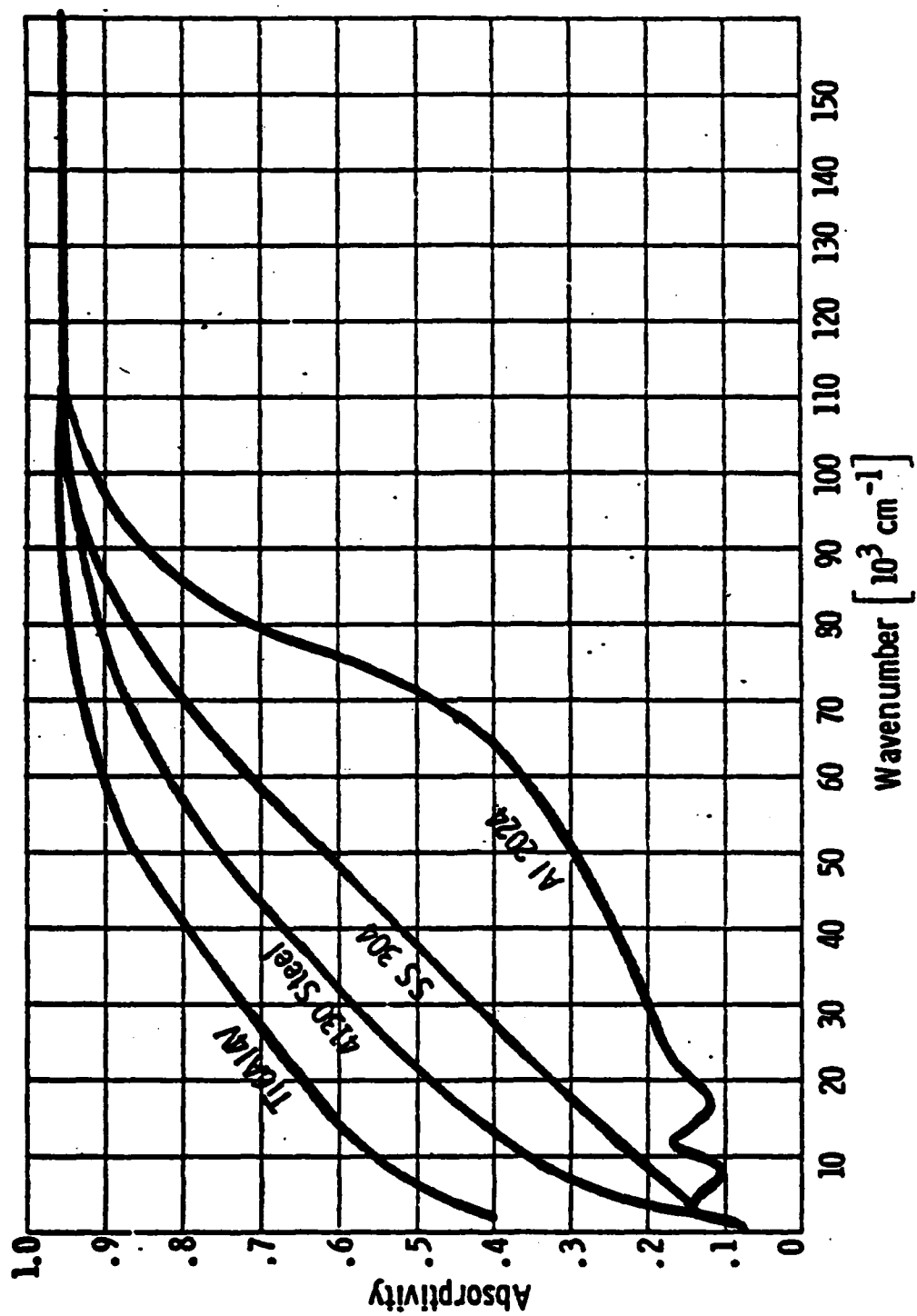


Figure 22. Absorptivity of Common Aerospace Materials vs. Wavenumber (38:53)

theory can be used. In this case, it has been shown that the surface reflectance becomes an exponential function of the square of the laser frequency (39:18). Another very important surface effect is the existence of thin films, either introduced by man or the result of oxide growths. These films act much like interference filters where certain wavelengths are selectively reflected depending on the thickness of the film (39:18). This effect is also, of course, very dependent on the angle of incidence of the laser wave. Finally, the spectral absorptance curve of a material is often dominated by other factors such as the thermal history of the material, chemical preparations, alloying, lattice orientation, impurities, and the presence of paint (39:18).

Being confronted with these complexities proved to be a difficult problem for this study, since it was desired not to make some specific assumptions concerning the target composition. The use of actual target spectral data would quickly classify this study as well. All this led to the decision to scale the wavelength dependence of the target interaction with the simplified Drude free electron theory as in equation (97). For this study, we will define a value of target 'efficiency' between zero and one. The best efficiency will occur at the short wavelength end of the spectrum of interest for this study, i.e.  $29000\text{ cm}^{-1}$  or .3448 micrometers. For longer wavelengths, efficiency values will be scaled proportionally downward from one. The expression used in the

program will be the following.

$$\text{Target efficiency} = \left[ \frac{.3448 \text{ (microns)}}{\lambda \text{ (microns)}} \right]^{\frac{1}{2}} \quad (98)$$

The program will be structured in such a way that more realistic target data can easily be inserted at a later time.

#### Discussion of the Approach

The approach we have selected is based on two rather questionable assumptions: 1) the effectiveness of a laser weapon is more a function of the bulk properties of the target material rather than the surface properties of the target and 2) the bulk properties can be approximated through the Drude free electron model and a  $\lambda^{-\frac{1}{2}}$  scaling. In this section, we will further examine the validity of these assumptions.

An Air Force Weapons Laboratory technical report describes two distinct mechanisms for the removal of paint from a metallic target surface (40:3). At relatively low laser intensities on the order of kilowatts/cm<sup>2</sup>, the paint apparently decomposes and chars, leaving the metal target blackened, and thus, highly absorbing (40:25). In this case, the existence of a paint actually enhances target coupling. However, at higher laser intensities (approximately 10 KW/cm<sup>2</sup>), the paint becomes quickly vaporized and leaves behind little res-

idue. In this case, the average absorptance of the painted target approaches the absorptance of the unpainted metal (40:26).

The second assumption we have made concerning the scaling of target interactions can be justified based on experimental data. Such data on the radiative properties of materials can be found in Reference 39 for common aerospace alloys. We selected two common alloys: Aluminum-2024, a wrought alloy with copper as the principal alloying agent (39:27), and Auminum-7075, also a wrought alloy with zinc as the alloying agent (39:114). Each experiment cataloged consisted of absorption measurements at various wavelengths for the given sample of material. These experiments represented a wide variety of surface preparations and thermal histories for the material samples as well. The raw data from these experiments are found on pages 37, 42, 109, 115, 119, and 136 of Reference 39. For our analysis, the raw absorption coefficients resulting from each experiment were normalized to one at the value corresponding to .35 micrometers. In all, 49 data points were used.

In this analysis, we assumed a statistical model where the normalized absorption data is proportional to  $\lambda^{-\frac{1}{2}}$ . The data was transformed in order to achieve a linear relationship between the independent variable of wavelength and the, now transformed, dependent variable of absorption. The data was

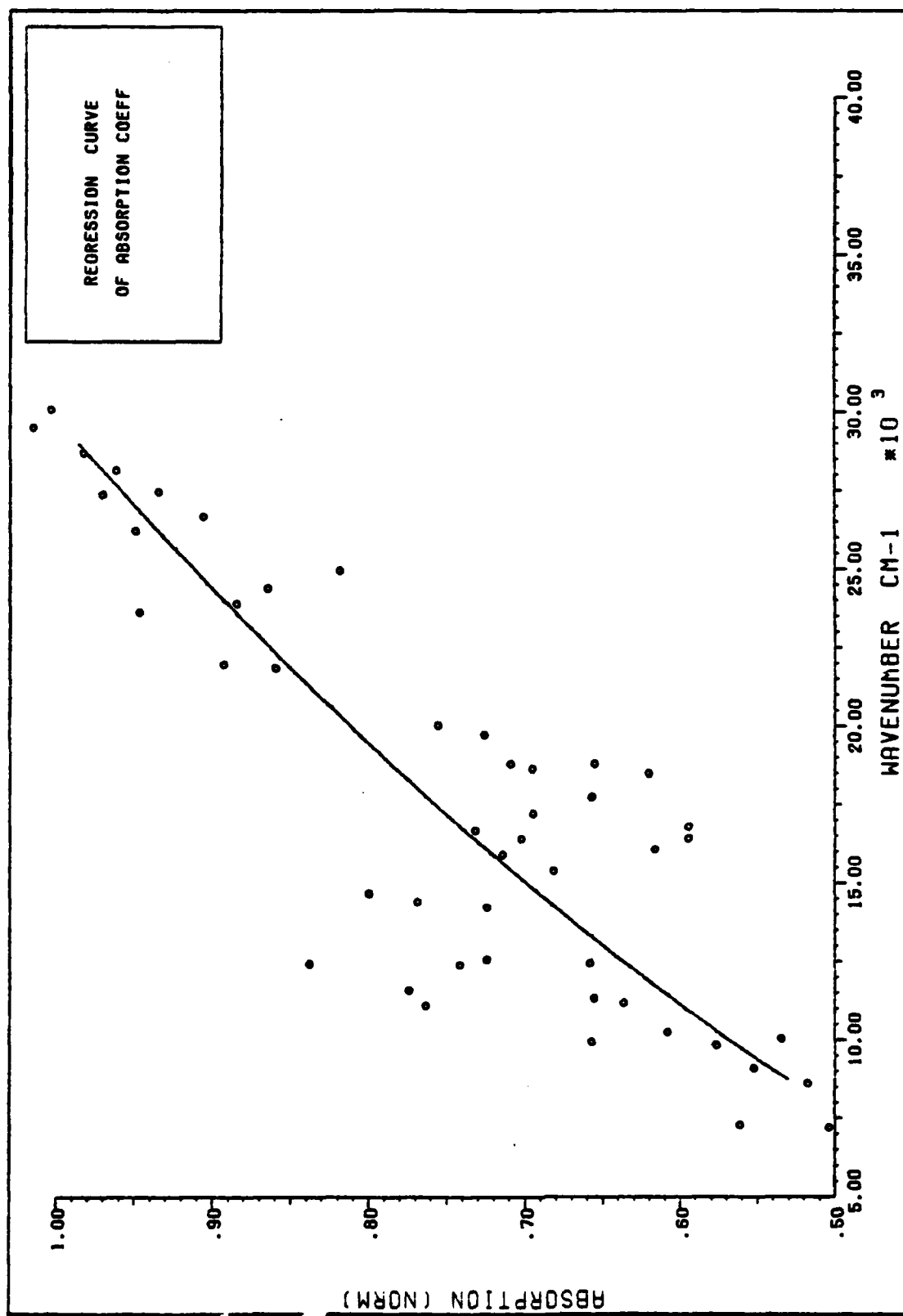


Figure 23. Regression Curve of Experimental Absorptivity Data of AL-2024 and AL-7075

then inserted into a simple univariate linear regression routine.

The two variables were found to be well correlated under this assumed model. The correlation coefficient from the regression was .794, indicating that 79.4% of the variation of the data can be explained through our assumed model. Much of the variation in the data is from the resonance absorption feature in aluminum at approximately  $12000 \text{ cm}^{-1}$  (.83 micrometers). The linear regression line between the transformed variables was found to be:

$$\text{Absorption} = -.0608 + 3.1604 \lambda \text{ (micrometers)} \quad (99)$$

This relationship, transformed back to the original variables, is plotted in Figure 23 along with the experimental data from which it was determined. The data is displayed in wavenumbers to keep consistency with other spectral plots in this report. The maximum deviation between the regression curve and our target efficiency expression, equation (98), is 3.6%.

This analysis is far from conclusively showing that all laser beam/target interactions can be described through equations (97). The subject of target energy coupling is extremely complex, and perhaps, can only be fully treated empirically for a specific target material.

## V. The Program

The theory developed in the previous chapter provided the foundation for the model. This chapter outlines the actual program which was used to examine the relationship between wavelength and the ground based laser weapon system efficiency to include propagation, device, and target coupling efficiencies. To those readers not interested in the actual program, this chapter may be skipped without loss of continuity.

The program was coded in FORTRAN V for use on a Control Data Corporation Cyber 6600 series computer with the NOS/BE 1 operating system. The overall program flow requires the execution of five separate programs as depicted in Figure 24. At Wright-Patterson AFB, all of the molecular absorption line data for the program FASCODE is contained on magnetic tape. This is preferred for two reasons: 1) to reduce storage requirements on the computer, and 2) to minimize input/output operations during execution of FASCODE. Thus, the first step is to read this data from tape to disk computer memory. This data is independent of the atmospheric model or transmission geometry chosen by the user; therefore, this data can be transferred once for a portion of the spectrum and accessed during multiple runs of FASCODE. The Air Force Geophysics Laboratory makes available programs for this purpose, thus assuring compatibility with the main program, FASCODE (24:68).

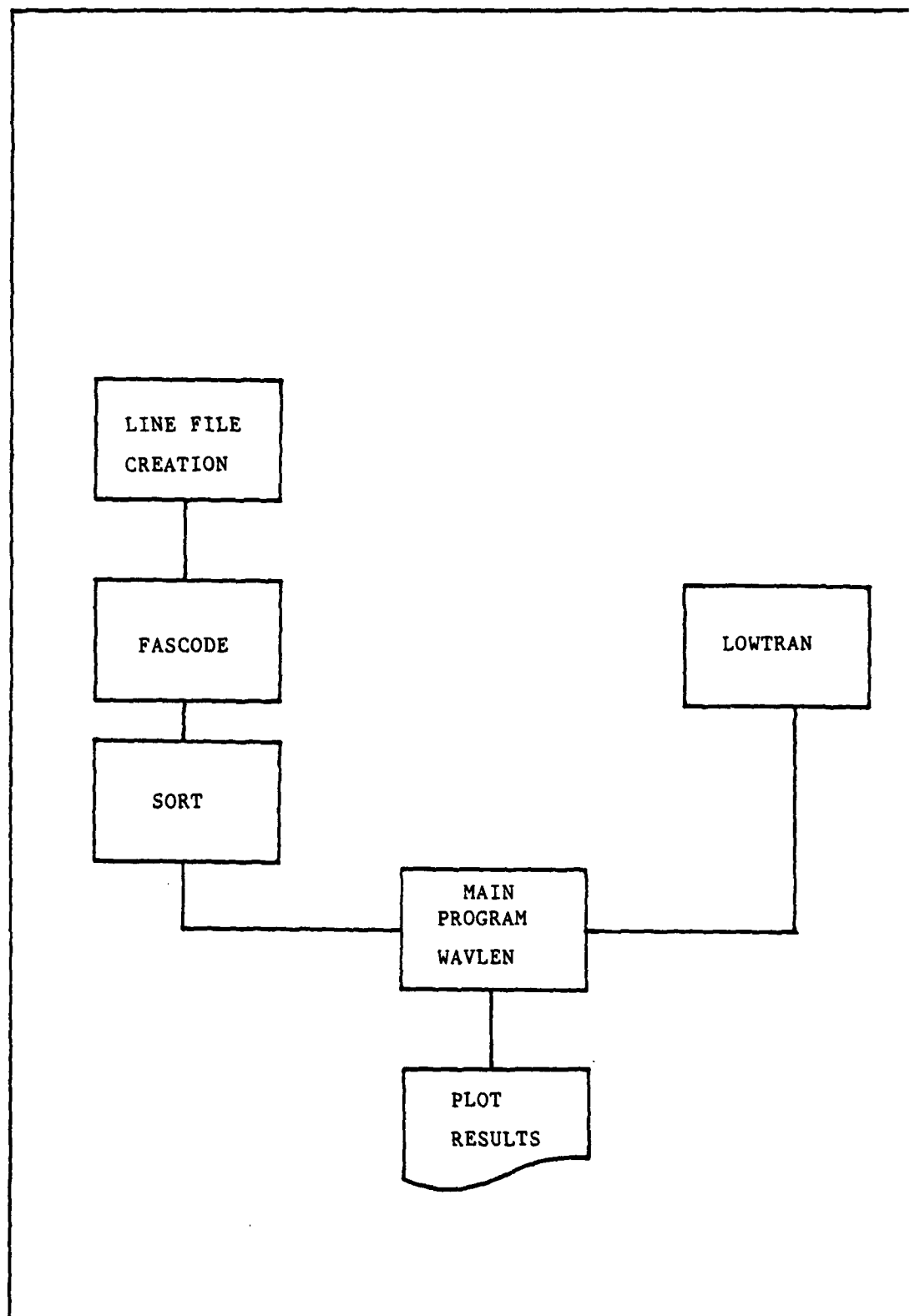


Figure 24. Program Flow for the Analysis

The program FASCODE was modified to provide molecular absorption optical depths for each of 32 layers of the atmosphere so that thermal blooming effects could be calculated. The modifications to FASCODE are discussed in Appendix B. The term optical depth is that value where the laser beam is attenuated by a factor of  $1/e$ . It is computed by simply multiplying the attenuation coefficient,  $\alpha$ , described by equation (63), by the path length,  $\Delta z$ . In this case, the path length is the width of each altitude layer.

Unfortunately for this study, FASCODE computes optical depths for all desired wavenumbers for an entire layer at a time. However, our main program, WAVLEN, requires absorption data for all layers, one wavenumber at a time. This incompatibility required that a program to sort the FASCODE absorption data to a usable format also be developed. This program, SORT, is included in Appendix C. The sorting process produces a data file of optical depths called FCDATA.

The program LOWTRAN calculates its optical depths in a format compatible with the main program and thus requires no additional data manipulation. As modified, LOWTRAN creates a data file called LTDATA which contains the attenuation coefficients of Rayleigh scattering, aerosol absorption, aerosol scattering, continuum absorption, and ozone molecular absorption for each altitude layer. The modification of LOWTRAN is described in Appendix A.

Both FASCODE and LOWTRAN use identical atmospheric models

in their calculations. These values of temperature, pressure, and density at the various altitudes are also required in the main program, WAVLEN. It was arbitrarily decided that LOWTRAN would provide this data by creating a data file called MODEL during the execution of LOWTRAN.

These three data files provide input to the main program, WAVLEN. Since this program is the guts of the computer model, it will be discussed in some detail. A listing of program WAVLEN is found in Appendix D.

The purpose of the program is to calculate a weapon system efficiency for a range of wavenumbers separated by a specified interval. Through inspection of the program output, an optimum efficiency is then determined. Therefore, the structure of the program is identified by one large wavenumber loop. A flow chart for program WAVLEN is depicted in Figure 25 for reference. The program requires ten input parameters for operation. These are:

- AVGPWR -- Average laser output power in Watts
- RO -- The radius of the output optics in meters
- V1 -- Beginning wavenumber to be calculated in cm-1
- V2 -- Ending wavenumber to be calculated in cm-1
- RANGE -- Range from the laser to the target in kilometers
- FOCRNG -- Focal range of the output optics in kilometers
- BEAMQ -- Beam quality, times diffraction limited
- JITTER -- Mean single axis jitter in microradians
- HOL -- Height above mean sea level of laser in kilometers
- COMPEN -- Percentage of the turbulence induced beam radius corrected by adaptive optics

All distance measurements in the program are converted to meters for consistency. In fact, MKS units are used exten-

sively. One of the first functions performed by WAVLEN is to read in the atmospheric data from the data file MODEL. Subroutine MDLATM performs this operation. Values of pressure in millibars, temperature in degrees Kelvin, and density in grams/cubic cm for both the altitude boundaries and average values for each altitude layer are read. Density values are converted to kilograms/cubic meters, as well.

The next operation begins the calculation of Yura's coherence diameter,  $\rho_0$ . This is done now, outside of the main wavelength loop, to save computer time since much of the calculations are wavelength independent. Two different models are used for the refractive index structure parameter variation with altitude. From ground level to 1000 meters, corresponding to the first temperature inversion, Wyngaard's model is used. The environmental conditions chosen for this model represent mid-morning or mid-afternoon sun angles during a clear day. Further, the height of the laser is assumed to be 50 meters above dry, open fields. The summation for Yura's coherence diameter proceeds in 50 meter increments for these first 1000 meters. For this model, a value for the change in refractive index for a change in temperature is required and is provided by the external function, DNDT. The arguments for this function are local temperature, pressure, and wavelength. An average value of .6 microns is used. Intermediate values of temperature are found through linear interpolation. How-

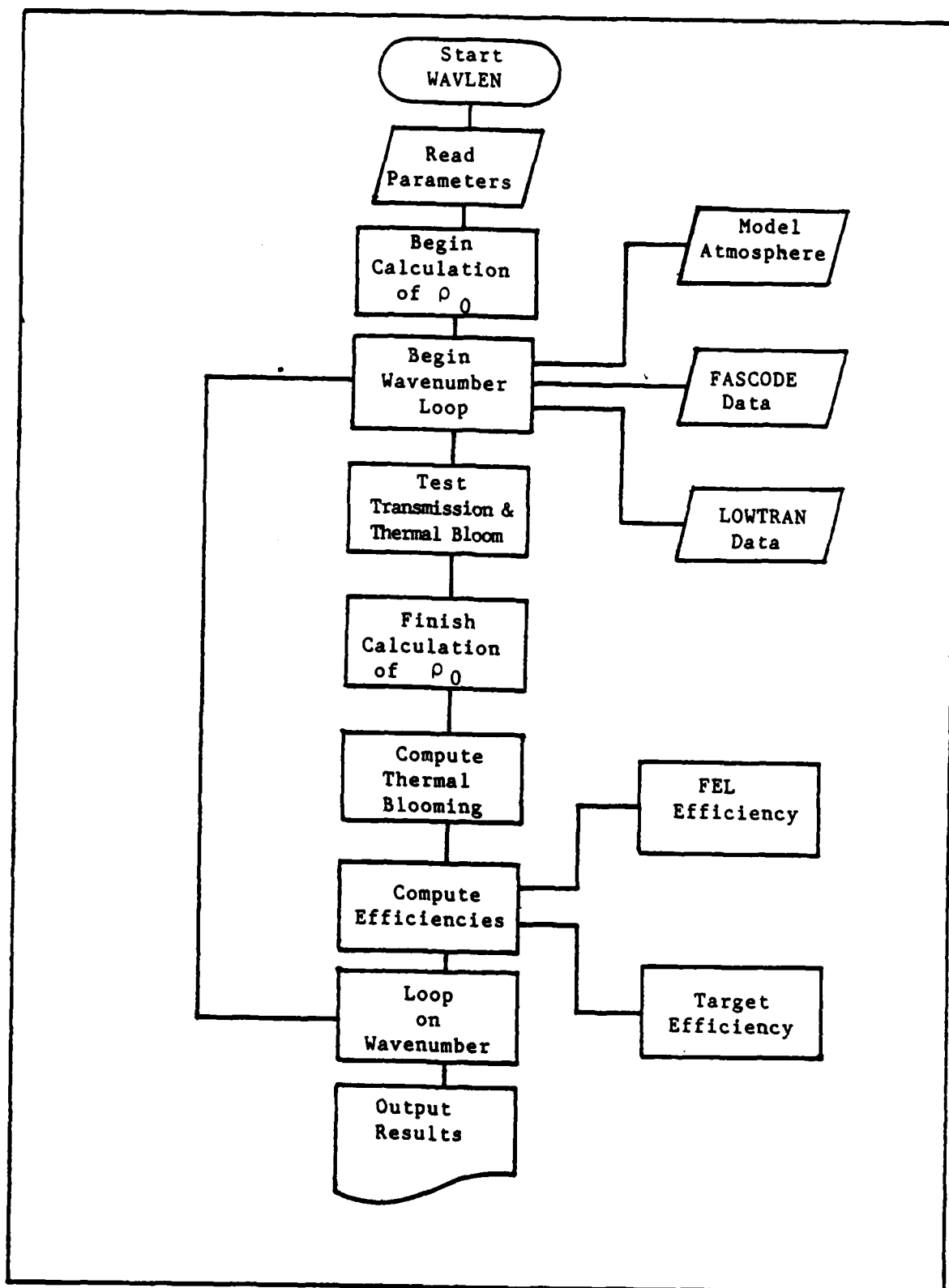


Figure 25. Flow Chart of Program WAVLEN

ever, exponential interpolation is used to determine values of pressure. Here, we have assumed

$$\frac{P}{T} \propto \text{DENSITY} \propto \exp (-z/\text{SCALE HEIGHT}) \quad (100)$$

For any generic exponential function,  $f(z)$ , the graph of the natural logarithm of  $f(z)$  is a straight line. Therefore, intermediate values between  $z=a$  and  $z=b$  can be determined by first employing linear interpolation.

$$\ln f(z) = \ln f(a) + \left( \frac{z - a}{b - a} \right) \ln \left( \frac{f(b)}{f(a)} \right) \quad (101)$$

Taking the exponential of both sides of equation (101) yields:

$$f(z) = f(a) \left( \frac{f(b)}{f(a)} \right)^{\left( \frac{z - a}{b - a} \right)} \quad (102)$$

Above 1000 meters to a height of 25 kilometers, Hufnagel's model of the refractive index structure parameter is employed. Here, the summation to determine  $\rho_0$  is in increments of 1000 meters.

The program WAVLEN next enters the wavenumber loop and calls subroutine FCREAD to read in the molecular absorption information from the data file FCDATA. The wavenumber read by FCREAD determines that wavenumber value to be used throughout the rest of the program. A provision is made in the program to accomodate runs which transition over the end of the spectral

region covered by FASCODE (approximately  $18000\text{ cm}^{-1}$ ). When this point is reached, the variable IFLAG is set to one and the program continues with a specified wavenumber interval (we have chosen  $1.0\text{ cm}^{-1}$ ) and using just the LOWTRAN data for input.

The program passes the wavenumber read by FCREAD when it next calls subroutine LTREAD. This subroutine reads in the information contained in the data file LTDATA. This data is separated by  $5.00\text{ cm}^{-1}$  wavenumber intervals. With one exception, simple linear interpolation is used to find the layer attenuation for the wavenumber of interest. In the case of Rayleigh scattering, however, the interpolation is scaled by wavenumber values to the fourth power. If an end-of-file condition is experienced on the file LTDATA, the program sets IFLAG to two and processing ceases.

To save computer time, WAVLEN makes a quick determination of atmospheric transmission and thermal blooming to see if it is worthwhile proceeding with further calculations for the current wavenumber. The total transmission is determined by adding the contributions from all of the atmospheric attenuation processes. A rough value of Gebhardt's thermal blooming distortion parameter, based on conditions in the first altitude layer, is also calculated. If either the transmission is less than 10% or the thermal blooming distortion parameter is greater than 30 (corresponding to a 98% irradiance loss in the laser beam), then the overall efficiency of the weapon system is set

to zero.

Following completion of the wavelength dependent portion of the computation of Yura's coherence diameter,  $\rho_0$ , the program begins the thermal blooming calculations. The double integration involved in computing the thermal blooming distortion parameter, NI, requires two altitude intervals over which to sum. In the outer summation, the interval is simply the width of the individual altitude layers. For the inner summation, however, each interval is reduced by a factor of one fourth. Tests showed that there is no problem of convergence of the integral with these chosen intervals; reducing the intervals did not alter the final result.

As with the previous calculation of Yura's coherence diameter, intermediate values of temperature are found through linear interpolation and pressure through exponential interpolation. Once these local values of temperature and pressure are determined, they are then used to scale the density.

The determination of the absorption and attenuation coefficients for the thermal blooming calculations requires some explanation. The optical depths computed by FASCODE and LOWTRAN both represent mean values for a given altitude layer. Since the optical depths are proportional to the number density of absorbers or scatterers, which in turn generally scale exponentially with altitude, the mean value of optical depth does not coincide with the middle of the altitude layer. If we as-

sume a constant scale height for the atmosphere of 7.0 kilometers and borrow the concept of 'expected' or mean value from statistics (41:135), we see that

$$\bar{Z} = \int_0^1 Z e^{-Z/7.0} dZ = .46 \quad (103)$$

Therefore, the mean value of the optical depth occurs, not at the midpoint, but rather at an altitude which is 46% from the bottom of the layer. Using these points as references, we can now determine intermediate values of optical depth with exponential interpolation. Finally, to convert the optical depth to an absorption or attenuation coefficient, one must divide by the width of the altitude layer.

To complete the thermal blooming calculations, function REFIDX provides the local index of refraction given the local pressure and temperature and the propagating wavelength and function VX supplies a nominal value of the horizontal wind for a given altitude. Once the thermal blooming distortion parameter, NI, is computed, it becomes the argument to function IREL to determine the irradiance reduction factor for the beam.

The  $1/e^2$  radius of the laser beam at any point along the propagation path is determined by subroutine RADIUS. It combines, in a root-sum-squared technique, the characteristic

radii resulting from the effects of turbulence, jitter, and diffraction and focusing. For focused laser beam, the actual focal range of the output optics is used; however, if a collimated laser beam is desired, the user should input a value of zero for the focal range. The program then sets the focal range to infinity (actually  $10^{25}$  meters) for all beam radius calculations. For turbulence, the program includes the ability to specify the percentage that atmospheric compensation by adaptive optics systems reduces the turbulence induced beam radius.

The last portion of program WAVLEN determines the different efficiencies at a given wavenumber and outputs the results. A propagation efficiency is computed according to equation (54). The free electron laser efficiency with energy recovery is supplied by subroutine FELOPT and a target coupling efficiency is provided by function TGTEFF. These three efficiencies are then multiplied together to arrive at an overall weapon system efficiency for that wavenumber. The program automatically keeps track of the best propagation efficiency and best overall efficiency over the run.

#### Program Limitations

Aside from the basic assumptions in the theory and the assumptions we have chosen to make, the program possess certain limitations. Even though LOWTRAN and FASCODE can compute optical depths for slant paths through the atmosphere, WAVLEN

can only accomodate vertical propagation paths. Primarily, this is due to the many altitude dependent parameters used in the turbulence and thermal blooming calculations. Also, the program is structured to use the entire atmosphere, i.e. the selected range to the target must be greater than 100 kilometers. Finally, the height of the laser must correspond to one of the boundaries of the altitude layers. In essence, this requires that the laser height be specified to the nearest kilometer above sea level. The parameter, COMPEN, which adjusts the effects of atmospheric turbulence on the beam radius, is strictly a scaling factor and should not be confused with degrees of compensation quoted for actual adaptive optics systems.

It should be emphasized that the efficiency values derived by the program do not represent actual values. In some cases, proportionality constants have been excluded. The purpose of the study is to assess the relative efficiencies between wavelengths and not to determine the actual values.

## VI . Analysis Results

The model developed for this study and presented in the preceeding chapters, was exercised in order to examine the interactions between the wavelength dependent relationships in the system and to select a 'best' wavelength for operation. This chapter presents the results of this analysis.

### Selection of Parameters for the Baseline Case

A baseline case was used as a point of departure for this analysis and to validate some of the factors within the model. Therefore, the selection of input parameters for this baseline case was somewhat critical. This section will discuss that selection process.

A mid-latitude, summer atmospheric model was used for the baseline calculations. In addition, a Rural boundary layer aerosol model with a 23 km visibility was initially assumed.

An important consideration for this analysis is, of course, the wavelength region to be examined. This region must be within the expected capabilities of the free electron laser device and should include areas where the atmospheric attenuation is low. Presumably, this region falls in or near the visible portion of the spectrum. We have chosen the wavelength range from 1.14 micrometers to .34 micrometers ( $8750.0 \text{ cm}^{-1}$  to  $29000.0 \text{ cm}^{-1}$ ) for this study. At wavelengths shorter than .34 micrometers, it is expected that Rayleigh scattering and the onset of significant ozone attenuation in

the ultraviolet region will combine to negate any advantage to shorter wavelengths. Likewise, at wavelengths longer than 1.14 micrometers, the spectral atmospheric transmission curve enters a strongly absorbing region due to water vapor (see Figure 12) and would preclude laser operation there.

The selection of laser power and radius of the output optics went hand in hand. In advocating short wavelengths laser systems for the military, Canavan uses the scaling parameter of 'brightness' to assess the capabilities of different laser systems (42:3). Brightness is the power per solid angle illuminated by the laser system and can be approximated by the following expression.

$$\text{Brightness} = \frac{PD^2}{\lambda^2} \quad (104)$$

where P is the laser power, D is the diameter of the output optics, and  $\lambda$  is the laser wavelength. Ignoring atmospheric losses, Canavan claims that in order to accomplish a strategic defense mission against ballistic missiles, a laser system would have to produce a brightness on the order of  $10^{21}$  watts/steradian (42:7). For wavelengths in the visible, this brightness can be achieved through a 10 megawatt laser with 5 meter optics.

Such a combination of power and optics could easily accomplish an anti-satellite mission for any conceivable orbit altitude. However, the ballistic missile defense mission would require relay mirrors in 1000 to 2000 km orbits

(43:79). If one restricts oneself to shooting through the atmosphere at zenith angles no greater than 45 degrees, simple geometry tells us that two such mirrors would be required and would result in a total propagation distance from laser to target on the order of 20,000 km. Therefore, for this baseline study, a selected range of 20,000 km appeared appropriate. In addition, a focal range of 20,000 km was chosen, equaling approximately one half of the average Rayleigh range.

The choices of 1.2 for beam quality, 0.2 microradians for jitter, 1000 meters for the mean sea level altitude of the laser and .85 for the degree of turbulence compensation were, admittedly, somewhat arbitrary. The beam quality for a free electron laser is expected to be quite good, and the chosen value represents this assumption. The free electron laser does not contain large mechanical moving parts, and therefore, is not expected to suffer significantly from jitter. The value of .2 microradians represents an optimistic jitter component. Presumably, the laser weapon would not be placed at a sea level altitude, and therefore, 1000 meters might represent a suitable starting point. As mentioned earlier, the factor used in this model for turbulence compensation is not to be compared to actual compensation factors quoted for adaptive optics systems; it is simply treated as a scaling parameter. In the visible region, approximately 85% of the total turbulence induced beam spread is due to the instantaneous, small scale beam spread component (44:30). A choice of .85 for the baseline case, thus, represents outstanding

compensation for this small scale component and places the turbulence induced beam radius on the same order of magnitude as those of diffraction and jitter effects.

Therefore, to summarize, the baseline case for this analysis will include the following.

Average laser power	= 10 megawatts
Radius of output optics	= 2.5 meters
Initial wavenumber	= $8750.0 \text{ cm}^{-1}$
Final wavenumber	= $29000.0 \text{ cm}^{-1}$
Propagation range	= 20,000 km
Focus range	= 20,000 km
Beam quality	= 1.2
Single axis jitter	= .2 microradians
Height of laser (MSL)	= 1000 meters
Turbulence compensation	= .85

#### Baseline results

The following 12 pages (Figures 26 through 37) contain the plotted results of the baseline case. The plots have been mistakenly normalized such that an efficiency value of one corresponds to  $18200.0 \text{ cm}^{-1}$ . Although this results in displayed efficiencies greater than one, the relative efficiencies between wavenumbers remains the same.

As expected, the structure of the efficiency curve is dominated by the variations caused by atmospheric molecular absorption. Most of the absorption lines in the region between  $8750$  and  $13000 \text{ cm}^{-1}$  are caused by water vapor and carbon dioxide, and in some places, completely negates laser operation there.

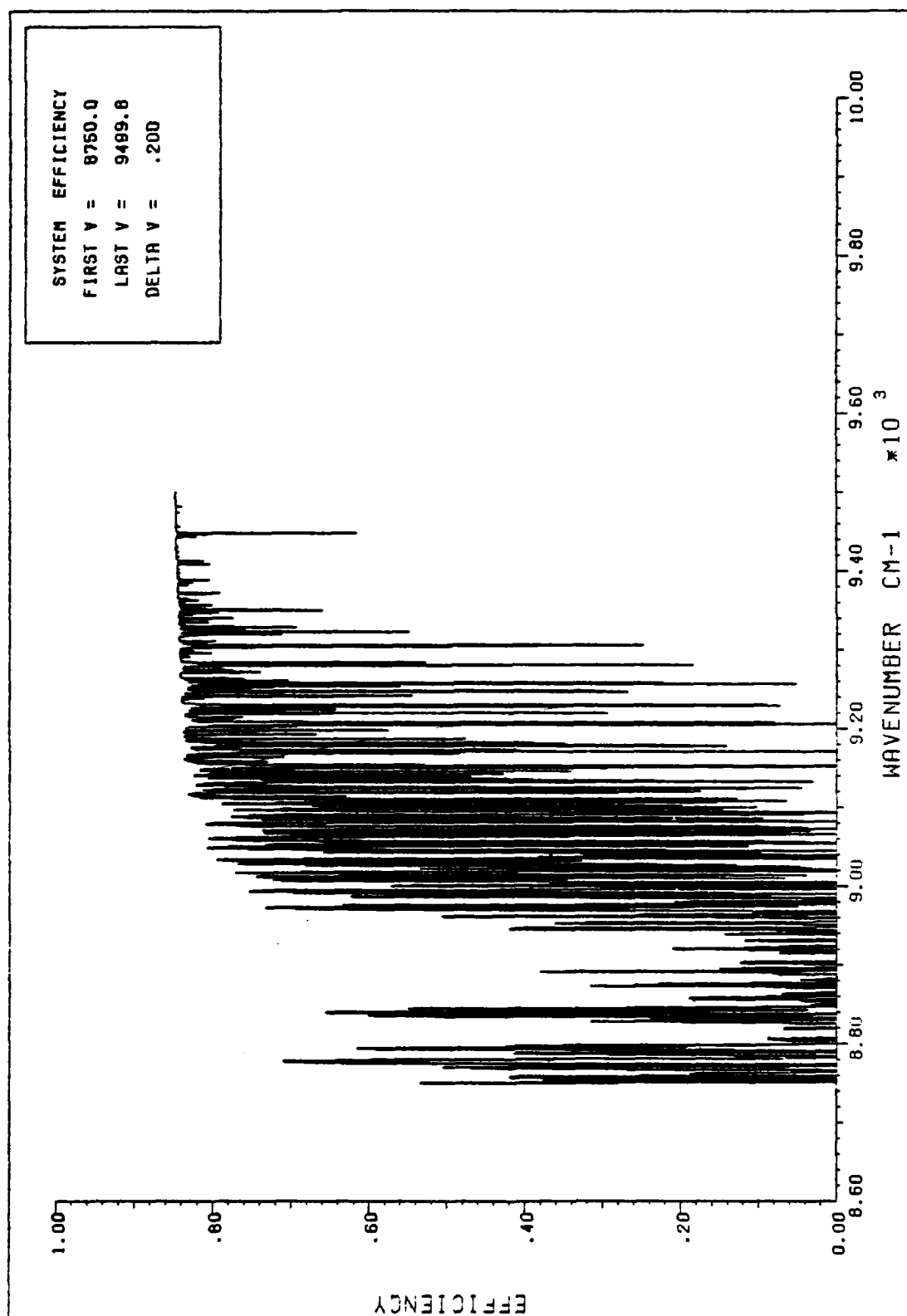


Figure 26. Overall System Efficiency ( 8750 - 9500  $\text{cm}^{-1}$  )

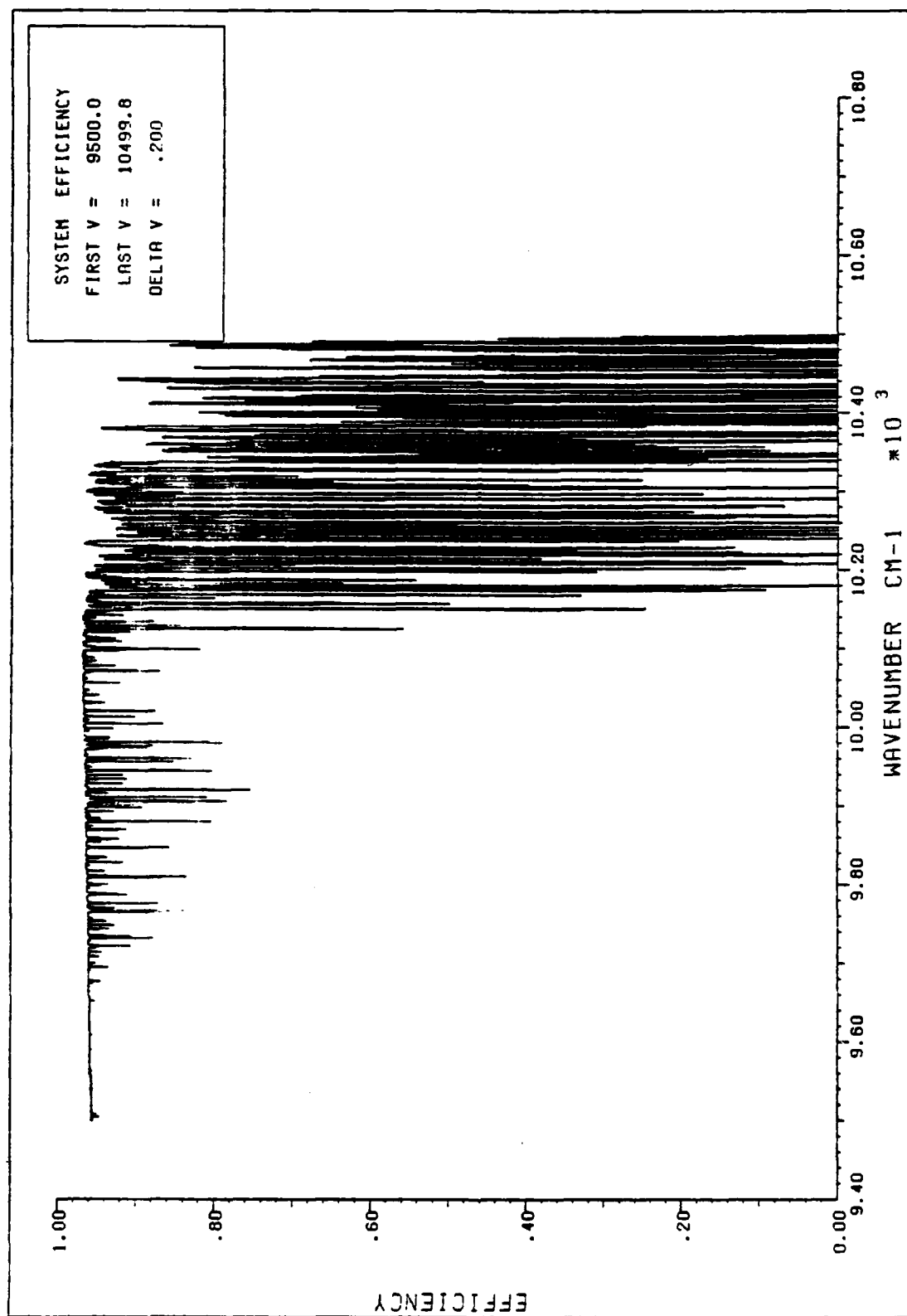


Figure 27. Overall System Efficiency ( 9500 - 10500  $\text{cm}^{-1}$  )

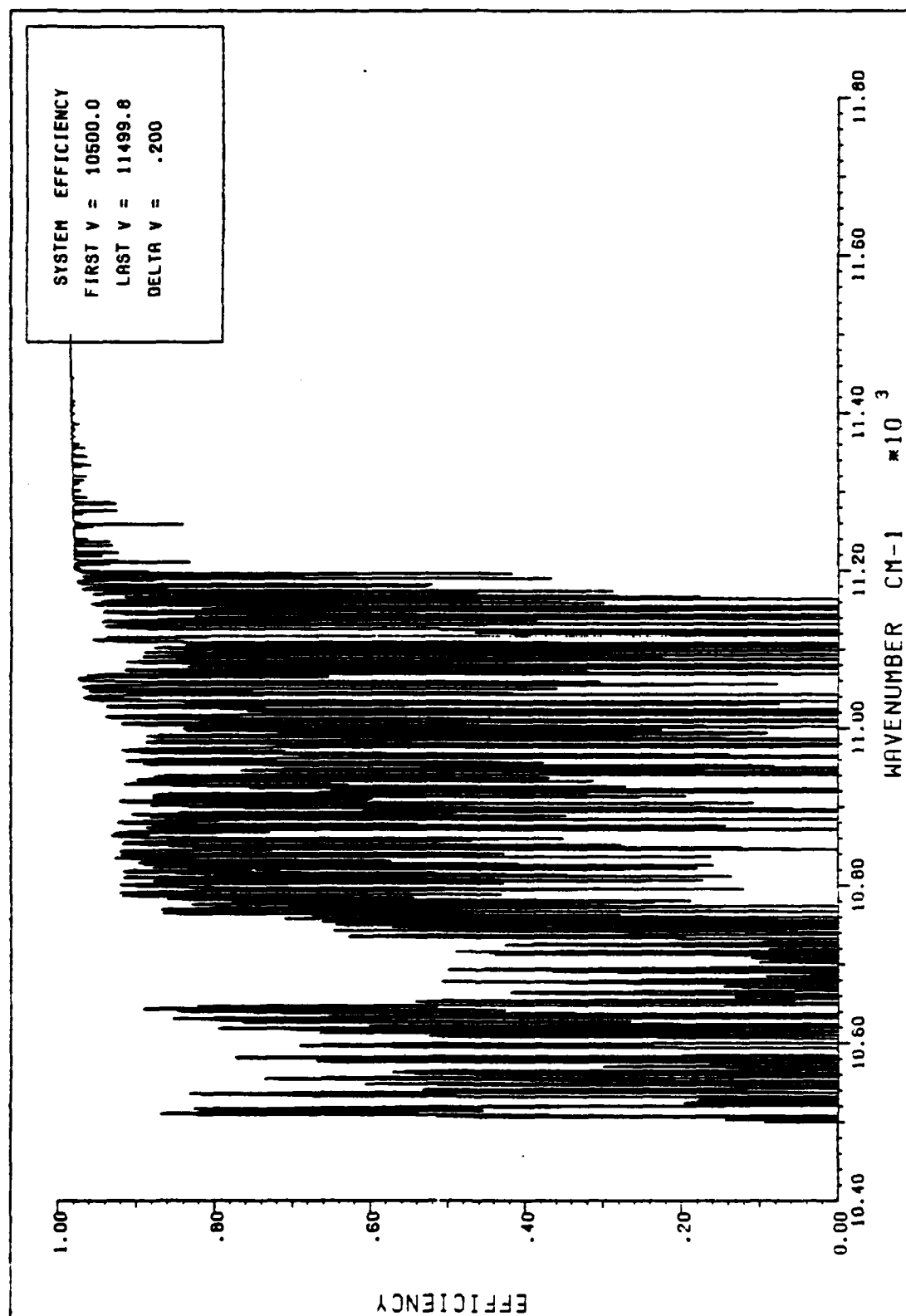


Figure 28. Overall System Efficiency ( 10500 - 11500  $\text{cm}^{-1}$  )

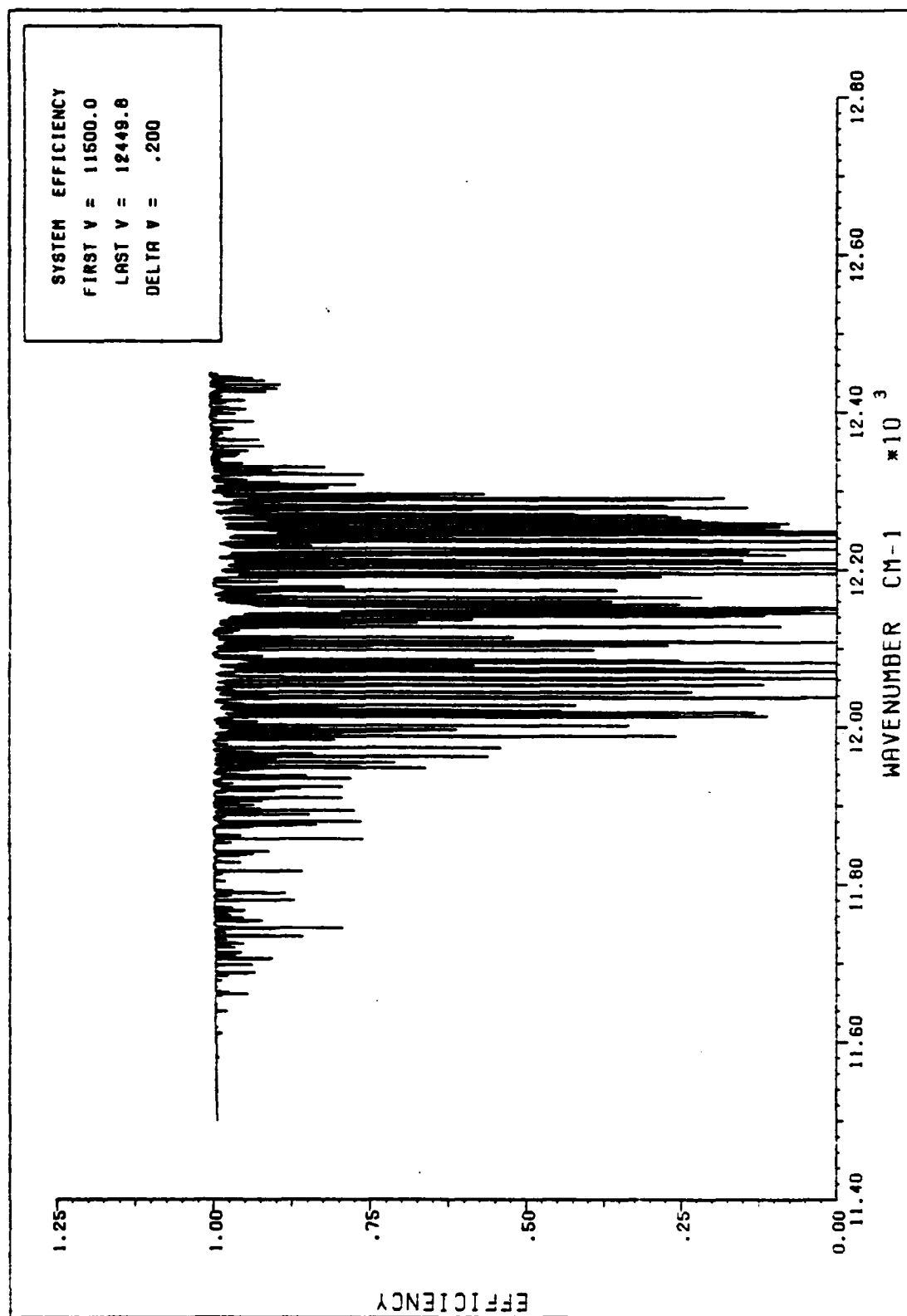


Figure 29. Overall System Efficiency ( 11500 - 12450  $\text{cm}^{-1}$  )

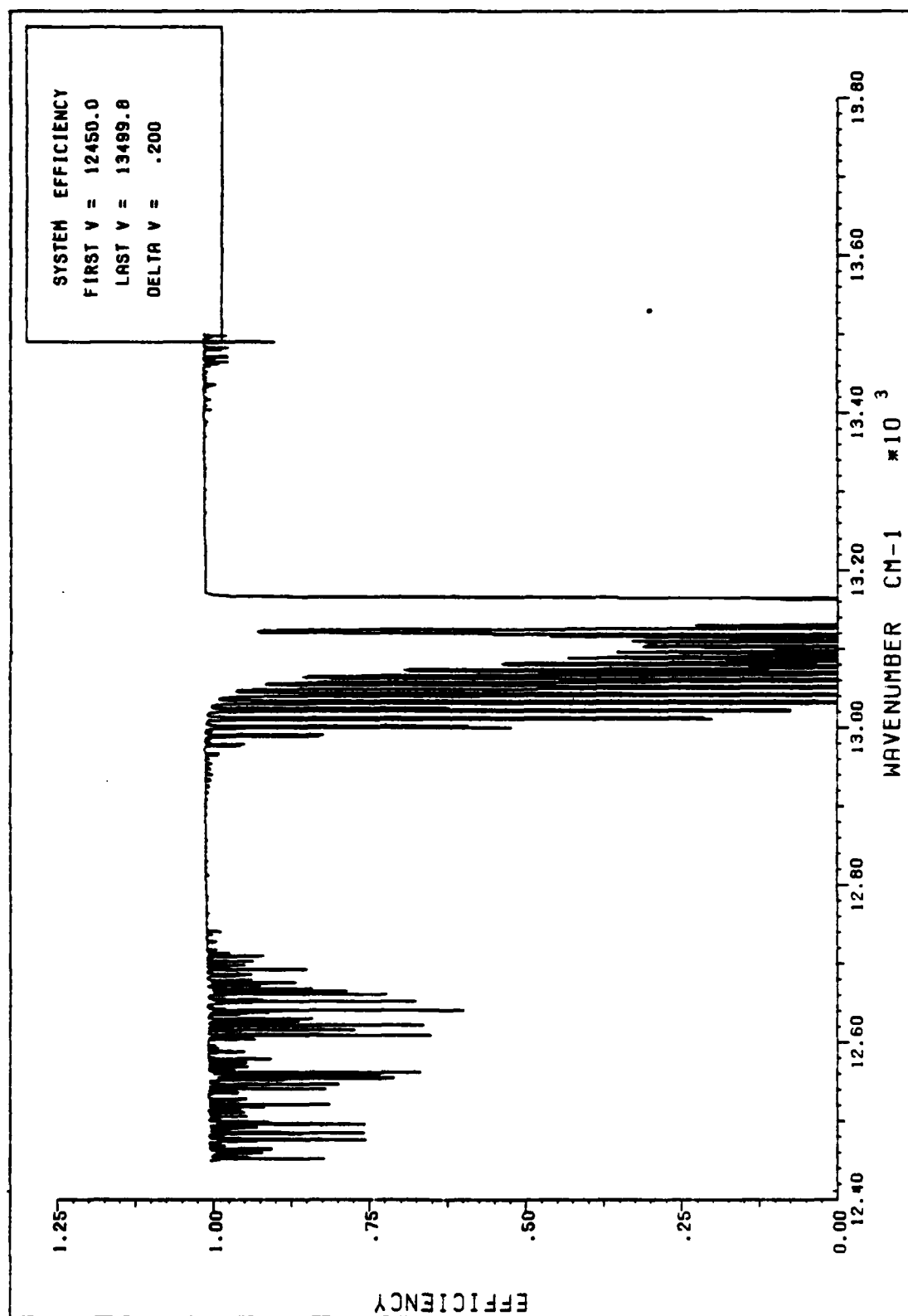


Figure 30. Overall System Efficiency ( 12450 - 13500 cm<sup>-1</sup> )

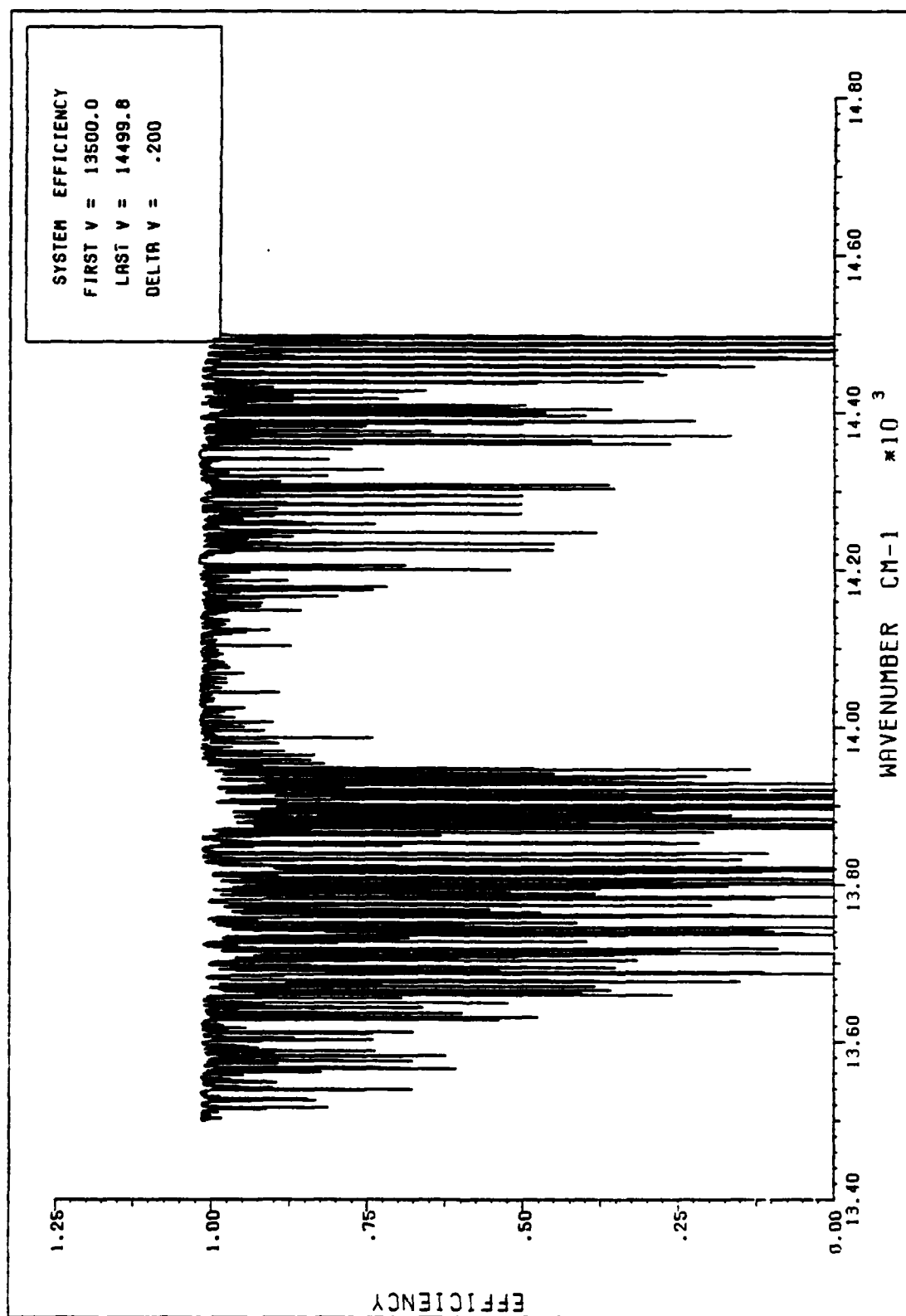


Figure 31. Overall System Efficiency ( 13500 - 14500  $\text{cm}^{-1}$  )

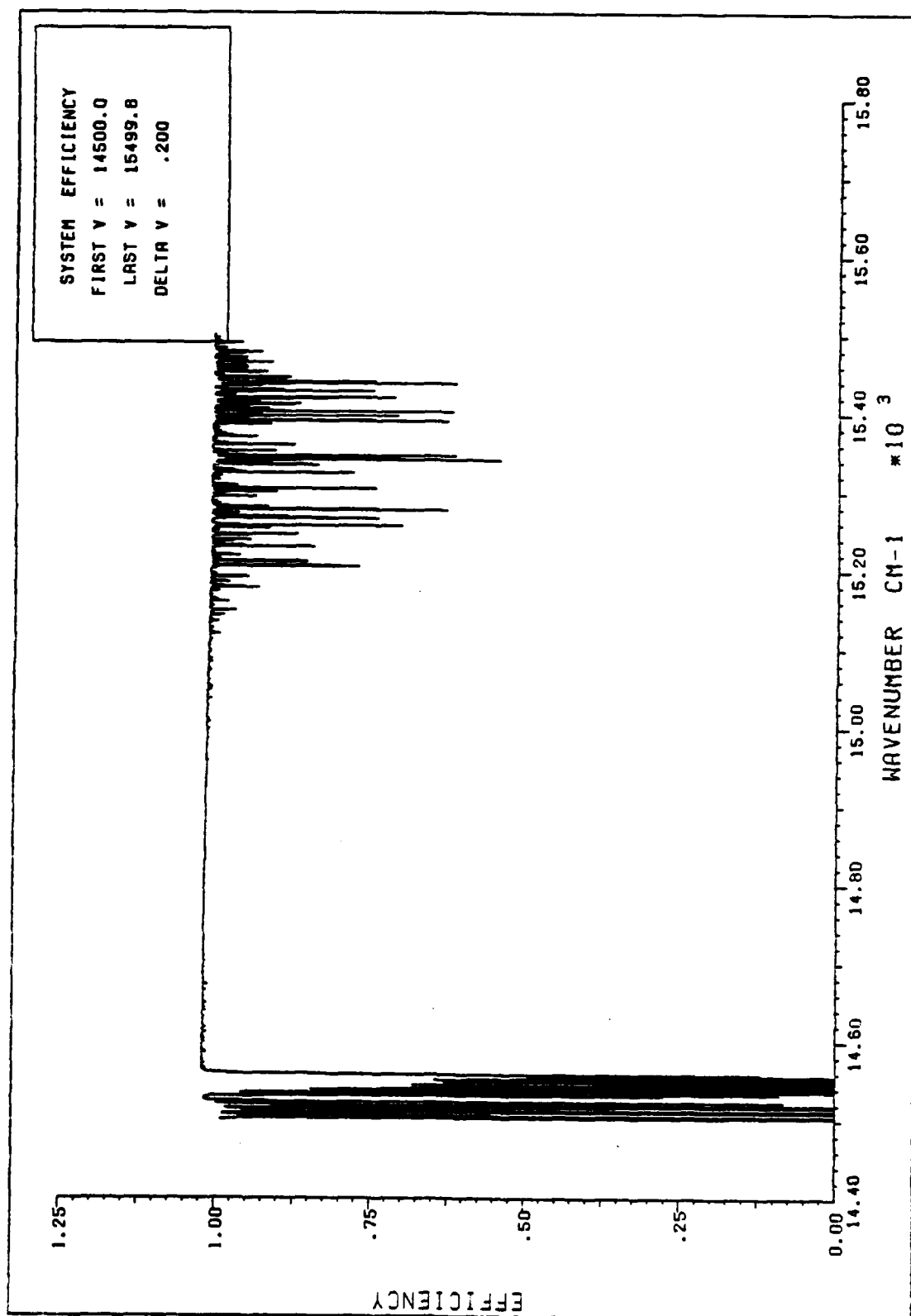


Figure 32. Overall System Efficiency ( 14500 - 15500 cm<sup>-1</sup> )

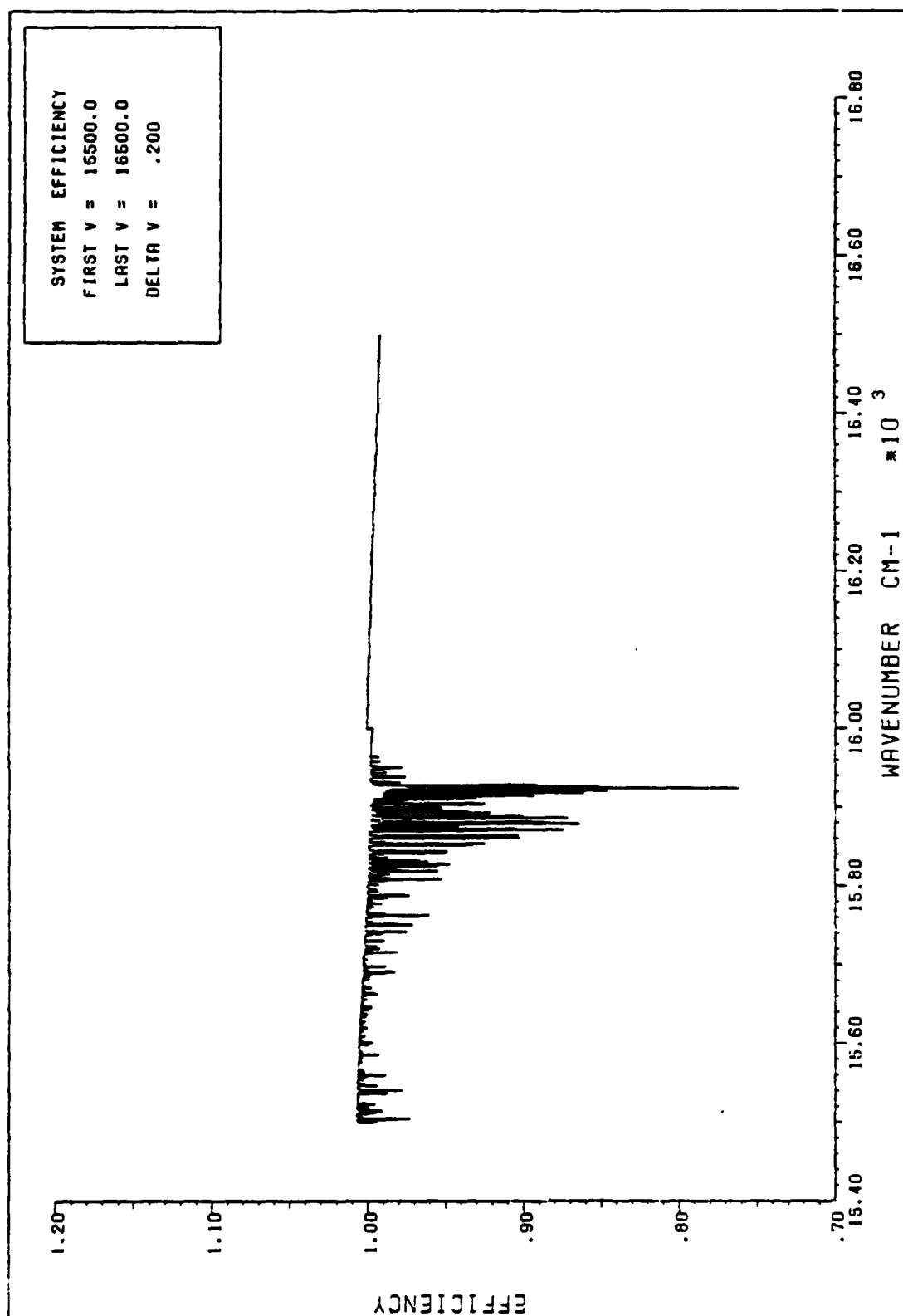


Figure 33. Overall System Efficiency ( 15500 - 16500  $\text{cm}^{-1}$  )

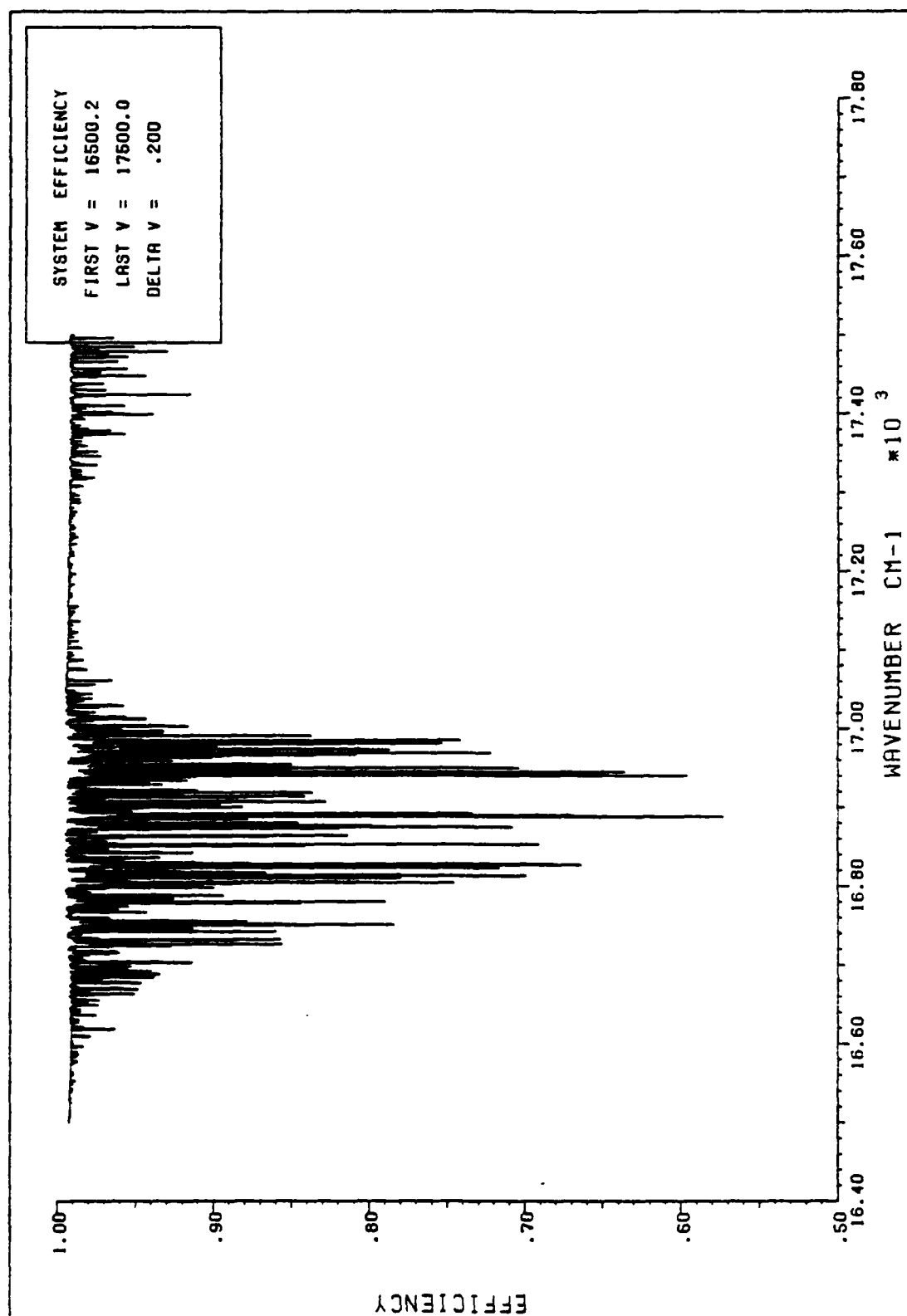


Figure 34. Overall System Efficiency ( 16500 - 17500  $\text{cm}^{-1}$  )

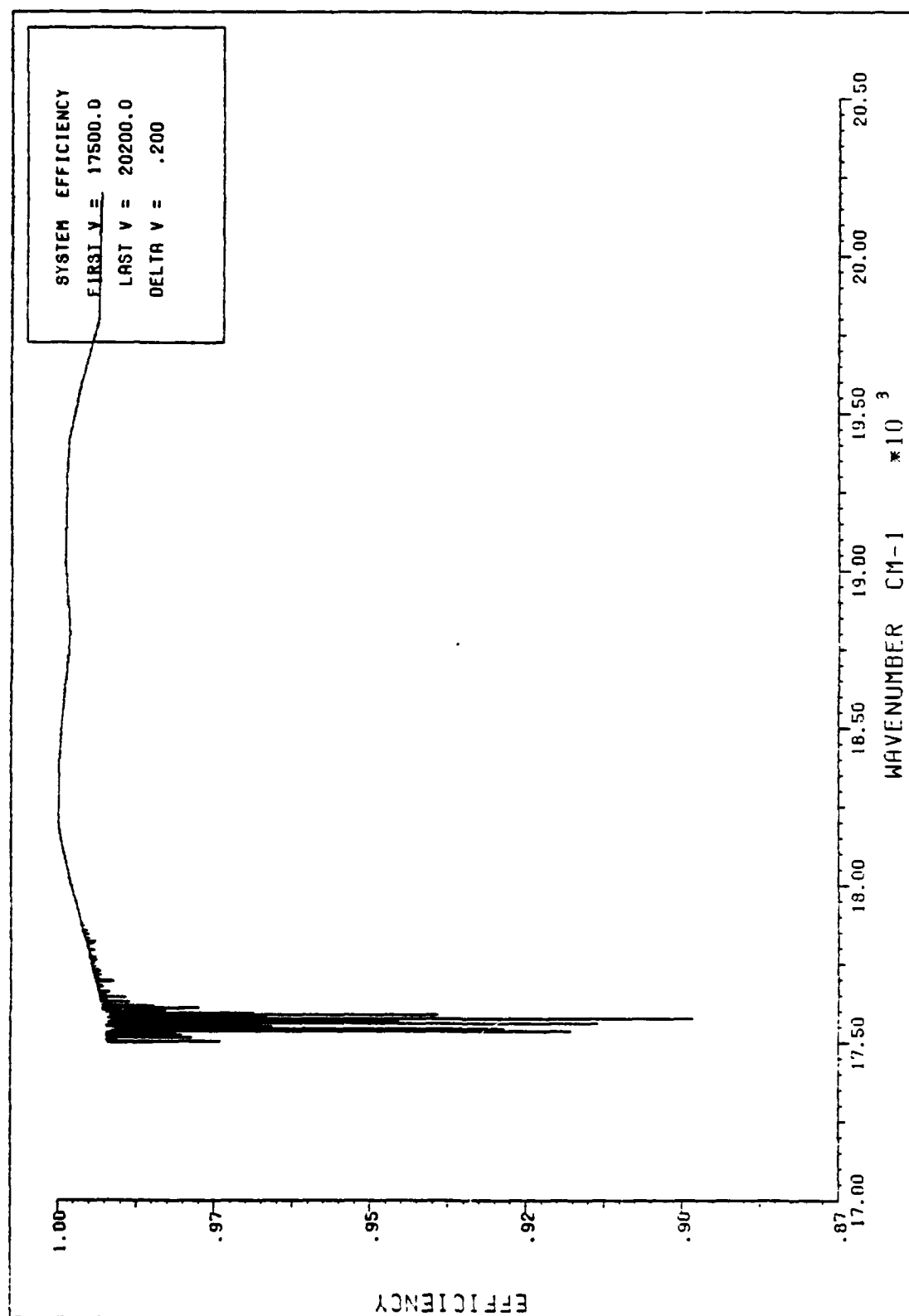


Figure 35. Overall System Efficiency ( 17500 - 20200 cm<sup>-1</sup> )

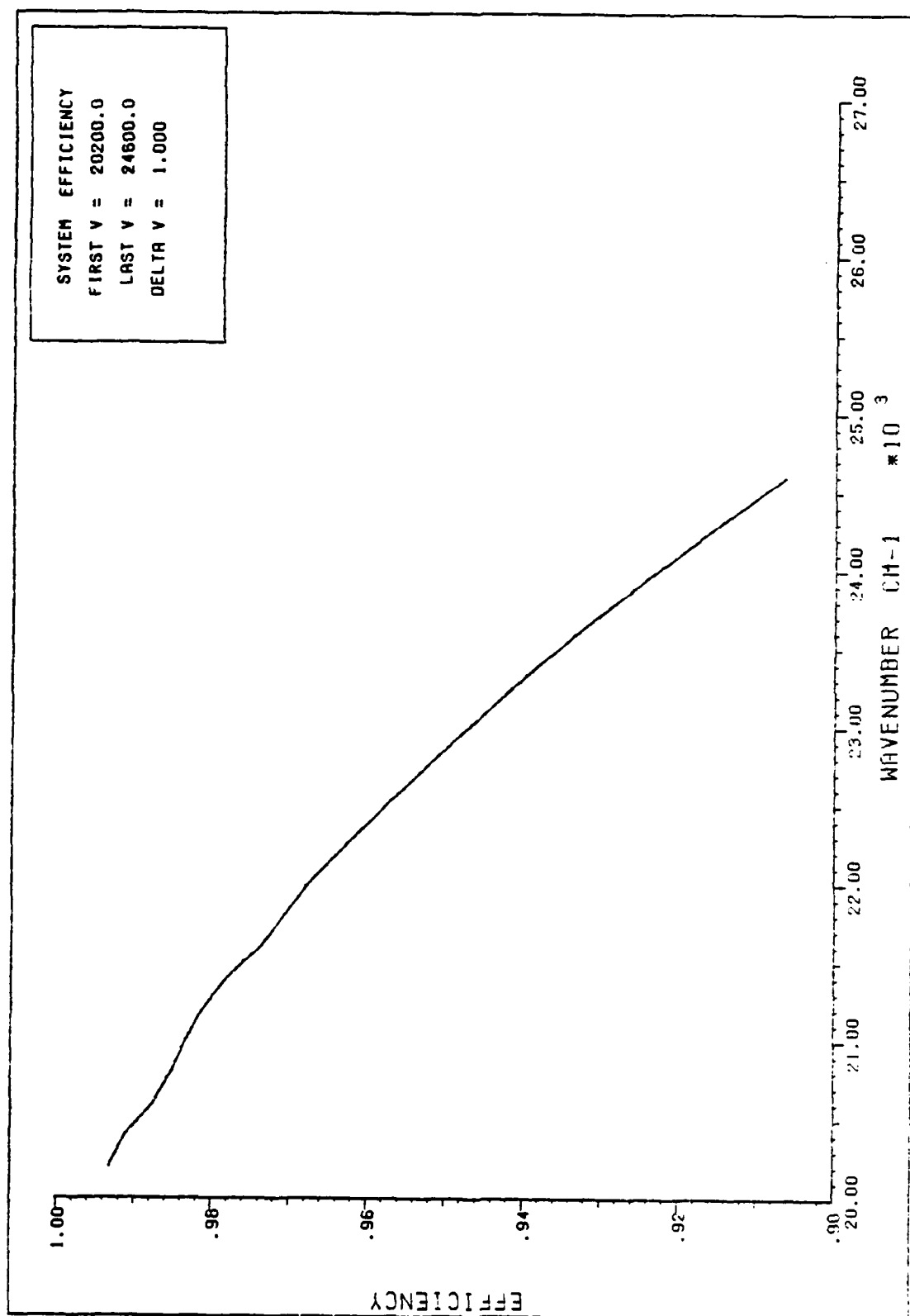


Figure 36. Overall System Efficiency ( 20200 - 24600  $\text{cm}^{-1}$  )

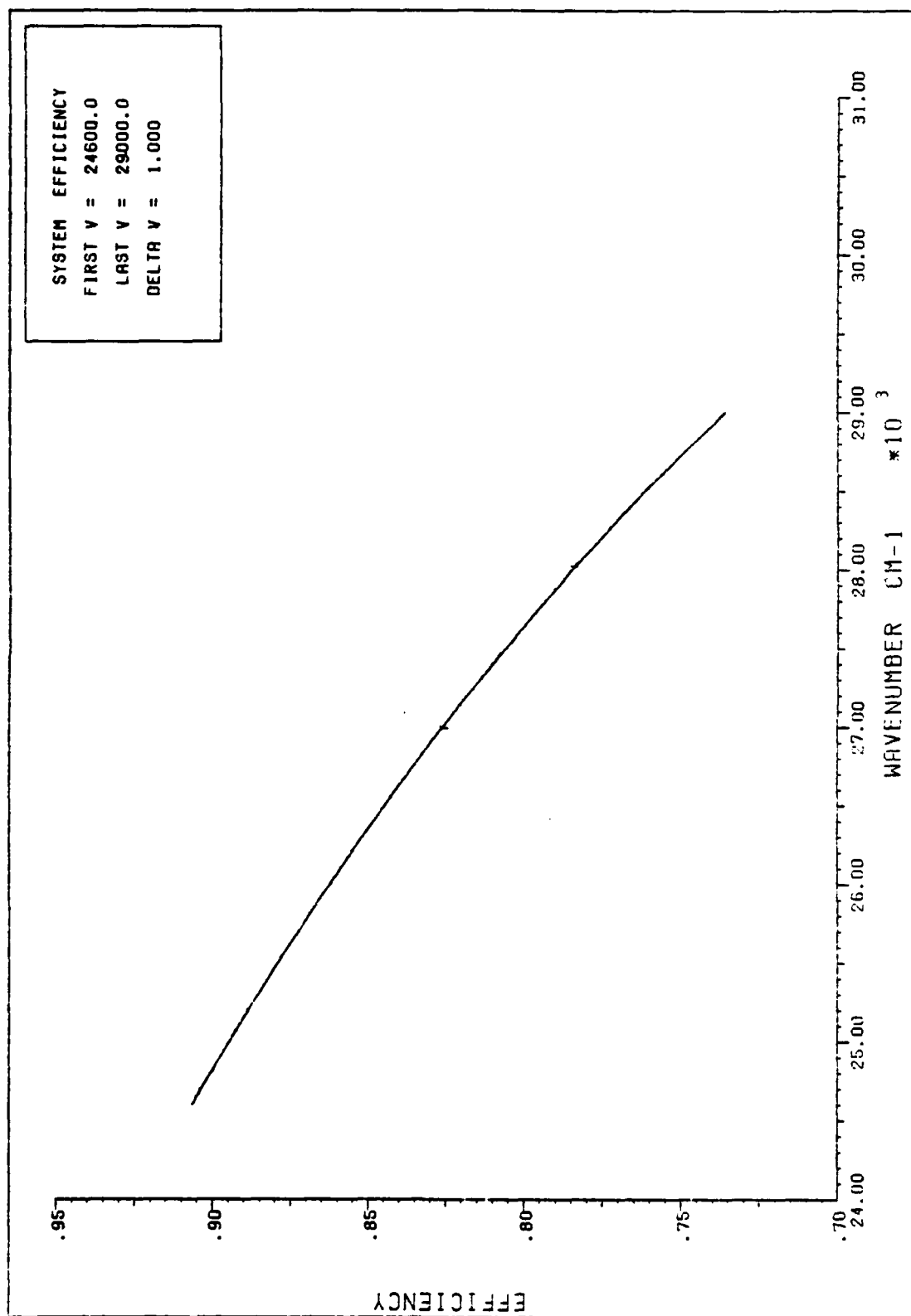


Figure 37. Overall System Efficiency ( 24600 - 29000 cm<sup>-1</sup> )

The optimum wavenumber for this baseline scenario occurs at  $14347.2 \text{ cm}^{-1}$  ( .697 micrometers) with a computed efficiency of .5079%. Yet, the term 'optimum' must be used with caution. Efficiencies within 1% of this optimum value can be found from  $12476.0$  to  $15225.6 \text{ cm}^{-1}$  (approximately .657 to .801 micrometers). Of course, the cumulative errors and basic assumptions within the model far exceed 1%. The relatively flat nature of the top line structure or 'envelope' of the efficiency curve between  $10000$  and  $17500 \text{ cm}^{-1}$  was not expected. It would appear at first glance that the competition among the wavelength dependent relationships produces an overall system efficiency which changes very little over a relatively broad region. Any wavelength selected within this region, as long as it avoided a molecular absorption feature, would essentially be equally efficient. In the next sections, we will proceed to examine these relationships further in an attempt to understand exactly what is driving the top level structure of the efficiency curve.

Thermal Blooming. With the parameters chosen for the baseline case, thermal blooming effects were not significant. Tests runs were accomplished where the laser power was increased in 10 megawatts increments. Not until a laser power of 50 megawatts was reached did the results change appreciably. Even then, only regions of significant molecular absorption were affected. In no instant did thermal blooming affect the overall efficiency when the wavelength did not

coincide with a molecular absorption feature. The aerosol absorption in the atmosphere computed by LOWTRAN proved to be a very small percentage of total atmospheric absorption. Therefore, aerosols did not contribute to heating the atmosphere to any significant degree. Another reason for the minor impact of thermal blooming, even within absorbing regions, was perhaps the model we selected for the local wind. At the 1000 meter altitude of the laser, the local wind was computed to be 11.2 meters/sec or 25 miles per hour. This value seems rather large and could perhaps, in and of itself have prevented the onset of thermal blooming in those cases involving modest laser powers and weakly absorbing atmospheric conditions.

Atmospheric Transmission. The individual optical depth due to aerosols, ozone and Rayleigh scattering were extracted during program execution and summed over the applicable atmospheric layers. With these values, a transmission factor attributable to each effect was determined. These were used to examine the overall structure of the efficiency curve and to validate this portion of the model as well.

The individual spectral transmission curves for these three effects are found in Figures 38, 39, and 40. As expected, aerosol transmission tended to favor the longer wavelengths (lower wavenumbers). This factor proved to be a rather significant issue, varying by a factor of two throughout the spectral range of the study. The slight undulation

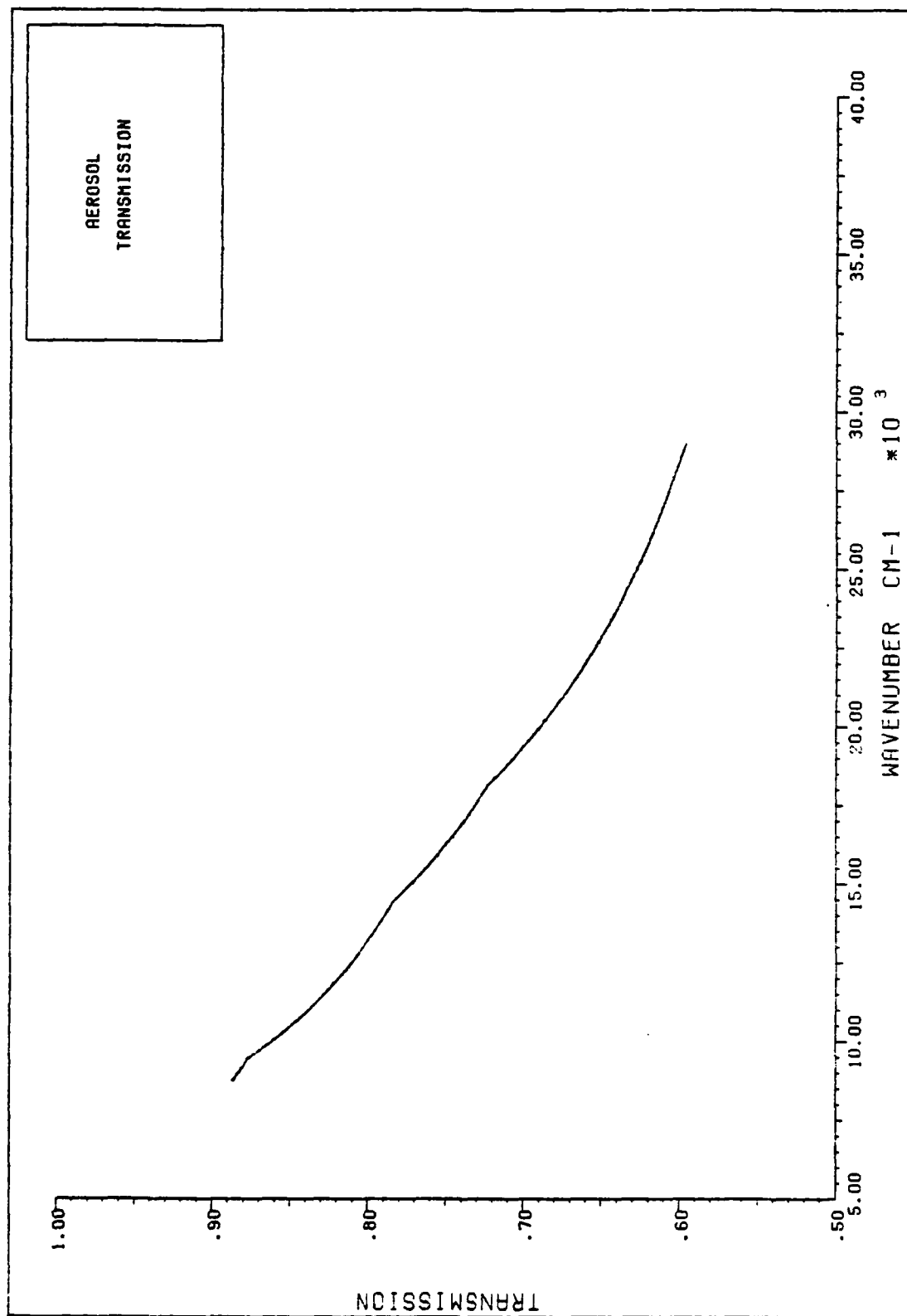


Figure 38. Aerosol Transmission

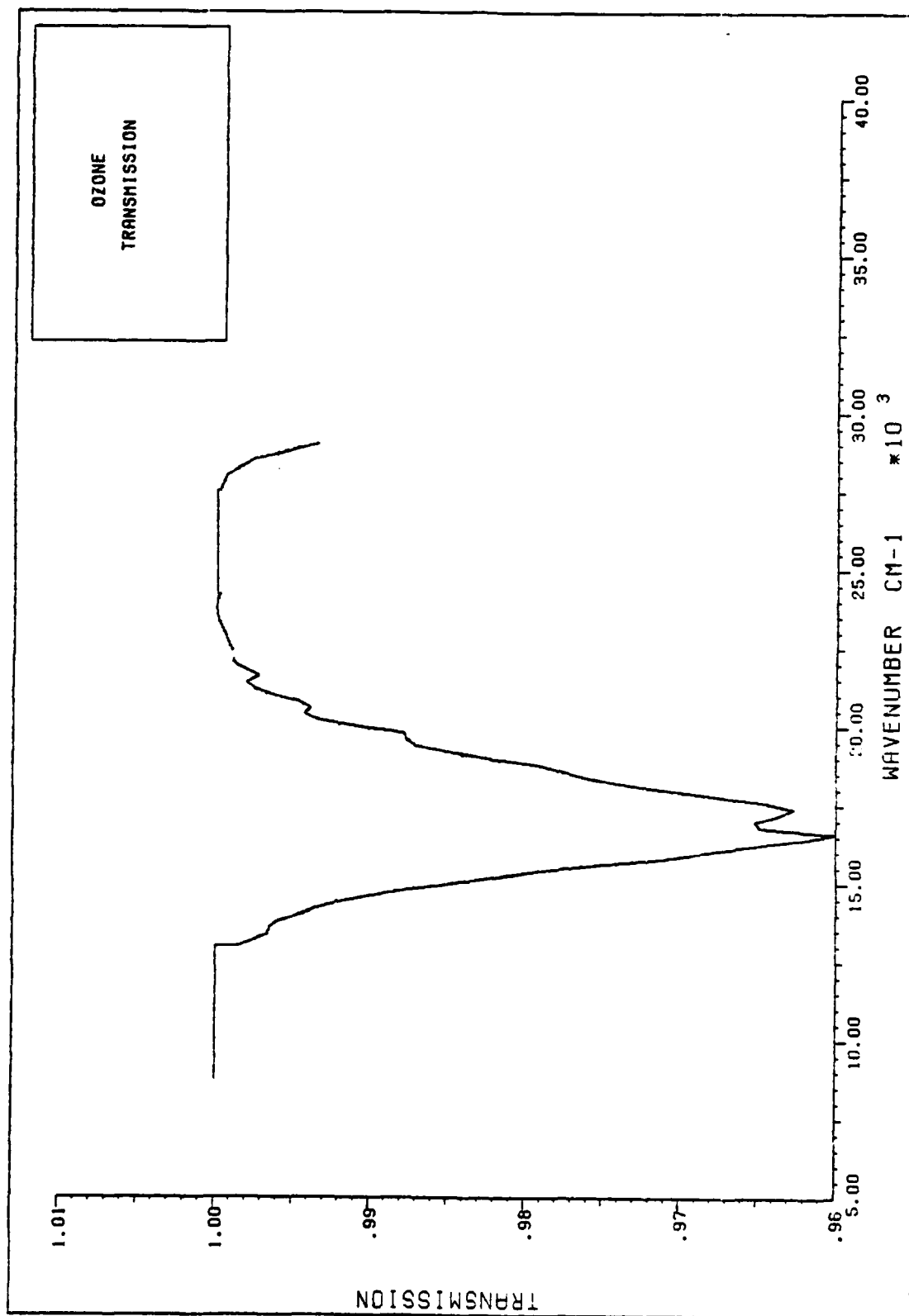


Figure 39. Ozone Transmission

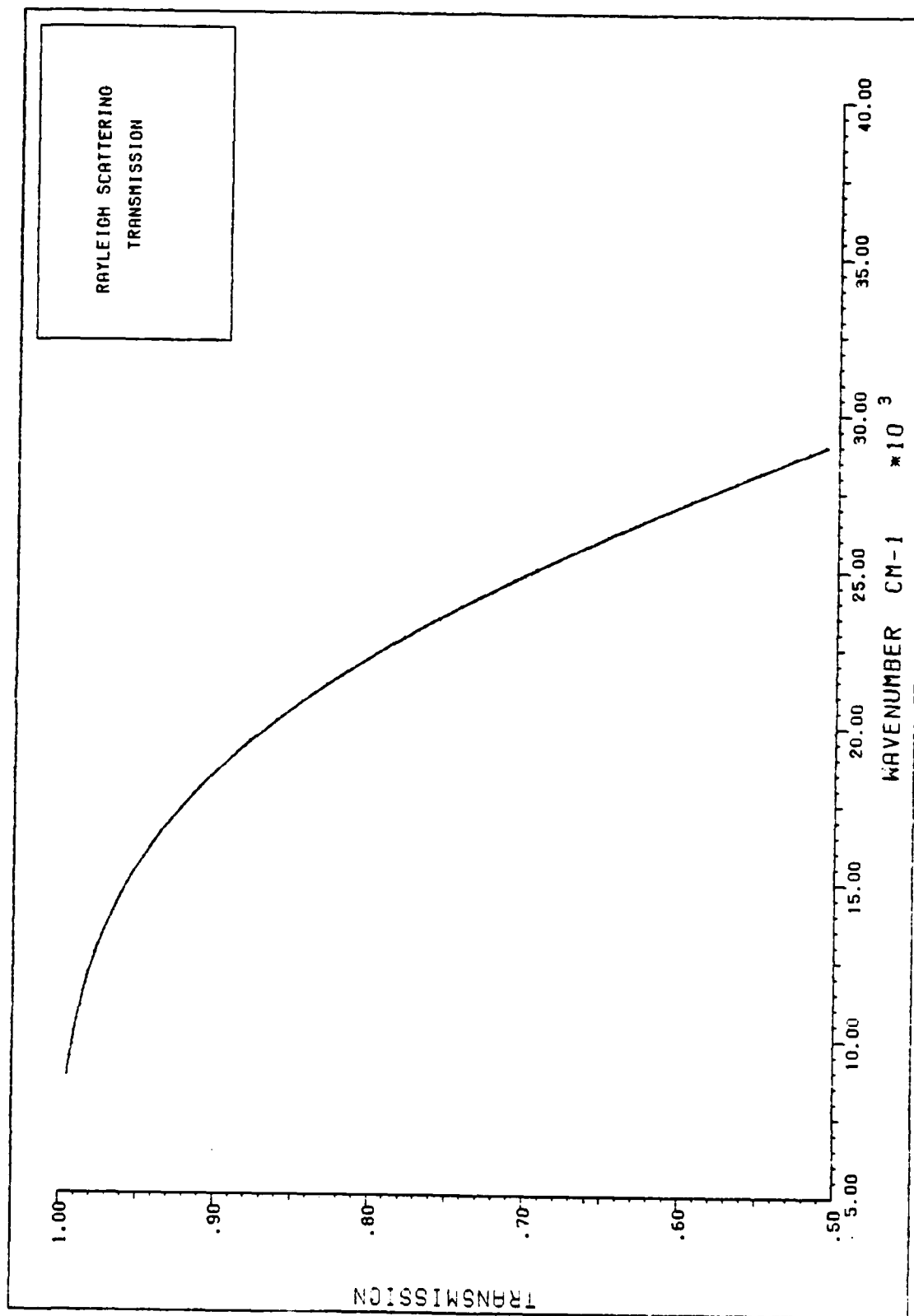


Figure 40. Rayleigh Scattering Transmission

in the curve are presumably caused by LOWTRAN's use of specific aerosol size distributions in computing attenuation coefficients, as explained in Chapter III. Interpolation within both LOWTRAN and our program undoubtedly lead to further inaccuracies.

The ozone transmission curve reflects the weak absorption feature of ozone in the midportion of the visible spectrum. This curve is identical to the curve in Figure 16. This absorbing region causes the shallow yet significant, dip in the computed efficiency curves between 15000 and 18200  $\text{cm}^{-1}$ . Also, one can note the beginnings of the ultra-violet ozone absorption in the far right of the curve in Figure 39. Since the majority of ozone attenuation occurs at higher altitudes, the height of the laser is expected to have little bearing on this curve.

Finally, the Rayleigh scattering curve depicts the strong wavelength dependence of this effect. In fact, it can be shown that in the high wavenumber region of the spectrum, Rayleigh scattering is indeed the dominant factor. The slope of the Rayleigh scattering curve in Figure 40 between 27000 and 28000  $\text{cm}^{-1}$  is within 10% of the slope in the efficiency curve, Figure 37, for the same region.

Beam Radius. The total efficiency of the laser system scales as one over the square of the laser beam radius at the target, therefore, beam radius determination should be very significant. As in the case of atmospheric transmission, values of the individual components of the beam radius were

output from the main program for examination.

The beam radius which results from beam diffraction effects was expected to scale inversely with the wavenumber of the laser radiation, favoring higher wavenumber. Examination of the plot in Figure 41 indicates that this was indeed the case and hand calculations confirmed the values. Further, the effects of focusing can be seen as the beam radius at the target is, for high wavenumbers, reduced to values smaller than the laser output optics. Although not plotted, the effects of jitter produced the expected constant radius across the spectrum.

For this analysis, we purposely selected atmospheric conditions which were unfavorable for turbulence. This choice proved to be very significant. The beam radius which results from turbulence effects was expected to be a very weak function of wavenumber (to the  $1/5$  power) and to favor the lower wavenumbers. Figure 42 shows this weak wavenumber dependence. One might reasonably expect that the stronger wavenumber dependence in the diffraction effect to win out over the weaker dependence in turbulence. However, this proved not to be the case. Even with our 85% reduction in turbulence induced beam radius to account for some degree of atmospheric compensation, this radius was, in the low wavenumber end of the spectrum, twice the diffraction radius and fully 10 times the diffraction radius in the high wavenumber end of the spectrum. The result being that, when the individual beam effects are combined, the total beam radius,

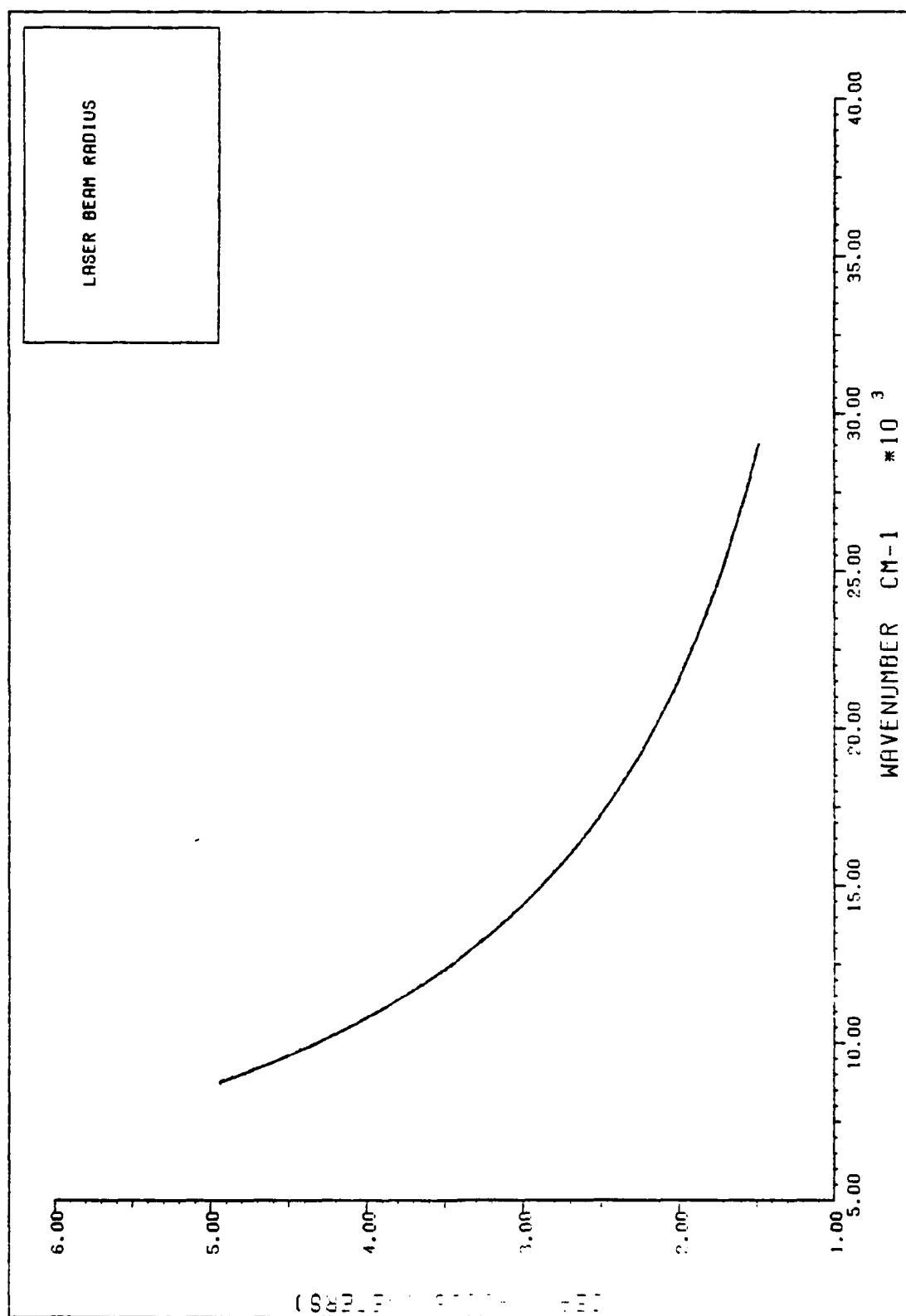


Figure 41. Beam Radius Due to Diffraction

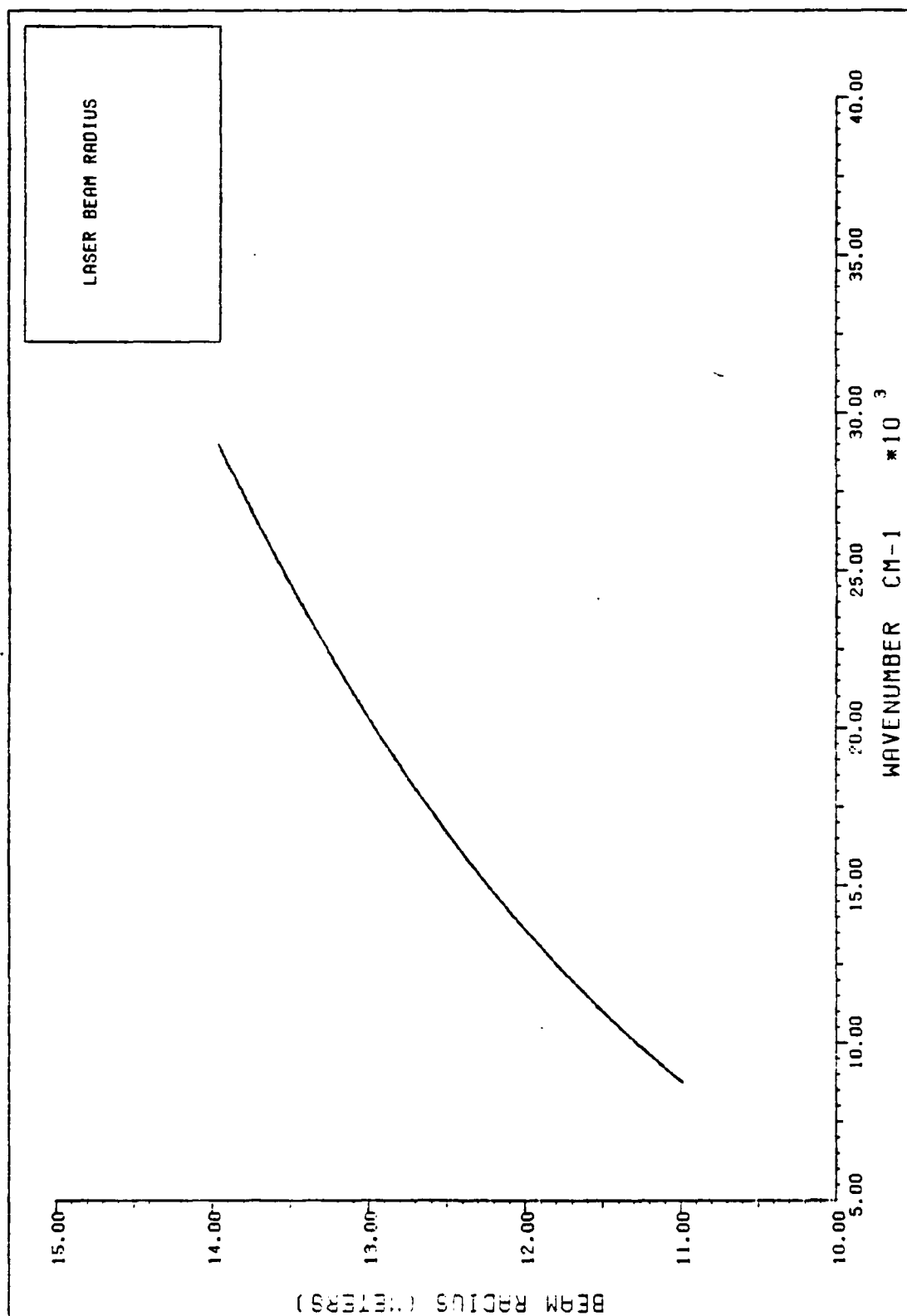


Figure 42. Beam Radius Due to Turbulence

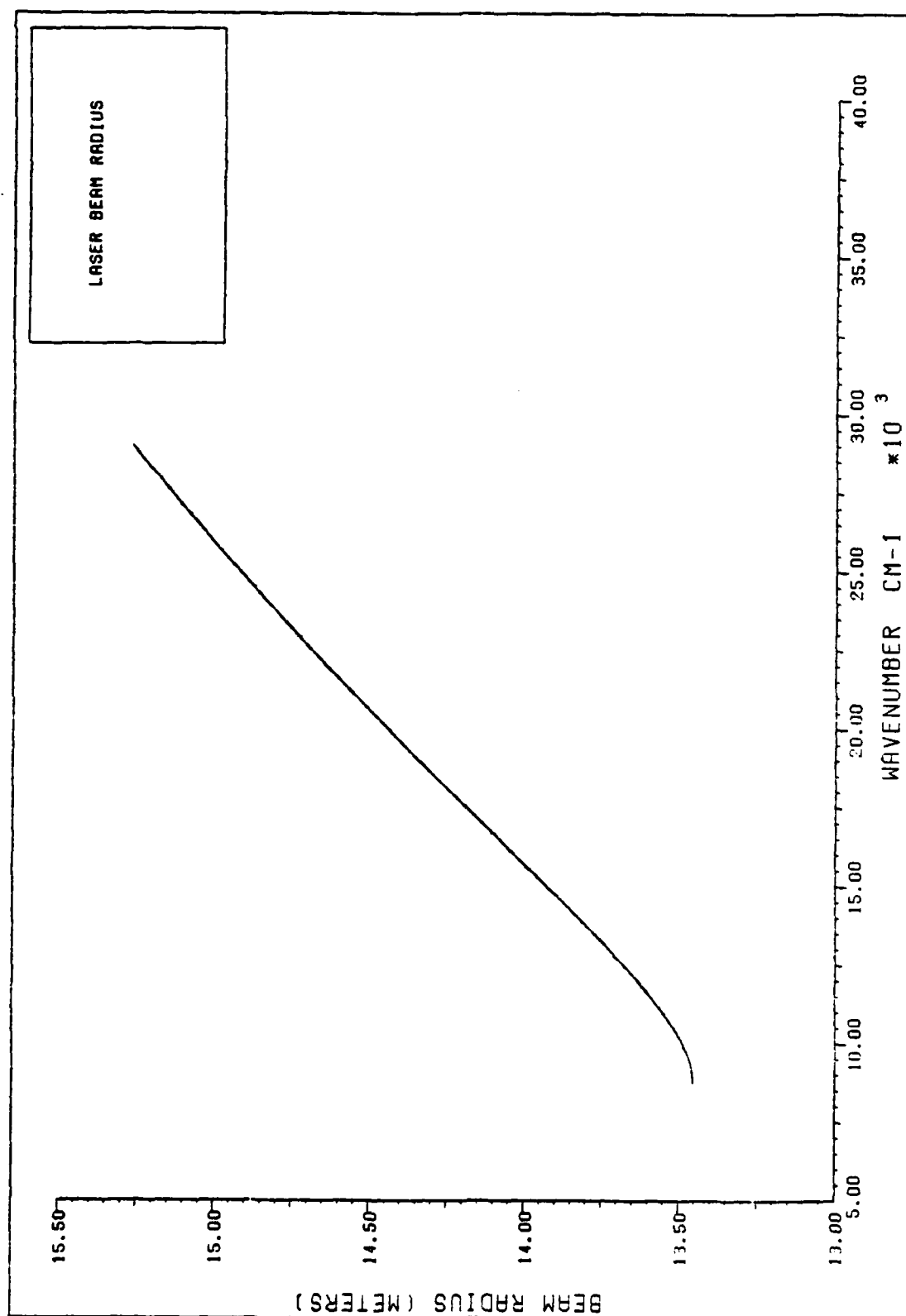


Figure 43. Total Beam Radius

rather than decreasing, increases slightly with rising wavenumbers. Likewise, the overall system efficiency decreases. The total beam radius is depicted in Figure 43. It was clear that with the original choice of parameters, turbulence induced effects dominated the total beam radius.

FEL efficiency and target efficiency were not examined separately since their values did not depend upon the selection of baseline parameters. From Figure 11, it can be seen that the FEL efficiency is a weak function of wavenumber, favoring lower wavenumbers. On the other hand, the target efficiency scales somewhat more strongly and favors the higher wavenumbers. Target efficiency ranges from a value of 1.0 to .55 over the selected wavenumber region.

When just the effects of aerosols, ozone absorption, Rayleigh scattering, beam radius, FEL efficiency, and target efficiency are combined, a curve is formed which perfectly duplicates the top line structure of the efficiency curves computed by the model. This curve is plotted in Figure 44. In its compressed wavenumber scale, the optimum peak is clearly more discernable, although no more valid. Also more discernable is the weak ozone attenuation which proves to be a dominating factor in the 15000 to 18200  $\text{cm}^{-1}$  region.

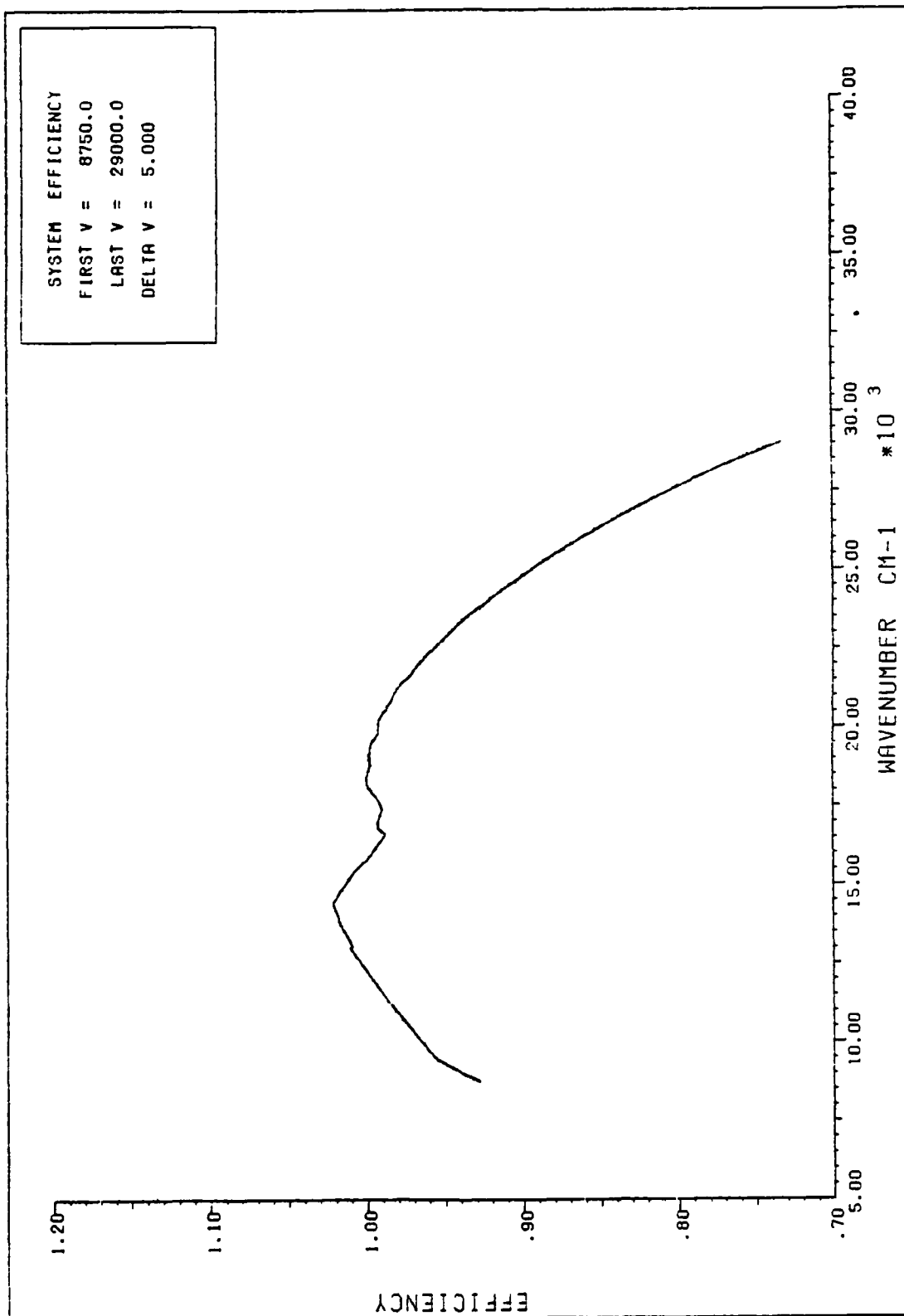


Figure 44. Top Line Structure of the Baseline Case

### Extensions to the Base Case

With the representative parameters chosen for the laser system, we were able to define an optimum wavenumber value. However, within a relatively broad wavenumber region either side of this optimum value the system efficiency was approximately equal and the wavelength selection essentially indifferent. Furthermore, the assumptions and inaccuracies inherent to the model tend to make the concept of an optimum wavenumber even more ambiguous. Nonetheless, the concept is useful in examining the sensitivities in the wavelength selection process for the free electron laser. In the remainder of this report, we will concentrate on how the optimum wavenumber departs from the value found in the baseline analysis when certain controllable and uncontrollable parameters are altered.

To do this, the analysis process will be greatly simplified. First, thermal blooming effects will be ignored. Further, the molecular absorption data from FASCODE will be excluded. By doing so, the overall system efficiency becomes a smooth function of wavenumber, resembling the curve in Figure 44. Through such an analysis, the approximate location of the peak can be determined. Undoubtedly, this point may, at times, fall on a molecular absorbing feature; yet, the purpose is not to determine an exact wavenumber for FEL operation but rather to examine the degree of impact that certain parameters have on fixing the spectral region where

such a wavenumber can be found.

Using this simplified approach, the baseline case was recalculated. This time, in the absence of molecular absorption data, the peak wavenumber occurred at  $14405.0 \text{ cm}^{-1}$  with a computed efficiency of .5085%. This wavenumber does indeed fall on an absorption feature, and explains the slight shift in the peak wavenumber ( $\sim 58 \text{ cm}^{-1}$ ) and efficiency from the results from the full model.

Effect of Turbulence Compensation. As discussed above, the effects of turbulence actually caused the beam radius to increase with increasing wavenumbers in the baseline case, rather than decrease. Therefore, it is expected that turbulence effects would have a profound influence upon the peak wavenumber along the efficiency curve. An experiment was conducted with the simplified model, maintaining all laser parameters equal to the baseline case except for the scaling term for atmospheric compensation. This was varied from .75 to 1.00 in intervals of .025. The results of this analysis can be found in Table I.

It can be seen that altering the degree of atmospheric compensation, drastically affects the peak in the efficiency curve; nearly the entire spectrum under study is covered by this experiment. However, even more significant are the order of magnitude increases in overall system efficiency one achieves with enhanced compensation. When the beam radius approaches its diffraction limited value, both

TABLE I - Variation of Turbulence Compensation

Degree of Compensation	Peak Wavenumber $\nu$ $\text{cm}^{-1}$	Peak Efficiency $\eta$ %	Wavenumber Shift from Baseline Case
.750	9435	.1333	-4970
.775	12910	.1728	-1495
.800	14005	.2335	-400
.825	14390	.3324	-15
.850	14405	.5085	0
.875	14405	.5836	0
.900	20200	1.8306	+5795
.925	22200	3.9726	+7795
.950	23010	5.8346	+8605
.975	27870	24.7141	+13465
1.000	28995	32.3936	+14590

TABLE II - Variation of Turbulence Compensation  
(No Ozone Absorption)

Degree of Compensation	Peak Wavenumber $\nu$ $\text{cm}^{-1}$	Peak Efficiency $\eta$ %	Wavenumber Shift from Baseline Case
.750	9435	.1333	-4970
.775	12910	.1728	-1495
.800	14005	.2335	-400
.825	14390	.3412	-15
.850	14405	.5125	0
.875	15270	.9233	+865
.900	16800	1.3812	+2395
.925	18185	2.8573	+3780
.950	23010	5.8346	+8605
.975	27870	24.7141	+13465
1.000	29000	34.7182	+14595

efficiency and peak wavenumber increase dramatically. A plot of the results for 100% turbulence compensation is found in Figure 45 to illustrate this point.

Admittedly, these results are somewhat artificial for two reasons: 1) the degree of compensation does not take into account the fact that limits do exist as to how much correction can actually be accomplished through adaptive optics on a real laser beam, and 2) we have left the contribution from ozone absorption in the calculations, causing the efficiency peaks to remain on either side of the weak ozone absorption feature in the mid-visible. To address the latter inconsistency, a second experiment was accomplished. This time, the contributions from ozone attenuation were excluded. The results of that analysis can be found in Table II.

Without the ozone contributions, the baseline peak wavenumber remains the same, yet, the system efficiency changes slightly. In this experiment, peak values of system efficiency shifted at somewhat more regular intervals, yet the results and conclusions remain essentially the same.

Effects of Altitude and Aerosols. The height above sea level of the laser and the selected aerosol model were analyzed together. The baseline case assumes a 'best case' aerosol model based on a rural environment and high visibility (23 km) conditions. The height of the laser in the baseline case (1.0 km) was admittedly pessimistic. In this section we will examine the effects of increasing the laser

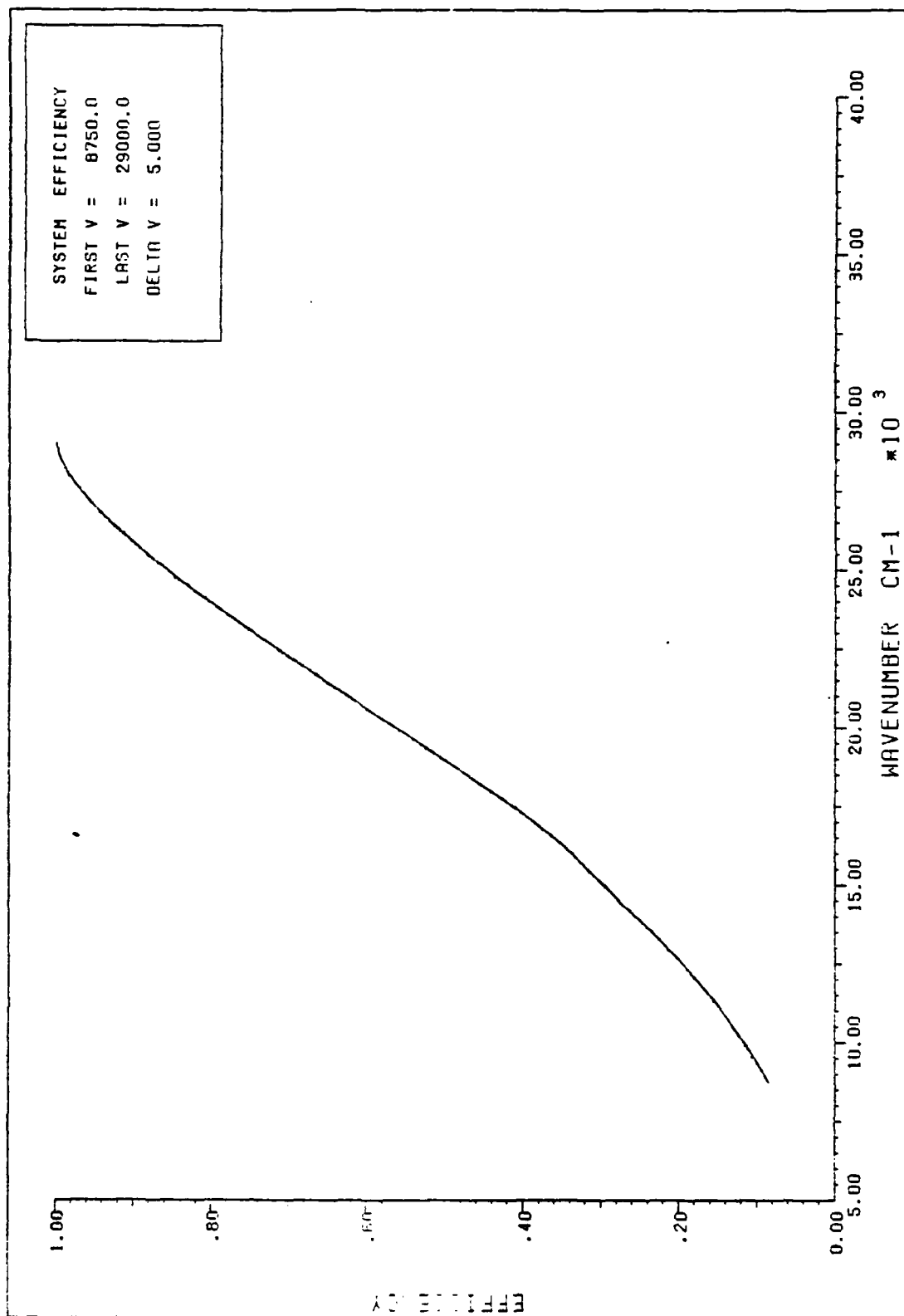


Figure 45. Efficiency Curve with 100% Turbulence Compensation

altitude and decreasing the visibility due to aerosol constituents in the atmosphere.

Sea level visibilities of 5, 15, and 23 km were chosen for the aerosol model in LOWTRAN while the Rural aspect of the model in the boundary layer was retained. The height of the laser was increased in 1.0 km increments to 3.0 km. The results of this third experiment are found in Table III.

As expected, both the peak wavenumber and the peak efficiency decrease as the visibility decreases when the laser remained at 1.0 km. The decrease is slight between 23 km and 15 km visibilities, but becomes significant between 15 km and 5 km.

At 2.0 km and above, the laser is out of LOWTRAN's boundary layer model, and hence, the differences in sea level visibility have no effect. This is, of course, not realistic. Even at 3.0 km. surface effects will determine actual aerosol concentrations. Unfortunately, LOWTRAN assumes that the surface is at sea level even though the initial altitude for its calculations might be 3.0 km. The user can work around this problem by inserting his own aerosol model. However, these results can illustrate certain points. Raising the height of the laser from 1.0 to 2.0 km results in a dramatic shift in the peak wavenumber to higher wavenumbers. Increasing the altitude by another kilometer, shifts that peak still farther, even though the aerosol attenuation is approximately the same. This is, of

TABLE III - Variation of Altitude and Sea Level Visibility

Laser Altitude	Sea Level Visibility					
	5.0 km		15.0 km		23.0 km	
	Peak $\nu$ cm <sup>-1</sup>	Peak $\eta$ %	Peak $\nu$ cm <sup>-1</sup>	Peak $\eta$ %	Peak $\nu$ cm <sup>-1</sup>	Peak $\eta$ %
1.0 km	12930	.4454	14305	.4979	14405	.5085
2.0 km	22200	.6535	22200	.6535	22200	.6535
3.0 km	23910	.7147	23910	.7147	23910	.7147

TABLE IV - Variation of Turbulence Compensation  
( Laser at 3.0 km Altitude )

Degree of Compensation	Peak Wavenumber $\nu$ cm <sup>-1</sup>	Peak Efficiency $\eta$ %	Wavenumber Shift From Baseline Case
.75	23645	.1811	-265
.80	23850	.3208	-60
.85	23910	.7147	0
.90	24505	1.4328	+595
.95	25600	4.1161	+1690
1.00	29000	59.3192	+5090

course, due to the much decreased Rayleigh scattering contribution. The atmospheric density is down by a factor of  $3/4$  from the sea level value at an altitude of just 3.0 km and the strong wavenumber dependence in Rayleigh scattering causes a significant shift in the efficiency peak. The computed efficiency curve for a 3.0 km laser altitude is depicted in Figure 46.

Effects of Turbulence Compensation - (2). The significant impact of the height of the laser on the peak wavenumber suggested a re-examination of the effects of turbulence compensation when the laser is raised to a much higher altitude. An experiment was accomplished with the laser at an altitude of 3.0 km and with a 23 km visibility, Rural aerosol model. The turbulence compensation factor was varied from .75 to 1.00 in intervals of .05. The results of this experiment are found in Table IV.

The effect of turbulence compensation on the efficiency of the system is still great, changing two orders of magnitude over the selected range of the compensation parameter. Although, compensation is still quite important in determining the peak wavenumber, the impact is much less at the higher laser altitude. Here, enhanced aerosol and Rayleigh scattering transmission tend to play a much greater role in determining the overall weapon system efficiency.

Effects of Aperture Size. The radius of the laser output optics was probably under estimated in the baseline case;

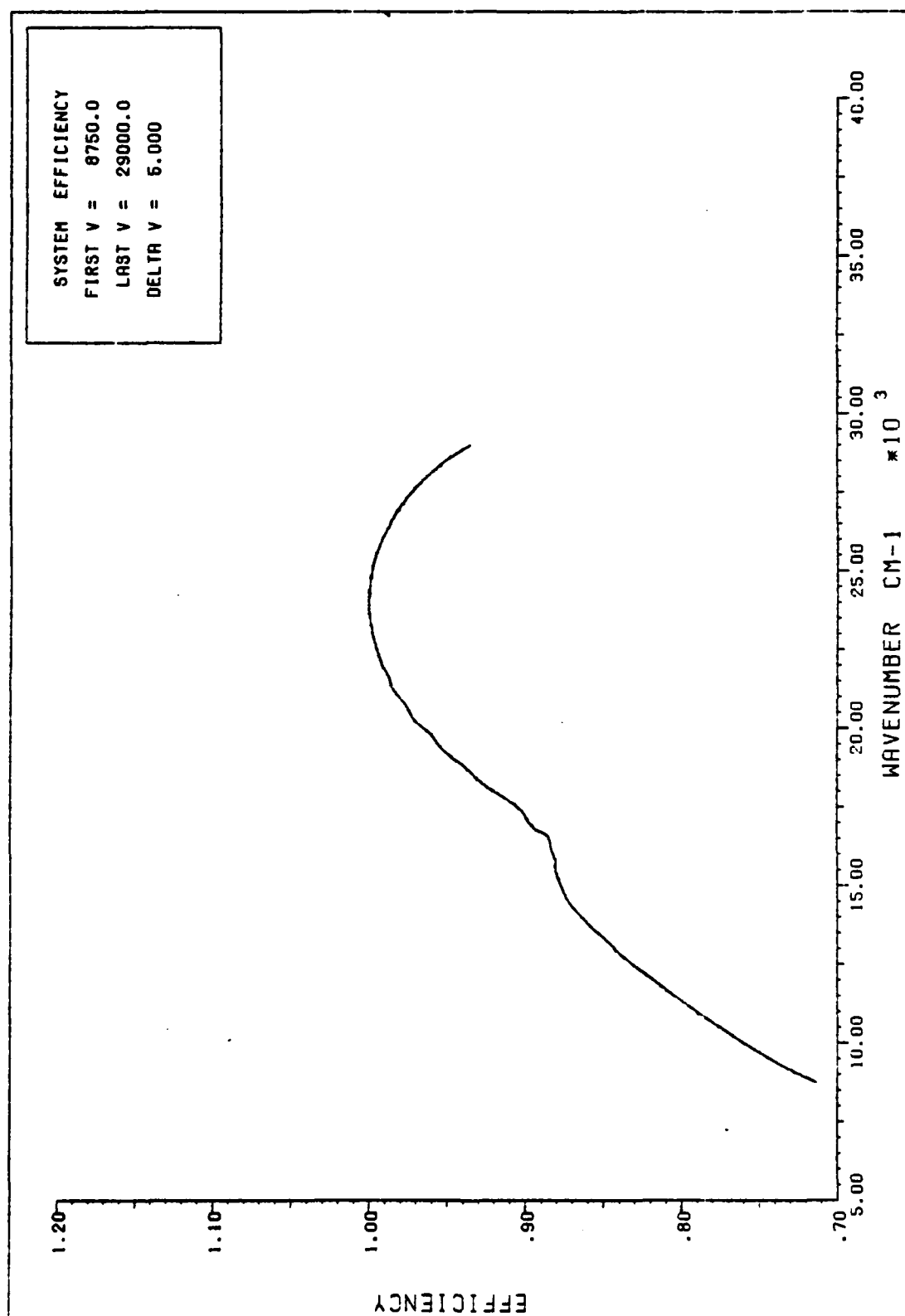


Figure 46. Efficiency Curve with Laser at 3.0km Altitude

therefore, this section will examine the effects of increasing the size of the optics on the weapon system efficiency and peak wavenumber. First, the baseline case was re-calculated using a collimated laser beam rather than a focused beam. Even though the system efficiency changed slightly when this was done, the peak wavenumber did not change, indicating the dominance of other beam effects over the focusing of the laser optics. The radius of the output optics was then increased in 1.0 meter intervals from 2.5 to 5.5 meters. Unrealistically, the jitter component of the beam was not increased for increasing optics. The results of this experiment are found in Table V.

TABLE V - Variation of Aperture Size

Radius of Output Optics	Peak Wavenumber $\nu \text{ cm}^{-1}$	Peak Efficiency $\eta \%$	Wavenumber Shift From Baseline Case
2.5	14405	.4890	0
3.5	14390	.9492	-15
4.5	14390	1.5121	-15
5.5	14305	2.1444	-100

With larger optics, the same diffraction angle of the laser beam can be achieved through longer wavelengths (lower wavenumbers); therefore, as the results show, increasing the size of the optics decreases slightly the peak wavenumber. However, the effect on the value of the peak wavenumber is very small. A more significant impact is found on the overall efficiency of the weapon system.

## VII. Conclusions and Recommendations

Unfortunately, time precluded a more thorough examination of the factors which impact the selection of an optimum wavelength. This chapter, however, will summarize those conclusions we have made during the study and briefly offer recommendations for further research.

### Conclusions

Many wavelength dependent relationships which might impact upon the selection of an operating wavelength for a ground based free electron laser weapon system, were considered in this study. Thermal blooming was found not to be a factor in the selection process. During the analysis, no single wavelength, nor even a small range of wavelengths, could be unambiguously identified as optimum for the strategic mission. For the system parameters we chose, an optimum wavelength was determined to be 0.697 micrometers ( $14347 \text{ cm}^{-1}$ ). However, this result is inconclusive for a number of reasons.

System efficiencies within only 1% of the optimum value could be found over a  $3000\text{-}4000 \text{ cm}^{-1}$  wavenumber region surrounding the peak wavenumber. Taking into account the errors and inaccuracies in the model, which we have

estimated to be 5%, the optimum wavenumber could fall anywhere between  $11000\text{ cm}^{-1}$  (0.91 micrometers) and  $24000\text{ cm}^{-1}$  (0.42 micrometers).

In addition, it is expected that the laser system parameters which were chosen for the analysis, could be unrealistic or inappropriate for a specific mission. Realizing this fact, we sought to determine how sensitive our optimum wavenumber value was to changing parameters.

When the degree of compensation for atmospheric turbulence is varied, the peak in the efficiency curve shifts significantly. Even with the excellent compensation factor we chose for the analysis, the turbulence induced beam radius dominates the total beam radius and a modest change in the ability of an adaptive optics system to correct for turbulence can have a dramatic influence on the selection of a wavelength. Turbulence has the most profound effect on the overall system efficiency which can change two orders of magnitude depending on the degree of compensation. The major conclusion which can be drawn from this discussion is already well known. Unless one does an excellent job of correcting for atmospheric turbulence, the beam radius, and hence the system efficiency, becomes quickly dominated by turbulence effects and little advantage accrues from having shorter wavelengths, larger apertures, focusing and high beam quality. We would add that the degree of compensation has a direct and significant bearing on the selection of laser wavelength.

When the mean sea level altitude of the laser is raised, the peak wavenumber increases dramatically due to the greatly reduced aerosol concentrations and Rayleigh scattering effects. At an altitude of 3.0 km, the optimum wavelength shifts to approximately 0.41 micrometers. Raising the altitude of the laser produces a modest increase in efficiency as well. At the higher altitudes, the impact of turbulence compensation on the peak wavenumber lessened but still significant. However, the ability to correct for turbulence remains just as important at the higher altitudes to the overall weapon system efficiency.

Increasing the size of the output optics will greatly enhance the system efficiency, yet has little impact on the optimum wavenumber for laser operation.

In summary, laser altitude is a strong influence on the peak wavelength while turbulence compensation also produces large shifts in peak wavelengths but enormous changes in the overall system efficiency.

### Recommendations

This analysis has hopefully examined most of the factors bearing on the problem; however, the actual selection process will likely be determined by further study.

The amount of correction for atmospheric turbulence which is eventually demonstrated will impact heavily on the selection decision. In fact, the peak wavelength may be

totally determined by the wavelength dependence in an adaptive optics system. In retrospect, there should have been more of an attempt to include realistic adaptive optics capabilities in this analysis.

In addition, the efficiencies of optical devices, such as cavity mirrors and focusing elements, ignored by this study, will likely have an important influence once a nominal wavelength is found and the optical materials selected.

Lastly, the wavelength dependence in the target coupling efficiency remains a very open question. It will probably be eventually answered through experimental studies rather than theoretically scaling relationships. The program for this analysis has been constructed in such a way as to easily allow the addition of specific spectral target data at a later time.

## APPENDIX A

### Modifications to the Code - LOWTRAN

This appendix describes the modifications which were accomplished during this study on the code LOWTRAN, version 6. The purpose was two-fold: 1) to extract absorption and scattering optical depths for each of the 32 altitude layers in LOWTRAN, and 2) to extract information on the atmospheric model for use in the main program. These modifications are listed as follows:

A. In the main program, LWTRN6, two files, TAPE8 and TAPE15, are declared in the PROGRAM statement, line 110.

B. In subroutine STDMDL, input/output unit 15 is opened between lines 250 and 255, and designated the file name, MODEL. Into this file, the atmospheric data will be written. Later in this subroutine, between lines 650 and 655, a WRITE statement is inserted to extract the atmospheric pressure, temperature, and altitude of the 33 altitude boundaries in LOWTRAN. An implied DO Loop structured is utilized.

```
WRITE (15) ( PM(I), TM(I), ZM(I), I=1,33 )
```

C. After LOWTRAN computes the path geometry through the atmosphere, the average values of pressure, temperature, and density for each of the 32 altitude layers are also written to the file MODEL. This is accomplished in subroutine RFPATH. This subroutine loops through each layer and computes these values but does not store them. Therefore, it is necessary to create arrays in which to store these values. This is done in the DIMENSION statement in line 200 with the addition of variables PBAR (35), TBAR(35), and RHOBAR(35). Within the layer loop, arrayed variables are substituted for the single dimension variables of PBAR, TBAR, and RHOBAR. This is done at lines 560-570 and at lines 860-870. Finally, outside of the layer loop, the arrays are written to the file MODEL after line 915. The file is closed immediately following this operation.

```
WRITE (15) ( PBAR(I), TBAR(I), RHOBAR(I), I=1,32 )
```

D. The most convenient place to extract absorption and scattering data is in subroutine TRANS. This is accomplished by first accessing a pre-existing common block of data through a COMMON statement.

```
COMMON / RFRPTH / ZP(35),PP(35),TP(35),RFNDXP(35),SP(35),  
1 PPSUM(35),TPSUM(35),RHOSUM(35),DENP(16,35),AMTP(16,35)
```

The arrayed variable AMTP(X,Y) from above represents the column density of the atmospheric constituent X over the altitude layer Y. Next, the arrayed variables RSCAT(35), AEXT (35), ABBS(35), CONT(35), and OZONE(35) are dimensioned, and the input/output unit 8 is opened and given the file name, LTDATA. These variables represent the contributions of Rayleigh scattering, aerosol scattering, aerosol absorption, continuum absorption, and ozone absorption. The arrayed variable ABB(X) from LOWTRAN corresponds to the cross-sectional probability for constituent X. The following is then inserted between lines 1250 and 1255.

```

DO 350 N=1,32

RSCAT(N)= ABB(6) * AMTP(12,N)

A= XX1 * AMTP(7,N) + XX2 * AMTP(12,N)
B= XX3 * AMTP(13,N) + XX4 * AMTP(14,N)
AEXT(N)= A + B

A= YY1 * AMTP(7,N) + YY2 * AMTP(12,N)
B= YY3 * AMTP(13,N) + YY4 * AMTP(14,N)
ABBS(N)= A + B

CONT(N)= ABB(5) * AMTP(5,N) + ABB(9) * AMTP(9,N) +
1 ABB(10) * AMTP(10,N)

OZONE(N)= ABB(8) * AMTP(8,N)

350  CONTINUE

WRITE (8) V, (RSCAT(I),AEXT(I),ABBS(I),OZONE(I),
1 CONT(I), I=1,32)

```

Outside of the wavenumber loop in subroutine TRANS, after line 1565, the unit 8 can be closed.

## APPENDIX B

### Modifications to the Code - FASCODE

This appendix describes the modifications on the code FASCODE which were accomplished to extract molecular absorption data for each altitude layer. These modifications are as follows:

A. In the main program, FASCOD1, an additional file, TAPE14, is declared in the PROGRAM statement, line 110. Also, this input/output file is opened and assigned the name, FCDATA, following line 1362 in the main program. An ENDFILE statement and a CLOSE statement on this file are then inserted following line 1470.

B. Subroutine LAYER controls the program looping over the altitude layers. In order to distinguish these different layers in the data on file FCDATA, it was necessary to place a marker after each layer calculation. This is accomplished by inserting between lines 5020 and 5025 the following.

```
LL = 0  
XX = 0.0  
WRITE (14) XX,XX,LL
```

C. In subroutine PATH, the sampling interval for FASCODE is computed. We wished to fix this interval to 0.2

wavenumbers. Therefore, line 7530 of this subroutine is replaced by:

```
30 DV = 0.2
```

D. In subroutine PANEL, line 16470 is modified to pass the number of the current layer to subroutine R1PRNT. One must remember to specify a value greater than zero for the parameter NPTS on the FASCODE input cards in order for this subroutine to be called.

```
IF (NPTS .GT. 0) CALL R1PRNT (R1,NLO,KFILE,LAYER)
```

E. Finally, subroutine R1PRNT is re-written entirely and is presented here in its entirety. The variable R1 is the optical depth for wavenumber VJ over altitude layer NUM.

```
SUBROUTINE R1PRNT (R1,JLO,MFILE,NUM)

COMMON/XPANEL/V1P,V2P,DVP,NLIM,NSHFT,NPTS
COMMON/IFIL/IRD,IPR,IPU,NOPR

DIMENSION R1(1)

JHI=JLO + NLIM - 1
DO 10 KK=1,NLIM
  J=JLO + KK -1
  VJ=V1P + FLOAT(J-JLO) * DVP
  WRITE (14) VJ, R1(J), NUM
10 CONTINUE
RETURN
END
```

## APPENDIX C

### Program Listing - SORT

This program is designed to sort the molecular absorption data generated by FASCODE into a format which is compatible to the main program and LOWTRAN. The program reads a block of 2000 wavenumbers for a given altitude layer, and then skips via the subroutine POST to the appropriate point in the next altitude layer. When all 32 layers have been read, the data is written to file and the process repeats with the next 2000 wavenumbers. The output on file SDATA now contains molecular absorption data over all layers for a single wavenumber. The program is as follows:

```
PROGRAM SORT

REAL MOLABS(2000,32),WAVNUM(2000),V,ABB
INTEGER I,LEVEL,KCOUNT

OPEN(14,FILE='FCDATA')
OPEN(12,FILE='SDATA')

I=0
KCOUNT=0

10  I=I+1
    DO 100 K=1,2000
        READ (14,END=500) V,ABB,LEVEL
```

```

      IF (LEVEL .EQ. 0) THEN
        IF (I .LT. 32) THEN
          IF (KCOUNT .EQ. 0) THEN
            GO TO 10
          ELSE
            CALL POST (KCOUNT)
            GO TO 10
          END IF
        ELSE
          STOP 1000
        END IF
      ELSE
        IF (I .NE. LEVEL) THEN
          STOP 2000
        END IF
        MAXNUM(K)=V
        MOLABS(K,LEVEL)=ABB
      END IF
100  CONTINUE

200  READ(14,END=250) V,ABB,LEVEL
      IF (LEVEL .NE. 0) THEN
        GO TO 200
      ELSE
        IF (I .LT. 32) THEN
          IF (KCOUNT .EQ. 0) THEN
            GO TO 10
          ELSE
            CALL POST (KCOUNT)
            GO TO 10
          END IF
        ELSE
          GO TO 250
        END IF
      END IF

250  DO 300 N=1,K-1
      WRITE (12) MAXNUM(N),(MOLABS(N,I), I=1,32)
300  CONTINUE

      KCOUNT=KCOUNT+1
      REWIND 14
      CALL POST(KCOUNT)
      I=0
      GO TO 10

500  DO 600 N=1,K-1
      WRITE (12) MAXNUM(N), (MOLABS(N,I), I=1,32)
600  CONTINUE

      END

```

\*\*\*\*\*

SUBROUTINE POST(KCOUNT)

INTEGER N,KCOUNT

N=KCOUNTX2000

DO 10 I=1,N

READ(14)

10 CONTINUE

END

# APPENDIX D

## Program Listing - WAVLEN

PROGRAM WAVLEN (INPUT,OUTPUT,TAPE5=INPUT,TAPE6=OUTPUT)

XX

\* PROGRAM BY  
\* CAPT DOUGLAS E. KOHLHEPP  
\* AFIT/ENS , GSO-83D  
\* WRIGHT-PATTERSON AFB, OHIO  
\*

\* THIS PROGRAM IS DESIGNED TO FIND THE OPTIMUM WAVELENGTH  
\* FOR A GROUND-BASED FREE ELECTRON LASER  
\*

XX

REAL MOLABS(32),AEXT(32),ABBS(32),RSCAT(32),OZONE(32),  
1 ATTEN(33),ABSORB(33),DELZ(32),P(33),T(33),ALT(33),  
2 PBAR(32),TBAR(32),RHOBAR(32),IAVG,PBEST,VBEST,JITTER,HOL,  
3 FOCRNG,LAMDA,HABG,HMSL,NI,IREL,ILASER,CONT(32),RANGE,  
4 COMPEN,EBEST,VPBEST,EFF,ETA,PROPEFF  
INTEGER H1,IFLAG,NSTEP

COMMON/OPDPTH/MOLABS,AEXT,ABBS,RSCAT,OZONE,CONT  
COMMON/ATH/P,T,ALT,PBAR,TBAR,RHOBAR  
COMMON/RAD/HOL,JITTER,BEAMQ,FOCRNG,RHOTURB,R0,COMPEN

DATA (DELZ(I),I=1,25)/25X1000.0/  
DATA (DELZ(I),I=26,30)/5X5000.0/  
DELZ(31)=20000.0  
DELZ(32)=30000.0

\* CONSTANTS AND STARTING VALUES

PI=3.1416  
IFLAG=0  
EBEST=0.0  
PBEST=0.0  
ATTEN(33)=0.0  
ABSORB(33)=0.0

\* OPEN DATA FILES

OPEN(8,FILE='LTDATA')  
OPEN(14,FILE='FCDATA')  
OPEN(15,FILE='MODEL')  
OPEN(10,FILE='EFFIC')

REWIND 8

```

REWIND 14
REWIND 15

*READ IN PARAMETERS FOR ANALYSIS
*READ CARD #1

      READ(5,100)AVGPMR,R0,V1,V2,RANGE
100  FORMAT (5F12.2)
      RANGE=RANGE*1000.0

*READ CARD #2

      READ(5,101) FOCRNG,BEAMQ,JITTER,HOL,COMPEN
101  FORMAT (5F12.2)
      FOCRNG=FOCRNG*1000.0
      H1=NINT(HOL) + 1
      HOL=HOL*1000.0

      IF (V1.GT.V2) THEN
        PRINT('WAVENUMBER PARAMETER ERROR')
        STOP 1000
      END IF

*READ IN ATMOSPHERIC DATA
      CALL MDLATM

* BEGIN COMPUTATION OF YURA'S COHERENCE DIAMETER FOR TURBULENCE
* SELECT AN AVERAGE WAVELENGTH OF .6 MICRONS
      LAMDA=.6E-6

*CONSTANTS AND INITIAL VALUES
      HABG=0.0
      SUM=0.0
      DELH=50.0
      Q=247.4
      USTAR=0.35

* BEGIN SUMMATION NEAR EARTH'S SURFACE WITH WYNGAARD'S MODEL

      DO 110 L=50,950,50

      HABG=L*(DELH/2.0)
      HMSL=HOL + HABG

      TEMP= T(H1) + ( (HABG/DELZ(H1)) * (T(H1+1) - T(H1)) )

      SCALE= P(H1+1) * T(H1)/( P(H1) * T(H1+1) )
      PRES= TEMP * ( P(H1)/T(H1)) * SCALE ** ( HABG/DELZ(H1) )

      DENOM= (14000.0 *(USTAR ** 3.0))/(HABG*Q)
      DENOM= (DENOM + 1.0) ** .667

```

```

CT2= (2.0E-3 * (Q ** 1.333) * (HABG ** (-1.333)))/DENOM
CN2= CT2 * (DN0T(PRES,TEMP,LAMDA) ** 2.0)
A=((RANGE-HABG)/RANGE) ** 1.667
A= A * CN2 * DELH
SUM=SUM + A
110 CONTINUE
DO 115 I=H1+1,25
DO 113 N=1,2
ZBAR=ALT(I) + (2.0XN -1.0)/(DELZ(I)*4.0) - HOL
CN2= 2.2*(1.0E-5 * 10.0**(-.3) * ZBAR) **10.0 * EXP(-ZBAR/1000.0)
CN2= CN2 + 1.0E-16 * EXP(-ZBAR/1500.0)
CN2= CN2 * 2.7
A=((RANGE-ZBAR)/RANGE) ** 1.667
A= CN2 * A * DELZ(I)
SUM=SUM + A
113 CONTINUE
115 CONTINUE
WRITE (6,117) SUM
117 FORMAT (' SUM= ',E12.4)
* BEGIN WAVENUMBER LOOP
* READ IN FASCODE DATA
120 IF (IFLAG .EQ. 0) THEN
CALL FCREAD (V,IFLAG,V1,V2)
END IF
IF (IFLAG .EQ. 1) THEN
V=V+1.0
DO 125 I=1,32
MOLABS(I)=0.0
125 CONTINUE
END IF
IF (V .GT. V2) THEN
GO TO 380
END IF
*READ IN LOWTRAN DATA

```

```

      CALL LTREAD (V,IFLAG)

      IF (IFLAG .EQ. 2) THEN
        GO TO 380
      END IF

      * CONVERT WAVENUMBER TO WAVELENGTH IN METERS

      LAMDA=1.0E-2/V

      * COMPUTE TOTAL TRANSMISSION AND THERMAL BLOOMING IN THE FIRST
      * LAYER TO DETERMINE IF IT IS WORTHWHILE PROCEEDING
      TRAN=0.0
      DO 150 I=H1,32

        ATEN(I)=MOLABS(I)+AEXT(I)+ABBS(I)+RSCAT(I)+OZONE(I)+CONT(I)
        ABSORB(I)=MOLABS(I)+ABBS(I)+OZONE(I)
        TRAN=TRAN+ATEN(I)

150  CONTINUE

      TRAN=EXP(-TRAN)

      NI=-DNDT(PBAR(H1),TBAR(H1),LAMDA) * AVGPWR
      NI=NI*ABSORB(H1)*DELZ(H1)*DELZ(H1)
      NI=NI/(PI*RHOBAR(H1)*980.0*UX(HOL)*R0*R0*R0)

      IF (TRAN .LE. 0.10 .OR. NI .GE. 30.0) THEN
        EFF=0.0
        WRITE(10) V,EFF
        GO TO 120
      END IF

      *FINISH WAVELENGTH DEPENDENT CALCULATIONS OF YURA'S COHERENCE DIAMETER
      RHOTURB=(5.80*PI*PI*SUM)/(LAMDA*LAMDA)
      RHOTURB=RHOTURB ** (-.60)

      *START THERMAL BLOOMING CALCULATIONS

      NSTEP=4
      NI=0.0

      *START OUTER LOOP

      DO 350 I=H1,32

        G=0.0
        ZZ=ALT(I) + DELZ(I)

      *INNER LOOP

```

```

DO 300 K=H1,I

ZMID=ALT(K) + .46*DELZ(K)
DZ=DELZ(K)/NSTEP
Z=ALT(K) + DZ/2.0

DO 250 N=1,NSTEP

TEMP= T(K) + ( (Z-ALT(K)) * (T(K+1) - T(K)) / DELZ(K) )

SCALE= P(K+1) * T(K)/(P(K) * T(K+1))
PRES= TEMP * (P(K)/T(K)) * SCALE ** ( (Z-ALT(K))/DELZ(K) )

DENS= (RHOBAR(K) * PRES * TBAR(K))/(PBAR(K) * TEMP)

CP=932.86 + 0.244*TEMP - 3.0742E-5*TEMP*TEMP

IF(ABSORB(K).LT.0.00001 .OR. ABSORB(K+1).LT.0.00001) THEN
ALFA=0.0
ELSE
ALFA=ABSORB(K)*(ABSORB(K+1)/ABSORB(K))**((Z-ZMID)/DELZ(K))
ALFA=ALFA/DELZ(K)
END IF

IF(ATTEN(K).LT.0.00001 .OR. ATTEN(K+1).LT.0.00001) THEN
EXT=0.0
ELSE
EXT= ATTEN(K)*(ATTEN(K+1)/ATTEN(K))**((Z-ZMID)/DELZ(K))
EXT= EXT/DELZ(K)
END IF

CALL RADIUS (LAMDA,Z,R)

A=ONDT(PRES,TEMP,LAMDA) * ALFA * EXP( -EXT * Z )
B=REFIDX(PRES,TEMP,LAMDA) * DENS * CP * VX(Z) * R * R

G= G + ( A * DZ / B )

Z=Z + DZ

250 CONTINUE
300 CONTINUE

CALL RADIUS ( LAMDA,ZZ,RR )

NI= NI + (4.89 * AVGPWR * G * DELZ(I))/(RR * PI)

350 CONTINUE

*DETERMINE IRRADIANCE ON TARGET
NI=ABS(NI)

```

```

      CALL RADIUS(LAMDA,RANGE,R)

      IAVG= (AUGPWR * TRAN * IRELAND)/(PI * R * R)
      ILASER= AUGPWR/(PI * R0 * R0)

      PROPEFF= IAVG/ILASER

      IF ( PROPEFF .GT. PBEST ) THEN
        PBEST=PROPEFF
        VPBEST=V
      END IF

      CALL FELOPT (ETA,LAMDA)

      EFF=PROPEFF * ETA *TGTEFF(LAMDA)

      IF (EFF .GT. EBEST) THEN
        EBEST=EFF
        VBEST=V
      END IF

      WRITE (10) V,EFF

      IF (IFLAG .NE. 2) THEN
        GO TO 120
      END IF

*END OF WAVENUMBER LOOP

380  WRITE(6,390) VPBEST,PBEST
390  FORMAT(' BEST WAVENUMBER FOR PROPAGATION=',F10.3,
1 ' WITH EFFICIENCY OF ',E12.4)

      WRITE (6,400) VBEST,EBEST
400  FORMAT (' BEST OVERALL WAVENUMBER=',F10.3,
1 ' WITH EFFICIENCY OF ',E12.4)

      END

*****
      SUBROUTINE MDLATH

* THIS SUBROUTINE READS IN THE ATMOSPHERIC PROFILE FROM 'MODEL'

      REAL P(33),T(33),ALT(33),PBAR(32),TBAR(32),RHOBAR(32)

      COMMON/ATM/P,T,ALT,PBAR,TBAR,RHOBAR

      READ (15) ( P(I),T(I),ALT(I), I=1,33)
      READ (15) (PBAR(I),TBAR(I),RHOBAR(I), I=1,32)

* CONVERT ALTITUDE TO METERS AND DENSITY TO KG/M3

```

```

DO 10 N=1,32
  ALT(N)=ALT(N) * 1000.0
  RHOBAR(N)=RHOBAR(N) * 1000.0
10 CONTINUE
  ALT(33)=ALT(33) * 1000.0

```

```

RETURN
END

```

```

*****
SUBROUTINE FCREAD (V,IFLAG,V1,V2)

```

```

* THIS SUBROUTINE READS IN MOLECULAR ABSORPTION DATA
* FROM THE FILE GENERATED BY FASCODE. IF END OF FILE IS
* REACHED, IFLAG IS SET TO ONE.

```

```

  REAL V,V1,V2,MOLABS(32),AEXT(32),ABBS(32),RSCAT(32),OZONE(32),
  1 CONT(32)
  INTEGER IFLAG,IENTER

```

```

  COMMON/OPDPH/MOLABS,AEXT,ABBS,RSCAT,OZONE,CONT

```

```

  DATA IENTER/0/
10 READ (14,END=100) V,(MOLABS(I), I=1,32)

  IF (IENTER .EQ. 0) THEN
    IF ( V .GE. V1 ) THEN
      WRITE (6,50) V
50   FORMAT(' STARTING WAVENUMBER WILL BE ',F10.4)
    ELSE
      GO TO 10
    END IF
  END IF

```

```

  IENTER=1

```

```

  IF ( V .LE. AINT(V2) ) THEN
    RETURN
  END IF

```

```

100 WRITE (6,150) V
150 FORMAT(' LAST WAVENUMBER READ BY FCREAD= ',F10.4)
  IFLAG=1
  RETURN
END

```

```

*****
SUBROUTINE LTREAD (V,IFLAG)

```

```

* THIS SUBROUTINE READS IN ABSORPTION AND SCATTERING DATA
* CREATED BY LOWTRAN6 AND PERFORMS INTERPOLATION

```

```

      REAL V,V1,V2,RSCAT(32),AEXT(32),ABBS(32),OZONE(32),CONT(32)
1     ,RSCAT2(32),AEXT2(32),ABBS2(32),OZONE2(32),CONT2(32)
2     ,RSCAT1(32),AEXT1(32),ABBS1(32),OZONE1(32),CONT1(32)
3     ,MOLABS(32)
      INTEGER IENTER,IFLAG

      COMMON/OPDPH/MOLABS,AEXT,ABBS,RSCAT,OZONE,CONT

      DATA IENTER/0/

      IF (IENTER .EQ. 0) THEN
        READ(8)V1,(RSCAT1(I),AEXT1(I),ABBS1(I),OZONE1(I),
1      CONT1(I),I=1,32)
        WRITE(6,100) V1
100    FORMAT(' FIRST WAVENUMBER READ BY LTREAD=',F10.4)
        READ(8)V2,(RSCAT2(I),AEXT2(I),ABBS2(I),OZONE2(I),
1      CONT2(I),I=1,32)

        IENTER=1

        IF(V .LT. V1) THEN
          WRITE (6,(' LTREAD ERROR '))
          STOP 2000
        END IF
      END IF

150  IF (V .GT. V2) THEN
        V1=V2
        DO 200 I=1,32
          RSCAT1(I)=RSCAT2(I)
          AEXT1(I)=AEXT2(I)
          ABBS1(I)=ABBS2(I)
          OZONE1(I)=OZONE2(I)
          CONT1(I)=CONT2(I)
200    CONTINUE

        READ(8,END=500) V2,(RSCAT2(I),AEXT2(I),ABBS2(I),OZONE2(I),
1      CONT(I),I=1,32)

        GO TO 150

      END IF

      FACT4=( VXX4.0 - V1XX4.0 )/( V2XX4.0 - V1XX4.0 )
      FACTOR=(V-V1)/(V2-V1)

      DO 300 I=1,32
        RSCAT(I)=RSCAT1(I) + FACT4 * (RSCAT2(I) - RSCAT1(I))
        AEXT(I)=AEXT1(I) + FACTOR * (AEXT2(I) - AEXT1(I))
        ABBS(I)=ABBS1(I) + FACTOR * (ABBS2(I) - ABBS1(I))
        OZONE(I)=OZONE1(I) + FACTOR * (OZONE2(I) - OZONE1(I))
        CONT(I)=CONT1(I) + FACTOR * (CONT2(I) - CONT1(I))
300

```

300 CONTINUE

RETURN

500 WRITE(6,600) V2

600 FORMAT(' LAST WAVENUMBER READ BY LTREAD=',F10.4)

IFLAG=2

RETURN

END

\*\*\*\*\*  
SUBROUTINE RADIUS (LAMDA,Z,R)

\* THIS SUBROUTINE COMPUTES THE 1/E2 RADIUS OF THE BEAM AT  
\* A SPECIFIED DISTANCE FROM THE LASER

REAL LAMDA,HOL,JITTER,BEAMQ,COMPEN,FOCRNG,DIST,RHOTURB

COMMON/RAD/HOL,JITTER,BEAMQ,FOCRNG,RHOTURB,R0,COMPEN

PI=3.1416

ROOT2=SQRT(2.0)

DIST=Z-HOL

JITTER=JITTER \* 1.0E-6

\* IF FOCAL RANGE IS ZERO, THE BEAM IS FOCUSED AT INFINITY

IF (ABS(FOCRNG-0.0) .LE. 0.01) THEN

FOCRNG=1.0E+25

END IF

\* COMPUTE TURBULENCE RADIUS

RTS=((ROOT2\*DIST\*(1.0-COMPEN)\*LAMDA)/(PI\*RHOTURB))\*2.0

\* COMPUTE JITTER RADIUS

RJS= 2.0\* ( (JITTER\*DIST) \*\* 2.0 )

\* COMPUTE DIFFRACTION AND FOCUS EFFECTS

RDS=((BEAMQ \* LAMDA \* DIST)/(PI \* R0 \* R0)) \*\* 2.0

RDS= RDS + ( 1.0- (DIST/FOCRNG) ) \*\* 2.0

RDS= RDS \* R0 \* R0

\* USE ROOT SUMM SQUARE TECHNIQUE TO COMPUTE FINAL RADIUS

R= SQRT( RDS + RJS + RTS )

RETURN

END

\*\*\*\*\*  
REAL FUNCTION REFDX (P,T,LAMDA)

\* THIS FUNCTION COMPUTES THE INDEX OF REFRACTION

```

REAL P,T,LAMDA

REFIDX=(5.85E-19 * P)/(T * LAMDA * LAMDA)
REFIDX= REFIDX + (7.76E-5 * P / T ) + 1.0

END

*****
REAL FUNCTION DNDT (P,T,LAMDA)

* THIS FUNCTION COMPUTES THE CHANGE IN REFRACTIVE INDEX
* FOR A CHANGE IN TEMPERATURE

REAL P,T,LAMDA

DNDT=-(5.95E-19 * P)/(T * T * LAMDA * LAMDA)
DNDT=DNDT - ((7.76E-5 * P)/(T * T))

END

*****
REAL FUNCTION IREL (NI)

* THIS FUNCTION COMPUTES THE FRACTION OF POWER LEFT IN THE BEAM
* AFTER THERMAL BLOOMING HAS TAKEN AFFECT. THE INPUT PARAMETER
* IS GEBHARDT'S DISTORTION NUMBER

REAL NI

IF (NI .LE. 0.1) THEN
    IREL=1.0
    RETURN
END IF

IF (NI .GE. 40.0) THEN
    IREL=0.0
    RETURN
END IF

IREL= 1.0/(1.0 + 0.0625 * NI * NI)

END

*****
REAL FUNCTION UX(Z)

* DETERMINES THE HORIZONTAL WIND AT ALTITUDE Z

REAL Z

UX=0.0

```

```

IF (Z .GE. 1.0E+5) THEN
  RETURN
ELSE IF (Z .GE. 24400.0) THEN
  UX=27.2 - 2.72E-4 * Z
  RETURN
ELSE IF (Z .GE. 12200.0) THEN
  UX=82.4 - 2.33E-3 * Z
  RETURN
ELSE
  UX=8.75 + 3.42E-3 * Z
  RETURN

```

```
END IF
```

```
END
```

```

*****
SUBROUTINE FELOPT(ETA,LAMDA)

```

```

* THIS SUBROUTINE COMPUTES THE DEVICE EFFICIENCY FOR
* A GIVEN WAVELENGTH

```

```

REAL ETA,LAMDA,LAMDAP,N,IPEAKB,IBARM,I0,EPSLON,THETAM,
1 LM,PBARA,PBARL,GAMMAB,GAMMA,KAPPA,X,G,FK,DELTA,VALUE

```

```
* DEFINE CONSTANTS AND NOMINAL DEVICE VALUES
```

```

PBARA=2.1E+6
PBARL=3.0E+6
LAMDAP=9.0E-3
N=2.0
IBARM=1.0E+11
IPEAKB=150.0
I0=1356.0
LM=50.0
THETAM=1.0E-6
EPSLON=0.1
PI=3.1416
GAMMAB=10.0

```

```
* COMPUTE KAPPA
```

```

KAPPA=((4.0*PI*EPSLON)/(LM*LM*LAMDAP*THETAM))**.667
KAPPA=KAPPA*(LAMDAP/(4.0*PI*N))**.20

```

```
* DETERMINE FROM CURVE FITS OPTIMUM VALUES OF X,G,FK GIVEN KAPPA
```

```
X=(-8.8528*KAPPA*KAPPA) + (4.0284*KAPPA) + .52725
```

```
G=(-3.6495*KAPPA*KAPPA) + (1.4410*KAPPA) + 1.76241
```

```

FK=((EXP(-G/X) * X * X) + KAPPA) ** (-1.5)
FK=FK * (EXP(-G/X) * X * X)

```

```

FK=FK * ( ((G*G) - 1.0)/(G*G) ) * ( (2/X) ** 1.5 )
FK=FK * ( KAPPA ** 1.25 )

* COMPUTE WIGGLER VECTOR POTENTIAL

AW=(KAPPA**(-.5)) * X * EXP(-G/(2.0*X))

* COMPUTE RESONANCE GAMMA AT ENTRANCE TO WIGGLER

GAMMA=((1.0+(AW*AW))*LAMDAP*X)/(LAMDA*2.0*(KAPPA**(.5)))
GAMMA=SQRT(GAMMA)

* COMPUTE DELTA

DELTA=((LAMDAP/LAMDA)**1.5)*(GAMMA-1.0)*PBARL*I0
DELTA=DELTA/(LM*LM*IBRM*PEAKB*FK*(GAMMA-1.0))

* FIND VALUE FROM CURVE FIT

VALUE=(11.9642*DELTA*DELTA) - (3.7919*DELTA) +.55284

* COMPUTE EFFICIENCY

ETA=((1.0/VALUE) + (PBARA/PBARL))**(-1.0)

RETURN
END

*****
REAL FUNCTION TGTEFF(LAMDA)

* THIS FUNCTION SCALES RELATIVE EFFICIENCY OF TARGET ABSORPTION
* WITH .3448 MICRONS BEING THE BEST

REAL LAMDA

TGTEFF=SQRT(.3448E-6/LAMDA)
END

```

## Bibliography

1. Robinson, Clarence A. "Panel Urges Defense Technology Advances," Aviation Week and Space Technology, 119: 16-18 (17 October 1983).
2. Brau, Charles, Director of the Free Electron Laser Project Office. Telephone interview. Los Alamos National Laboratory, New Mexico, 10 June 1983.
3. Brau, Charles A. "Free Electron Laser," Laser Focus, 22: 60-62 (January 1982).
4. Elias, Luis R. et al. "Observation of Stimulated Emission of Radiation by Relativistic Electrons in a Spatially Periodic Transverse Magnetic Field," Physical Review Letters, 36: 717-120 (29 March 1976).
5. Deacon, D. A. G. et al. "First Operation of Free Electron Laser," Physical Review Letters, 38: 892-894 (18 April 1977).
6. Colson, William B. "One-body Analysis of Free Electron Lasers," Novel Sources of Coherent Radiation, edited by Stephen F. Jacobs et al. Reading MA: Addison-Wesley Company, 1978.
7. Kroll, N. M. et al. "Variable Parameter Free-Electron Laser," Free-Electron Generators of Coherent Radiation, edited by Stephen F. Jacobs et al. Reading MA: Addison-Wesley Company, 1980.
8. Brau, Charles A. and Richard K. Cooper. "Variable Wiggler Optimization," Free-Electron Generators of Coherent Radiation, edited by Stephen F. Jacobs et al. Reading MA: Addison-Wesley Company, 1980.
9. Green, J. M. "Assessment of Free Electron Lasers," Optics and Laser Technology, 43: 245-251 (October 1981).
10. Brau, C. A. "Optimization of Free-Electron Lasers When Mirror Damage Limits the Laser Power in the Wiggler (Revised)," FEL Project Memorandum. Los Alamos National Laboratory, New Mexico, 23 July 1982.

11. Reilly, J. P. et al. A Study to Design a Free Electron Laser Experiment: Volume I, Revision I, 31 March 1978 - 1 May 1979. Contract DAAK40-78-C-0140. W. J. Schafer Associates, Inc., Wakefield MA, 25 May 1979 (AD-B038-207).
12. Kroll, Norman M. "Enhanced Energy Extraction in Free-Electron Lasers by Means of Adiabatic Decrease of Resonant Energy," Free-Electron Generators of Coherent Radiation edited by Stephen F. Jacobs et al. Reading MA: Addison-Welsey Company, 1980.
13. Brau, C. A. "Optimization of the Overall Efficiency of Free-Electron Lasers with Energy Recovery," FEL Project Memorandum, Los Alamos National Laboratory, New Mexico 30 July 1982.
14. Brau, C. A. "FELOPT - A Program to Compute Optimized Free-Electron Laser Performance," FEL Project Memorandum, Los Alamos National Laboratory, New Mexico, 6 August 1982.
15. Camphausen, F. High Energy Laser Irradiance Model (HELIM): Summary Report NWC-TP-6102. Naval Weapons Center, China Lake CA, June 1971 (AD-B039-541).
16. Lilly, J. Q. Simplified Calculation of Laser Beam Propagation through the Atmosphere: Technical Report RH-76-8. U. S. Army Missile Command, Redston Arsenal AL, January 1976 (AD-B010-223L).
17. Ground Up To Space (GUTS), Version 2, Revision K. Unpublished computer program. Air Force Weapons Laboratory, New Mexico, 7 June 1983.
18. Peckham, Capt. L. N. and Lt. R. W. Davis. A Simplified Propagation Model for Laser System Studies: Technical Report AFWL-TR-72-95 (Revised). Air Force Weapons Laboratory, New Mexico, April 1973 (AD-909-426).
19. Gebhardt, Frederick G. "High Power Laser Propagation," Applied Optics, 15: 1479-1493 (July 1976).
20. Yariv, Amnon. Introduction to Optical Electronics (Second Edition). New York: Holt, Rinehart and Winston, 1976.
21. Atmospheric Propagation by Lasers. Unpublished course notes developed by Engineering Technology, Inc., Waco, TX.
22. Handbook of Lasers with Selected Data on Optical Technology, edited by Robert J. Pressley. Cleveland: The Chemical Rubber Company, 1971.

23. McClatchey, R. A. and J. E. A. Selby, Atmospheric Attenuation of Laser Radiation from 0.76 to 31.25 Microns: Technical report AFCRL-TR-74-003. Air Force Cambridge Research Laboratory MA, 3 January 1974.
24. Smith, H. J. P. et al. FASCODE - Fast Atmospheric Signature code: Scientific Report No. 2, Contract F19628-77-C-0041. Visidyne, Inc., Burlington MA, 16 January 1978.
25. Kneizys, F. X. et al. Atmospheric Transmission/Radiance: Computer Code LOWTRAN5: Technical Report AFGL-TR-80-0057. Air Force Geophysics Laboratory MA, 21 February 1980 (AD-A088-215).
26. Clifford, S. F. "The Classical Theory of Wave Propagation in a Turbulent Atmosphere," Laser Beam Propagation in the Atmosphere, editor by J. W. Strohbehn. New York: Springer-Verlag, 1978.
27. Wyngaard, J. C. et al. "Behavior of the Refractive-Index-Structure Parameter Near the Ground," Journal of the Optical Society of America, 61: 1646-1650 (December 1971).
28. The Infrared Handbook, edited by William L. Wolfe and George J. Zissis, The Infrared Information and Analysis Center, Environmental Research Institute of Michigan, 1978.
29. Yura, H. T. "Atmospheric Turbulence Induced Laser Beam Spread," Applied Optics, 10: 2771-2773 (December 1971).
30. Kenemuth, J. R. et al. "Thermal Blooming of 10.6 Micron Laser Beam in CO<sub>2</sub>," Applied Physics Letters, 17: 220-223 (1 September 1970).
31. Gebhardt, Frederick G. and David C. Smith. "Self-induced Thermal Distortion in the Near Field for a Laser Beam in a Moving Medium," IEEE Journal of Quantum Electronics, Vol. QE-7: 63-73 (February 1971).
32. Walsh, J. L. and P. B. Ulrich. "Thermal Blooming in the Atmosphere", Laser Beam Propagation in the Atmosphere, edited by J. W. Strohbehn. New York: Springer-Verlag, 1978.
33. Born, M. and E. Wolf. Principles of Optics (3rd Edition). New York: Pergamon Press, 1965.
34. Handbook of Geophysics and Space Environments, edited by S. L. Valley. Air Force Cambridge Laboratory MA, 1965.
35. U. S. Standard Atmosphere 1962. Washington: U. S. Government Printing Office, 1962.

36. Watson, Jerry, FEL Project Office. Telephone interview. Los Alamos National Laboratory, New Mexico, 7 September 1983.
37. Reitz, John R. et al. Foundations of Electromagnetic Theory (Third edition). Reading MA: Addison-Wesley Publishing Company, 1980.
38. Root, R. G. et al. Analysis of Laser-Target Interaction, Volume I - Theory: Final Report, 16 December 1977 - 15 December 1978. Contract DAAK40-78-C-0010. Physical Sciences Inc., Woburn MA, March 1979 (AD-A089-211).
39. Thermophysical Properties of Selected Aerospace Materials, Part I: Thermal Radiative Properties, edited by Y. S. Touloukian and C. Y. Ho. Lafayette IN: Purdue University Publishing, 1976.
40. Predicting the Average Absorptance During the Continuous Wave Laser Penetration of Painted Alloys: Final Report, AFWL-TR-77-169. Air Force Weapons Laboratory, Kirkland AFB NM, November 1977 (AD-A061-607).
41. Devore, Jay L. Probability and Statistics for Engineering and the Sciences. Monterey CA: Brooks/Cole Publishing Company, 1982.
42. Canavan, Gregory H., Associate Physics Division Leader for Advanced Concepts. "Basics of Space Lasers." Unpublished report. Los Alamos National Laboratory, New Mexico, 1983.
43. Robinson, Clarence A. "Shuttle May Aid in Space Weapons Test," Aviation Week and Space Technology, 119: 74-78 (31 October 1983).
44. Laser Weapon Technical Effectiveness Determination, Volume V - Optometrics Analysis: Final Report. Contract DAAH01-80-C-1122, General Research Corporation, Huntsville AL, 30 September 1981 (AD-B062-593L).

## VITA

Captain Douglas E. Kohlhepp was born on 23 March 1951 in Baltimore, Maryland and graduated from the University of Maryland in 1972 with a Bachelor of Science in Physics. Upon graduation, he entered the United States Air Force and was commissioned through Officers' Training School. Captain Kohlhepp completed Undergraduate Navigator Training in December 1973, and was awarded the ATC Commander's Trophy and the Husik Memorial Trophy. He underwent combat crew training in the FB-111 aircraft and served as a crew navigator, instructor navigator, flight examiner, and offensive systems staff officer within the 509th Bombardment Wing, Pease AFB, New Hampshire. In 1978, Captain Kohlhepp earned a Master of Science in Systems Management from the University of Southern California. Captain Kohlhepp was a Major Command flight evaluator and inspector with the First Combat Evaluation Group, Barksdale AFB, Louisiana, prior to entering the Air Force Institute of Technology in June of 1982.

Permanent address: 5516 Leith Road  
Baltimore, Maryland

UNCLASSIFIED

SECURITY CLASSIFICATION OF THIS PAGE

## REPORT DOCUMENTATION PAGE

REPORT SECURITY CLASSIFICATION <b>Unclassified</b>			1b. RESTRICTIVE MARKINGS			
2a. SECURITY CLASSIFICATION AUTHORITY			3. DISTRIBUTION/AVAILABILITY OF REPORT Approved for Public Release; Distribution Unlimited			
2b. DECLASSIFICATION/DOWNGRADING SCHEDULE						
4. PERFORMING ORGANIZATION REPORT NUMBER(S) AFIT/GSO/ENP/83D-2			5. MONITORING ORGANIZATION REPORT NUMBER(S)			
6a. NAME OF PERFORMING ORGANIZATION School of Engineering		6b. OFFICE SYMBOL (If applicable) AFIT/ENG		7a. NAME OF MONITORING ORGANIZATION		
6c. ADDRESS (City, State and ZIP Code) Air Force Institute of Technology Wright-Patterson AFB, Ohio 45433			7b. ADDRESS (City, State and ZIP Code)			
8a. NAME OF FUNDING/SPONSORING ORGANIZATION		8b. OFFICE SYMBOL (If applicable)		9. PROCUREMENT INSTRUMENT IDENTIFICATION NUMBER		
8c. ADDRESS (City, State and ZIP Code)			10. SOURCE OF FUNDING NOS.			
11. TITLE (Include Security Classification) See Box 19			PROGRAM ELEMENT NO.		TASK NO.	WORK UNIT NO.
			PROJECT NO.			
12. PERSONAL AUTHOR(S) Douglas E. Kohlhepp, B.S., Capt, USAF			15. PAGE COUNT 189			
13a. TYPE OF REPORT MS thesis		13b. TIME COVERED FROM _____ TO _____		14. DATE OF REPORT (Yr., Mo., Day) 1983 December		
16. SUPPLEMENTARY NOTATION						
17. COSATI CODES			18. SUBJECT TERMS (Continue on reverse if necessary and identify by block number)			
FIELD	GROUP	SUB. GR.	Free electrons Laser beams Laser weapons			
20	5					
19. ABSTRACT (Continue on reverse if necessary and identify by block number)						
Title: Wavelength Selection for a Ground Based Free Electron Laser Weapon System						
Thesis chairman: John Erkkila, Lt Col, USAF						
<p>A computer model was developed to examine the wave length dependent relationships which would impact in a selection of the operating wavelength for a ground based free electron laser weapon system employed in a strategic role. The program considers the device efficiency of the free electron laser, the propagation of laser radiation in the atmosphere, and the coupling of laser energy into the target material. The program employs modified versions of the atmospheric transmission codes LOWTRAN and FASCODE.</p> <p>The optimum laser wavelength for a specific selection of laser parameters is determined. However, equally acceptable wavelengths could be found with (cont'd)</p>						
DISTRIBUTION/AVAILABILITY OF ABSTRACT			21. ABSTRACT SECURITY CLASSIFICATION			
UNCLASSIFIED/UNLIMITED <input checked="" type="checkbox"/> SAME AS RPT. <input type="checkbox"/> DTIC USERS <input type="checkbox"/>			Unclassified			
22a. NAME OF RESPONSIBLE INDIVIDUAL John Erkkila, Lt Col, USAF			22b. TELEPHONE NUMBER (Include Area Code) (513) 255-2012		22c. OFFICE SYMBOL AFIT/ENP	

DD FORM 1473, 83 APR

EDITION OF 1 JAN 73 IS OBSOLETE.

SECURITY CLASSIFICATION OF THIS PAGE

UNCLASSIFIED

SECURITY CLASSIFICATION OF THIS PAGE

Abstract (cont'd)

3 .2 micrometer region surrounding this optimum value. In addition, the wavelength selection process is very sensitive to the mean sea level altitude of the laser device and the degree to which atmospheric turbulence induced beam spread can be compensated for by adaptive optics.

UNCLASSIFIED

SECURITY CLASSIFICATION OF THIS PAGE

14-00000

FILMED